NASA Technical Memorandum 104594, Vol. 2

MODIS Technical Report Series

Volume 2, MODIS Level 1 Geolocation, Characterization and Calibration Algorithm Theoretical Basis Document, Version 1

John L. Barker, Joann M. K. Harnden, Harry Montgomery,
Paul Anuta, Geir Kvaran, Ed Knight, Tom Bryant,
Al McKay, Jon Smid, and Dan Knowles, Jr.

May 1994

NASA Technical Memorandum 104594, Vol. 2

MODIS Technical Report Series

Volume 2, MODIS Level 1 Geolocation, Characterization and Calibration Algorithm Theoretical Basis Document, Version 1

John L. Barker, Joann M. K. Harnden, and Harry Montgomery
Goddard Space Flight Center
Greenbelt, Maryland

Paul Anuta, Geir Kvaran, Ed Knight, Tom Bryant, Al McKay, Jon Smid, and Dan Knowles, Jr.
Research and Data Systems Corporation
7855 Walker Drive, Suite 460
Greenbelt, Maryland

National Aeronautics and
Space Administration

Goddard Space Flight Center
Greenbelt, Maryland
1994

Table of Contents

Executive Summary vii
Chapter 1: Introduction 1
Chapter 2: MODIS Instrument Calibration Requirements 7
2.1 Product Sensitivity to Calibration 7
2.2 MODIS Instrument Calibration Specification 8
2.3 Instrument Characteristics 9
2.4 Calibration Strategy 9
Chapter 3: Theoretical Basis for the MODIS Characterization and Calibration Algorithm 11
3.1 Geolocation 11
3.2 Pre-Processing: Characterization and Reduction of Known Systematic Noise 13
3.3 Characterization of On-Board Calibrator and Lunar-View Calibration Data, Including Calculation of Calibration Coefficients 15
3.3.1 The Solar Diffuser 15
3.3.2 Electronic Calibration 17
3.3.3 The Spectroradiometric Calibration Assembly (SRCA) 18
3.3.3.1 SRCA Radiometric Mode 18
3.3.3.2 SRCA Geometric Mode 19
3.3.3.3 SRCA Spectral Mode 19
3.3.4 Blackbody 19
3.3.5 Space Viewport 20
3.3.6 Earth Scan Characterization/Calibration Data 20
3.3.6.1 Lunar View Characterization 20
3.3.6.2 Noise Characterization 21
3.3.7 Calculation of Radiometric Calibration Coefficients in the Reflective Bands 22
3.3.8 Calculation of Radiometric Calibration Coefficients in the Emissive Bands 22
3.4 Compare OBC/Lunar coefficients to Projected Coefficients 22
3.5 Calibration: apply the best calibration coefficients to the data. 23
3.6 Generate Utility Masks 23
3.6.1 Dead/Failing Detector Elements 23
3.6.2 Classification Masking Algorithm Basis Overview 24
3.7 Image-Derived Characterization, Including Calculation of Potential Calibration Coefficients 25
3.7.1 Histogram Equalization 26
3.7.2 Automated Calibration-Site-Based Radiometric Rectification by Relative Multiband Normalization 28
3.7.3 Modulation Transfer Function (MTF) Correction 29
3.7.4 Calculation of Potential Calibration Coefficients 30
3.8 Generate Quality Assurance Metadata 30

3.9 Project Calibration Coefficients for the next orbit....30
3.10 Level-1 Algorithm Detailed Control Flow Diagram, with Illustrative Equations....31
Chapter 4: Error Budgets....41
Chapter 5: Summary;....49
Appendix A: MODIS Level-1A Earth Location Algorithm Theoretical Basis Document, Version 1.0;....51
1.0 Introduction....51
2.0 Overview and Background Information....52
2.1 Experimental Objective....53
2.2 Historical Perspective....54
2.3 Instrument Characteristics....54
2.4 Ancillary Input Data....55
3.0 Algorithm Description....56
3.1 Theoretical Description....56
3.1.1 Coordinate Systems....57
3.1.2 MODIS Viewing Geometry....60
3.1.3 Mathematical Description of Algorithm....61
3.1.4 Variance or uncertainty estimates....67
3.2 Practical Considerations....69
3.2.1 Numerical Computation Considerations....69
3.2.2 Programming/Procedural Considerations....69
3.2.3 Product Validation and Geometric Parameter Estimation....71
3.2.3.1 Product Validation....71
3.2.3.2 Geometric Parameter Estimation....72
3.2.4 Quality Control and Diagnostics....73
3.2.5 Exception Handling....74
4.0 Constraints, Limitations, Assumptions....74
Appendix B: Instrument Specification;....77
B.1 Introduction....77
B.2 Physical Instrument Requirements....77
B.3 Radiometric Requirements....79
B.4 Spectral Band Requirements....83
B.5 Geometric Requirements....86
B.6 Other Performance Requirements....87
B.7 Remaining Specification Requirements....90
B.8 Summary....92
Appendix C: Instrument Design;....93
Appendix D: MODIS Calibration Strategy....105
D.1 Overview of Calibration Strategy....105
D.2 Phasing of Calibration Scene Utilization....111
D.3 Calibration Algorithm Data Transformation Strategy....112
D.4 Integration of Multiple Calibration Source Data....119
Appendix E: Algorithm Theoretical Basis Document for the Vicarious, In-flight, Radiometric Calibration of MODIS;....123

TABLE OF CONTENTS

1.0 Introduction 123
1.1 Algorithm Identification and Data Product 123
1.2 Algorithm Overview 123
1.3 Document Scope 125
1.4 Document Organization 125
2.0 Overview and background information 126
2.1 Experimental Objective 126
2.2 Historical Perspective 126
2.3 Instrument Characteristics 126
3.0 Algorithm Description 127
3.1 Theoretical Description 127
3.1.1 Physics of Problem 127
3.1.2 Mathematical Description of Algorithm 130
3.1.3 Variance/Uncertainty Estimates 130
3.2 Practical Considerations 140
3.2.1 Implementation Plans 140
3.2.2 Programming/Procedural Considerations 140
3.2.3 Calibration and Validation 141
3.2.4 Quality Control and Diagnostics 141
3.2.5 Exception Handling 141
3.2.6 Data Dependencies 142
3.2.7 Output Product 142
4.0 Constraints, Limitations, and Assumptions 142
5.0 Component Algorithm Descriptions 142
6.0 References for Appendix E 144
Acronyms for Appendix E 147
Appendix F: Glossary; 149
Appendix G: Acronyms & Symbols; 155
G.1 Acronyms 155
G.2 Symbols 158
Appendix H: Bibliography and References; 161
Index 171

Executive Summary

Each EOS Science Team Member is required to prepare an Algorithm Theoretical Basis Document (ATBD) describing the physical and mathematical basis for his or her data products. This document is the Version 1 ATBD describing the MODIS Level-1 processing algorithms (products MOD01 and MOD02) and the associated MODIS Utility Mask (product MOD18). In this document, calibration refers to the application of calibration coefficients to instrument data to create radiance values. Characterization refers to any manipulation of instrument data to derive instrument characteristics, including the generation of calibration coefficients using data from on-board calibration systems built into the instrument.

Processing algorithms for the MODIS Level-1 data products are in a preliminary phase of development. As the engineering and protoflight models of the MODIS instrument are fabricated and tested, the instrument manufacturer, Santa Barbara Research Center (SBRC), will provide characterization and calibration equations suitable for initial use and a numerical error analysis addressing Level-1 data product uncertainties. At that point, critical instrument-specific information can be incorporated into this document to provide a more quantitative formulation of the algorithms and their theoretical basis.

The MODIS Characterization Support Team (MCST), working under the direction of the MODIS Team Leader, has the primary responsibility for developing the Level-1 ATBD. With review from MCST, the MODIS Science Data Support Team (SDST) is responsible for developing and implementing the MODIS geolocation algorithm, Level-1A product. MCST is responsible for developing the characterization and calibration algorithm, the Level-1B product. MCST is also responsible for development of the MODIS Utility Masking algorithm.

Processing level designations for MODIS data products are defined in Table 1. Level-0 data from the instrument are reformatted, the Earth coordinates of individual pixels are determined and appended to the instrument data, instrument calibration information and other ancillary and engineering data required for processing are provided, and the whole is archived as the Level-1A MODIS data product, MOD01. Level-1B processing accepts Level-1A data as input and completes the conversion from digital numbers generated within the instrument to physical observations expressible in SI units. Level-1B processing provides calibrated at-satellite radiances generated at the original instrument spatial and temporal resolution, which are some radiometric calibration techniques used in Level-1B (MODIS product MOD02) processing require knowledge of intrinsic pixel properties such as clear or cloudy, sea or land, pure or mixed terrain class, inoperative detector, etc. Pixel classification results obtained during Level-1B processing will be retained and provided for general reference by the scientific community in MODIS Standard Data Product MOD 18, the MODIS Utility Mask. The Utility Mask will contain a series of binary and octal data fields describing designated pixel characteristics. Level-2 data products

are derived from the Level-1 radiances and describe geophysical and other Earth phenomena that cannot be measured directly by satellite instruments but can be mathematically derived from radiance observations. Level-2 data include derived land, ocean, and atmospheric products. This document discusses the theoretical basis for Level-1 processing algorithms and the MODIS Utility Mask.

Table 1
MODIS Data Processing Levels

Raw Data	Data in the original space-to-ground transmission packets, as received from the observatory, unprocessed by EDOS.
Level-0	Reconstructed instrument data at original resolution, time ordered, with all possible space-to-ground transmission artifacts removed and duplicate packets eliminated.
Level-1A	Level 0 data, reformatted but not resampled, located in an Earth-referenced coordinate system, and packaged with needed ancillary and engineering data.
Level-1B	Radiometrically corrected and fully calibrated instrument data in physical units at the original instrument spatial and temporal resolutions.
Level-2	Environmental variables (e.g., ocean wave height, soil moisture, ice concentration) retrieved at original instrument spatial and temporal resolutions.
Level-3	Instrument data or retrieved environmental variables that have been spatially and/or temporally resampled, averaged or composited.
Level-4	Model outputs or environmental variables derived from lower level data that are not directly measured by the instruments. For example, new variables based upon a time series of Level-2 or Level-3 data.

To assure that essential processing routines are available at launch, initial development efforts will focus on a set of core processing algorithms that use characterization and calibration data from pre-launch tests, on-board calibrators, and vicarious calibration experiments. If instrument stability in the space environment is better then the required minimum, appropriate calibration may provide enhanced results. Special purpose algorithms to support special calibration techniques may be required, or remedial algorithms to correct for non-ideal instrument behavior in the space environment may be needed. Algorithms to exploit increased instrument stability or correct for non-ideal behavior will be developed in priority order as resources permit.

The design of the first MODIS instrument will be fixed at the Critical Design Review (CDR), scheduled for the end of 1993. In-depth analysis of on-board calibration

systems will be initiated after CDR. A Peer Review of the MODIS Calibration Plan, including both the SBRC Instrument Calibration Plan and the overall context into which it fits, is planned for Spring of 1994. The Engineering Model will be completed and tested in the spring of 1995. As test data from the Engineering Model becomes available for analysis, Level-1 algorithm requirements will again be reviewed and this document will be updated. Revised versions of this ATBD will be issued as is appropriate; the probable schedule for instrument delivery and ATBD revisions is given in Table 2.

Table 2
MODIS and Cal ATBD Delivery Schedules

MODIS Instrument	Sensor Delivery Date	Revised Cal ATBD
Engineering Model	Spring 1995	August, 1995
Protoflight Model	Summer, 1996	November, 1996
Flight 1 Model	Winter, 1998	March, 1999

On-board calibration systems built into the MODIS instrument can measure radiometric response, spectral response, Modulation Transfer Function (MTF), and band-to-band spatial registration. Previous on-board calibration systems in the MODIS precursor instruments usually provided only a radiometric capability, so MODIS calibration will likely be both more complex and more accurate than that of its precursor instruments. A program of surface and airborne measurements to provide vicarious instrument calibration is planned in the post-launch era. Other sources of calibration information are shown in Figure 2.

The MODIS Characterization Support Team (MCST) has the task of integrating all characterization and calibration resources. Calibration must support the radiometric accuracy levels shown in Table 3.

To meet these accuracy requirements and assure that calibration uncertainty contributes as little as possible to the error of scientific products, effects of correctable instrument-related imperfections, such as pointing bias, systematic noise, and image ghosting will be reduced in Level-1 processing. The calibration algorithm is required to calibrate MODIS data to an acceptable level of accuracy in a fully automated mode, i.e., without human intervention for extended periods of time. Components of the Level-1 characterization and calibration algorithm will be formally documented and presented for peer-review by the instrument and Earth science communities before they are finalized and implemented in operational data processing.

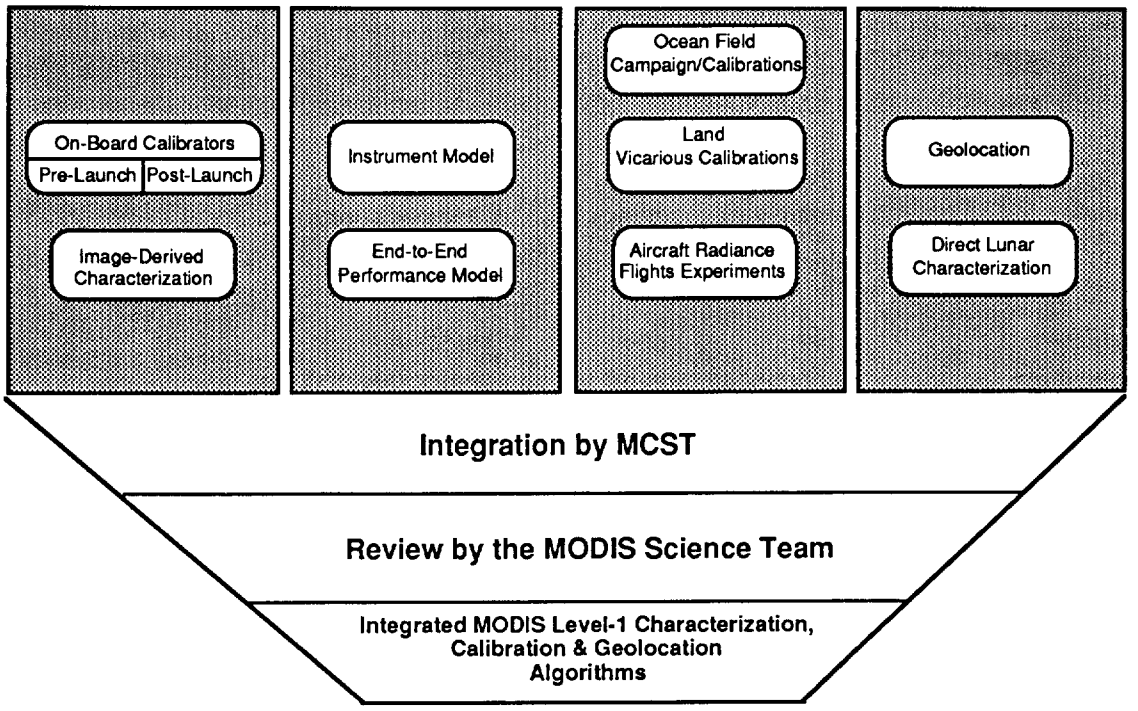

Figure 2. MODIS Characterization and Calibration Data Sources

Table 3
Radiometric Accuracy Required in the MODIS Specification

Wavelength	Required Accuracy at L_{typ}[a] ($\pm 1\sigma$, %)	Minimum Required Accuracy from $0.3*L_{typ}$[a] to $0.9*L_{max}$[a] ($\pm 1\sigma$, %)
< 3 μm	5	6
> 3 μm	1[b]	2
Reflectance Calibration[c]	2	3

a. Based on use of multiple samples of a uniform, extended, non-polarized source.
b. At L_{typ} Band 20 shall have minimum required radiometric accuracy of 0.75% with a goal of 0.50% and Bands 31 and 32 shall have an accuracy of 0.50% with a goal of 0.25%. The "high" ranges of bands 31 and 32 shall have an accuracy of 10%.
c. Calibration relative to the Sun using the solar diffuser plate and solar diffuser stability monitor.

A potential structure for the Level-1B processing algorithm is shown in Figure 3. This is the current baseline flow for on-orbit processing during the Operational Phase; the structure presented does not address exception handling or the special processing which will be required during the Activation and Evaluation (A&E) Phase, nor does it address Level-1 reprocessing or required off-line investigations. These issues will be addressed in future versions of this document. This processing flow does distinguish between processes that are considered to be indispensable for successful instrument calibration (core algorithm components), and those that enhance calibration accuracy, but can be implemented as subsequent software builds. The core algorithm will be given highest development priority; subsequent builds will be developed as resources permit. Individual algorithm components in the subsequent builds will be implemented only after it is shown that each improves the accuracy of the calibration.

Each pixel will be geolocated before its radiance is determined. Pixel geolocation begins with the determination of pixel viewing vectors (look vectors) in an instrument-referenced coordinate system. The look vectors are transformed through three intermediate coordinate systems (spacecraft, orbital, and Earth Centered Inertial) before the intersection of the look vectors with a suitable earth reference ellipsoid (probably WGS84) is determined in an Earth Centered Rotating coordinate system. Intersection points with the reference ellipsoid are then transformed to the desired geodetic coordinates. The final phase of the computation corrects for shifts in pixel location that occur because of terrain altitude deviations from the reference ellipsoid. Because the look vector might intersect the Earth surface in several locations at high look angles, an iterative procedure is used to determine the first (highest) intersection of the look vector with the surface. Besides the computations concerned with determining pixel geodetic latitude, geodetic longitude, and height above the Earth ellipsoid, other portions of the algorithm determine satellite zenith angle, satellite azimuth, range to the satellite, the solar zenith angle, and the solar azimuth. A more complete ATBD description of the geolocation algorithm is presented in Appendix E of this document.

The remaining processing components shown in Figure 3 (Box 2 and beyond) provide radiometric, spectral, and geometric characterization and calibration of the instrument. With sufficient measurement resources, radiometric calibration can achieve an absolute accuracy nearly matching the inherent radiometric stability of the instrument (NEdL). Radiometric processing begins with a pre-processing operation (Box 2 in Figure 3) to characterize known systematic noise components, i.e., determine their magnitude in the current dataset and reduce their effects. Pre-processing to reduce noise in this manner may improve the effective stability of the instrument and ultimately permit more accurate radiometric calibration. Examples of systematic noise sources which might be present include event-related noise (detected by its time correlation with events occurring within the MODIS instrument, on the orbiting platform, or within other payload instruments), coherent noise (periodic noise detected as a peak in the 1- or 2-dimensional Fourier transforms of the MODIS signals), image `ghosting', and crosstalk. This processing

phase will also detect and characterize any anomalous or exceptional behavior, such as might be caused by passing over the South Atlantic Magnetic Anomaly. Characterization results will be included in the metadata. Noise reduction procedures will be implemented only if all three of the following criteria are met:

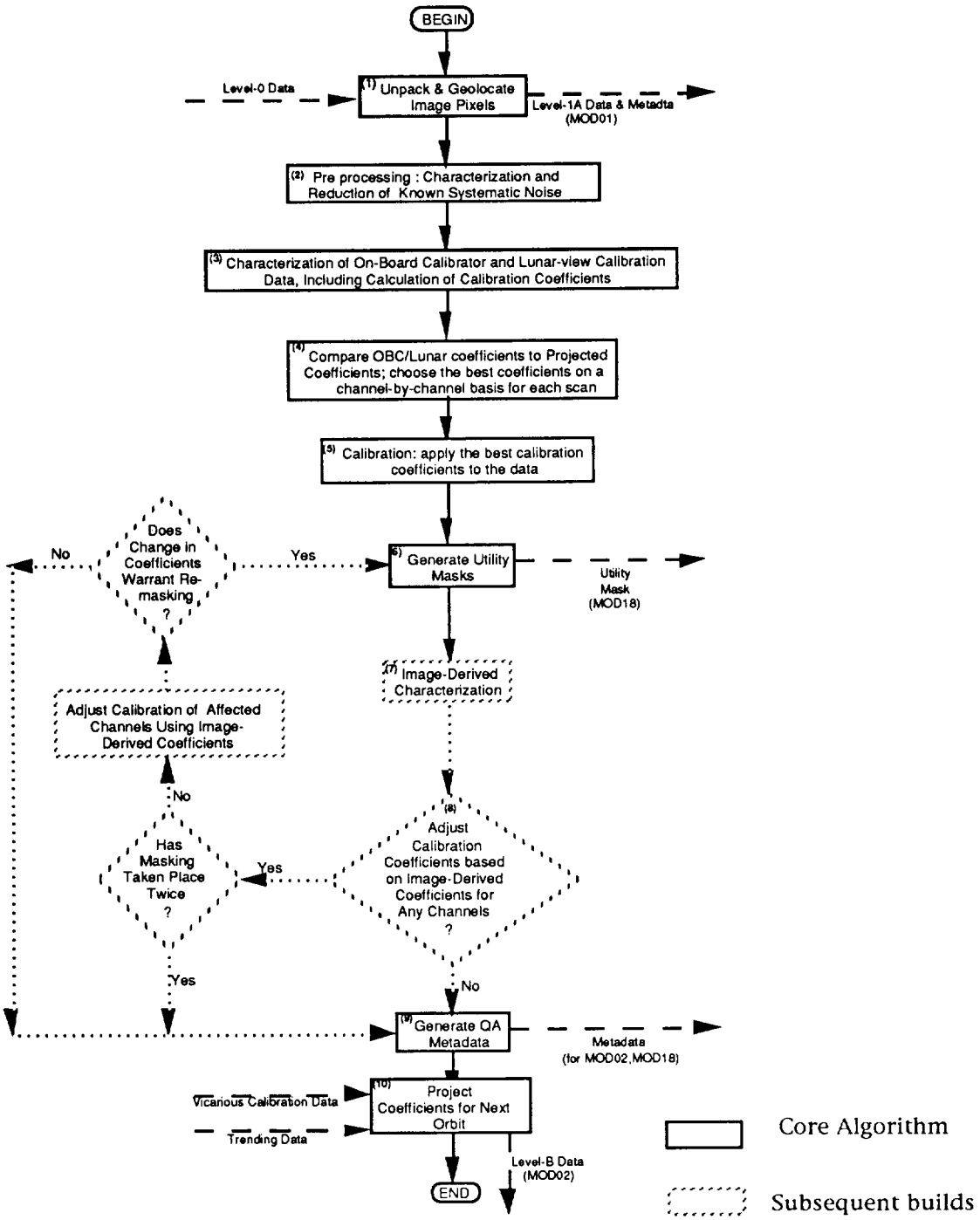

Figure 3. Level-1 Control Flow Diagram

(1) It is conclusively demonstrated that a particular type of noise (e.g., image ghosting) is present in the MODIS data.
(2) The noise can be predicted accurately enough that its effects can be reduced.
(3) The MODIS Science Team approves its reduction.

If noise reduction techniques are implemented, parameters used in the noise reduction process will also be retained in the metadata.

Systematic noise characterization and reduction is followed by instrument characterization and the determination of calibration coefficients using the on-board calibrators (OBCs) and the Moon (Figure 3, Box 3). The instrument manufacturer will provide the initial software to determine calibration coefficients based on the basic instrument design and measurements of instrument and OBC behavior obtained in the laboratory pre-launch, including the instrument response to on-board calibration systems. After launch, OBC characteristics will be studied in the context of all available calibration information, and the initial OBC characterization software supplied by the manufacturer will be modified to accommodate additional information developed as the instrument ages.

Lunar calibration observations may be obtained in a direct view mode in which normal platform attitude adjustments are suppressed for half an orbit to obtain a direct view of the lunar disk from the dark side of the Earth, and in a Space View mode that exploits 2-6 x per year when the Moon is visible through the MODIS Space Viewport. Lunar reflectance is a function of solar illumination angles as well as lunar surface coordinates and lunar libration angles. An Earth-based lunar reflectance measurement program has been initiated to provide the lunar radiance parameters required to use the Moon as an EOS calibration source.

The combined hardware/software system delivered by the manufacturer is required to meet the radiometric accuracy requirements of the specification (Table 3) without reference to the additional sources of calibration information that become available after instrument launch. The characterization & calibration algorithm processing flow assumes that the manufacturer has successfully met this requirement, and calibration coefficients used for processing are not allowed to deviate from the combined OBC/lunar values obtained in this processing phase by more than the probable error limits of these coefficients. However, it may be possible to improve on those error limits by using other sources of information such as vicarious calibration, trending data obtained from long-term instrument behavior studies, and past coefficient determinations from OBC and lunar data, as well as image-derived characterization (shown in Box 7 and described below). All of this data is combined to generate a "best guess" set of projected coefficients for the next orbit. If comparison of the last-available projected coefficients with the OBC/lunar coefficients (Box 4) shows that the projected coefficients are within the probable error limits of the OBC/lunar coefficient determinations, the projected coefficients are declared the "best" and these coefficients are used in subsequent processing. If the projected coefficients are outside the probable error limits for the OBC/lunar

coefficients, the OBC/lunar coefficients are declared "best" and these are used in subsequent processing. In the processing scheme as shown, no calibration coefficient that is inconsistent with the OBC and lunar coefficient determinations is ever used. The goal of the processing done after OBC and lunar coefficient determinations is to fully characterize and validate the calibration, and possibly to improve its precision and potential accuracy.

In the calibration phase (Box 5), calibration coefficients are applied to instrument data to obtain Level-1B data, and the calibrated Level-1B data then serves as input to utility mask processing (Box 6). The utility mask provides flags for important pixel characteristics such as cloudy/clear, land/water, pure/mixed terrain class, and inoperative detectors. In the processing flow, utility mask information is used to identify pixels that are cloud-free and otherwise suitable for image-derived processing techniques.

Image-derived characterization is based on intrinsic image characteristics and includes techniques such as image de-striping using histogram equalization, Modulation Transfer Function (MTF) characterization (and potential), and site-based radiometric monitoring of unsupervised calibration sites. If results of the image-derived techniques suggest that changes in calibration coefficients are warranted for some channels, new Level-1B radiometric data is created for those channels (first time through) and a decision is made as to whether the change in those calibration coefficients warrants recomputation of the Utility Mask. If not, processing proceeds to Quality Assurance (Q/A) Metadata generation. If so, the entire Utility Mask is recomputed and image-derived characterization is again applied based on the new pixel classifications.

Processing terminates after not more than two iterations through the Utility Mask and Image-Derived Characterization routines. With processing terminated at depicted, the radiometric calibration, the utility mask and the image-derived characterizations are consistent, i.e. the utility mask is based on the same radiometric information provided in the Level-1B product.

The flow now proceeds to quality assurance and metadata generation. MODIS Level-1B processing must maintain the radiometric accuracy and spectral and geometric characterization uncertainty required by the instrument specification (GSFC, 1993, Table 2, Appendix C) for the whole lifetime of the EOS program. The Q/A metadata will allow quantitative tracking of MODIS calibration performance.

Chapter 1

Introduction

The Moderate Resolution Imaging Spectroradiometer (MODIS) is being developed and launched as one of a series of Earth Observing System (EOS) instruments that will "advance scientific understanding of the entire Earth system by developing a deeper comprehension of the components of that system and the interactions among them (Asrar and Dokken, 1993)". Each of the EOS instruments is supported by a dedicated science team that is responsible for developing and validating the scientific for that instrument. Science team members are individually responsible for specific data products from their instrument, and as part of a documentation effort, each team member will generate and update an Algorithm Theoretical Basis Document (ATBD) describing the theoretical basis for the algorithms used to generate those data products. This document is Version 1 of an ATBD for the MODIS Level-1 Processing Algorithms, which include Level-1A, geolocation raw data (product MOD01), Level-1B geolocated radiance (Product MOD02) and the MODIS Utility Mask (product MOD18). This ATBD is produced by the MODIS Characterization Support Team (MCST), which is responsible for developing standard MODIS characterization and calibration procedures.

The algorithm to geolocate MODIS pixels is being developed in a separate effort undertaken by the MODIS Science Data Support Team (SDST) with review by MCST. The geolocation of MODIS data includes the determination of geodetic latitude, longitude, and elevation for the individual pixels and the determination of geometric parameters for each observation (satellite zenith angle, satellite azimuth, range to the satellite, solar zenith angle, and solar azimuth). Details of the proposed geolocation algorithm can be found in Appendix E of this document.

This Level-1 ATBD and its updates are written for MODIS data users who need to understand the strengths and limitations of the MODIS data for their own research, and for those people who are responsible for developing and implementing algorithms which utilize MODIS instrument data. This document with its appendices will present those features of MODIS characterization and calibration needed to understand the calibration algorithms. The MODIS calibration algorithm is currently in the early stages of development; consequently, this document presents a top-level overview of the algorithm with some illustrative equations. Calibration, in this document, refers to the application of calibration coefficients to instrument data to create radiance values. Characterization refers to any manipulation of instrument data to derive instrument characteristics, including the generation of calibration coefficients using on-board calibrator data. Initially, it is assumed that the instrument will meet its specification, and that no anomalies will arise. A set of characterization and calibration procedures to deal with this scenario is identified. This core algorithm is the minimum set of routines necessary for at-launch calibration processing; it will be given highest development priority. As pre-

launch instrument test data become available, additional calibration issues may arise, even though none are currently anticipated. If there are instrument anomalies such as systematic noise that must be removed in ground processing to meet specification requirements, then procedures to reduce those effects will receive the next highest development priority. Finally, an instrument that meets specifications may provide stability that exceeds minimum requirements. The approach to MODIS calibration outlined here includes provisions to exploit any such margins in the instrument performance to minimize calibration error and the associated uncertainty in the final scientific products; these procedures will be developed as resources are available.

MODIS instruments will be launched on the EOS spacecraft in a Sun-synchronous orbit. There are six such spacecraft planned, three in the AM series (in a descending orbit with a 10:30 AM equatorial crossing time) and three in the PM series (in an ascending orbit with a 1:30 PM crossing time). Each series will consist of an initial platform followed by two replacements launched on 5-year centers, for a total series life of 15 years. The schedule for successive MODIS instruments and the MODIS ocean precursor instruments (SeaWiFS and COLOR) is shown in Figure 1.0-1.

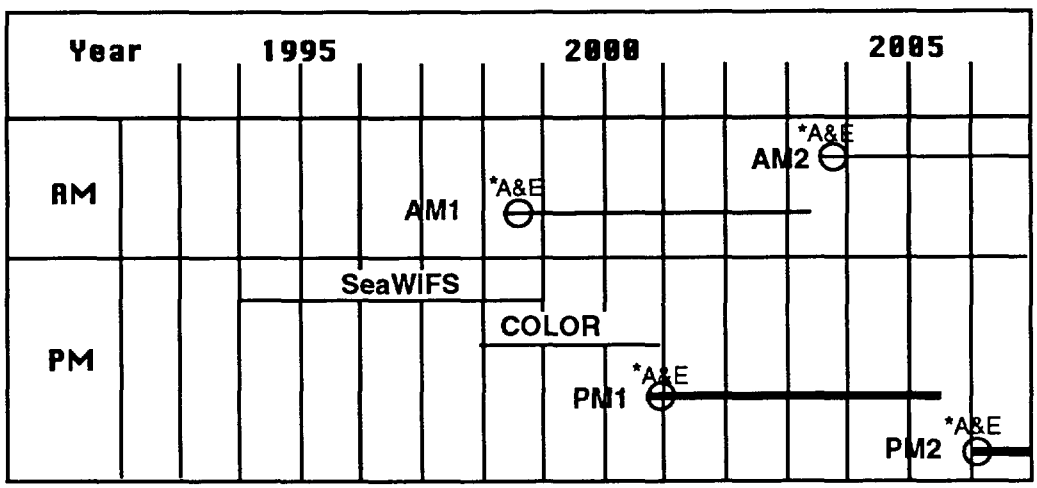

* A&E: Activation and Evaluation of the MODIS instruments

Figure 1.0-1. Launch schedule for the MODIS AM and PM instruments with ocean precursor instruments also shown.

MODIS requirements are laid out in other source documents (Salomonson et al., 1989; Salomonson and Toll, 1990; Ardanuy et al., 1991; Salomonson and Barker, 1992; Pagano, 1992; Barnes and Salomonson, 1993, and Pagano and Durham, 1993). MODIS heritage instruments include AVHRR, HIRS, Landsat TM (Markham and Barker, 1986; Salomonson and Barker, 1987; and Barker and Wanchoo, 1988) and MSS, Nimbus-7 CZCS, and SeaWiFS. To provide long-term observations of potential changes in Earth processes for succeeding decades, MODIS will maintain observational continuity with predecessor and successor instruments, and with

instruments that will provide correlative and ancillary data. The EOS mission requires a cohesive, calibrated data set composed of data from all six MODIS instruments. A scientifically useful data set composed of measurements from all MODIS instruments requires a calibration scheme to provide consistent radiance values across instruments, orbits, and time intervals.

An intensive series of instrument check-out, characterization and calibration activities is planned during the on-orbit Activation and Evaluation (A&E) period (3-6 months), immediately after each of the instruments is launched. As each MODIS instrument is launched and activated, MODIS characterization and calibration on-orbit procedures will:

- Establish initial estimates of MODIS instrument stability within an orbit and over many orbits, and from these, develop a schedule for the use of individual calibration techniques and an estimate of achievable instrument calibration accuracy;
- Determine the extent to which pre-launch instrument calibration has been successfully retained in orbit and make any adjustments necessary in the pre-launch characterization and calibration algorithm;
- Incorporate the results of vicarious calibrations as they are available.

An illustrative flow diagram for MODIS Level-1 processing is given in Figure 1.0-2.

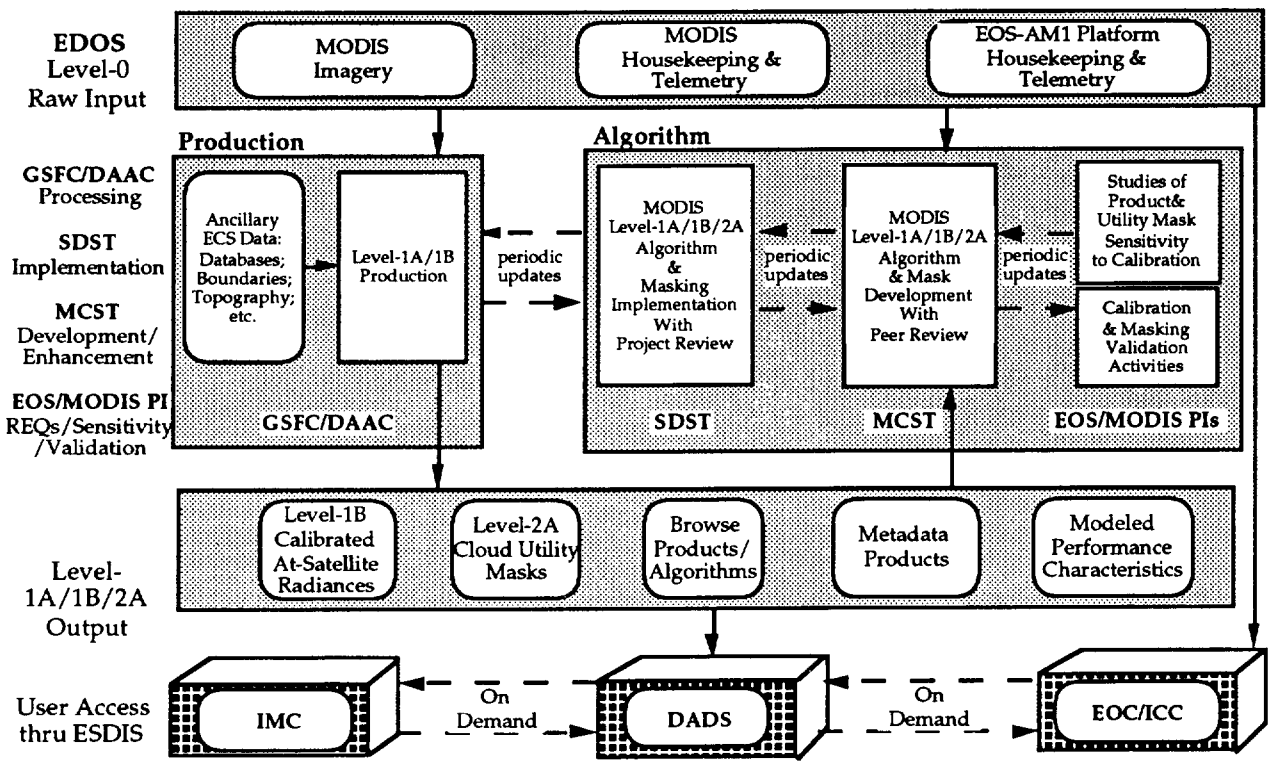

Figure 1.0-2. MODIS Level-1 Calibration & Utility Mask Products illustrative flow diagram

The MODIS Level-1 characterization and calibration algorithm consists of all the procedures required to produce radiometrically calibrated, spectrally characterized and geolocated MODIS data for distribution within the science community. The core algorithm will be based on pre-launch laboratory test results for the instrument and its on-board calibration systems as supplied by the instrument manufacturer. Successive versions of the algorithm will be augmented by some of the characterization and correction techniques discussed in this document. Changes to the calibration algorithm will be implemented only if it can be unambiguously shown that the changes produce a better product. In addition to absolute radiometric calibration and image-derived calibration techniques, processing may include noise removal, within-band and cross-band signal normalization, spectral band monitoring and geometric registration assessment, and possible (Modulation Transfer Function) inversion. A scene mask will be implemented indicating characteristics of each pixel such as dead or noisy channels, replaced channels, clear or cloudy, radiometrically homogeneous (pure) or heterogeneous (mixed), approximate water fraction, snow fraction, glint, solar irradiance level, etc.

Over a period of more than three years in the 1980s, the scientific investigators of the Landsat Image Data Quality Assessment (LIDQA) project characterized the performance of both the MSS and TM sensors (Markham and Barker, 1985). When correctable anomalies were found, it was no longer possible to change the ground processing system. The intention of the MODIS Level-1 processing effort is to provide the possibility of correcting for observed anomalies by having appropriate software in place for evaluation and potential use at the time of launch, and to provide for on-going post-launch up-grades.

MODIS Level-1 processing will produce Level-1A and Level-1B data sets. The Level-0 MODIS data is digitally quantized to twelve bits (one part in 4096). The Level-1A data processing de-packetizes the Level-0 data and re-formats it into 16-bit, byte-aligned words. Ancillary and engineering data which are needed for calibration processing will be appended; examples of such information include spacecraft location and attitude and the projected calibration coefficients, along with their uncertainties. The same Level-1A processing also geolocates the data, i.e., the Earth location of each individual pixel is determined, expressed in Earth-referenced coordinates, and included in the data set.

The MODIS Level-1B data product is a radiometrically calibrated and spectrally and geometrically characterized product. It is created from the application of radiometric processing routines to Level-1A data. If the symbol Q is used to represent the original 12-bit quantized Level-1A radiometric data from the instrument and L_λ represents the Level-1B at-satellite radiance obtained from calibration processing, then radiometric calibration processing is represented by the equation:

$$L_\lambda = f(Q)$$

where the functional form of f will be determined for each channel from pre-launch radiometric calibration activities and the coefficients for f will be determined on an on-going basis on-orbit. To facilitate the comparison of scenes taken under different conditions, some researchers may prefer to work in units of planetary albedo (for the solar reflective bands) or effective temperatures (for the thermal emissive bands). The effective at-satellite planetary reflectance ρ_p is given by

$$\rho_p = \frac{\pi \; L_\lambda \; d^2}{E_{SUN,\lambda} \; cos\,\theta_s}$$

where d is the Earth-Sun distance in astronomical units, $E_{SUN,\lambda}$ is the mean solar exoatmospheric irradiance and θ_s is the solar zenith angle. The effective at-satellite temperature T is given by:

$$T = \frac{K_2}{ln(\frac{K_1}{L_\lambda} + 1)}$$

where K_1 and K_2 are band-dependent constants.

The sections that follow address calibration requirements and potential algorithm structure and theoretical basis. The appendices cover the instrument specification, instrument design, calibration strategy, the geolocation algorithm, a draft Vicarious Calibration ATBD, and glossary, acronyms and symbols, and references.

Chapter 2

MODIS Instrument Calibration Requirements

The objectives of MODIS characterization and calibration are to:

- Calibrate and characterize each individual MODIS instrument;
- Maintain calibration consistency between successor MODIS instruments (AM1, AM2, and AM3 and PM1, PM2, and PM3);
- Maintain calibration consistency between the MODIS instrument series and other EOS-AM and EOS-PM instruments including ASTER, MISR, CERES, AIRS; and
- Maintain consistency with past and future Earth-observing instruments including Landsat TM, AVHRR, and the SeaWiFS and COLOR ocean observation programs.

To detect trends occurring over periods of years to decades and provide input for causal models of Earth processes, each MODIS instrument must be calibrated in absolute (SI) units. Since there are practical limits on the accuracy with which national and international SI calibration standards can be transferred to the instruments, EOS is planning a series of pre-launch cross-sensor calibration experiments. By circulating reference standards among the laboratories building the instruments, and by assuring that comparable procedures are followed in referencing these standards, the EOS program may obtain a measure of precision among observations from multiple instruments that exceeds absolute accuracy based on SI standards. The MODIS instrument will be included in EOS cross-calibration experiments.

2.1 Product Sensitivity to Calibration

As the MODIS Science Team members create sensitivity curves describing the uncertainty in their products as a function of the uncertainties of various instrument characterization and calibration parameters, potential product benefits can be analyzed as a function of instrument precision and accuracy improvements. Product sensitivities will be developed collaboratively by the MCST and Science Team members as the critical driving algorithms for Level-2 products are identified over the next several years. On-orbit, sensitivity relationships will be used to determine if a given Level-2 product would merit reprocessing using revised coefficients when new calibration information is developed. Products that are relatively insensitive to calibration may not need to be updated; other products strongly dependent on calibration accuracy may warrant re-processing.

2.2 MODIS Instrument Calibration Specification

The MODIS instrument specification (MODIS Spec., 1993) contains many performance, testing, calibration, and quality assurance requirements. The contractor must meet these requirements upon delivery of the instrument. The specification requirements are the minimum necessary for the success of the mission. Appendix B presents a detailed description of the specification, including exceptions and testing circumstances for each requirement. A brief summary is included below.

The Specification mandate includes physical instrument requirements (section B.2) such as mass and orbit.. It also covers characterization and calibration issues, including radiometric (B.3), spectral (B.4), geometric (B.5), and other performance requirements (B.6). Finally, there are requirements for instrument math models, and verification and calibration plans and procedures (section B.7)

The specification assigns each spectral band a noise equivalent radiance (NEdL), a typical radiance (Ltyp), a maximum radiance (Lmax), a cloud radiance estimate (Lcloud), and a desired Signal to Noise Ratio (SNR). Radiances must be able to be determined to an uncertainty of 5% for wavelengths below 3 mm and 1% for those above 3 mm (see footnote C to Table 2.1-1, below, for exceptions). Additionally, reflectances must be calibrated, using the solar diffuser and solar diffuser stability monitor, to within 2%.

Table 2.2-1
Calibration Accuracy Required in the MODIS Specification and Accuracy Predicted by the Instrument Manufacturer

Wavelength	Required Accuracy[a] ($\pm 1\sigma$, %)	Predicted Accuracy[b] ($\pm 1\sigma$, %)
< 3 μm	5	4
> 3 μm	1[c]	0.75
Reflectance Calibration [d]	2	TBD

a. Based on use of multiple samples of a uniform, extended, non-polarized source.

b. Pagano and Durham, 1993

c. At L_{typ} Band 20 shall have minimum required radiometric accuracy of 0.75% with a goal of 0.50% and Bands 31 and 32 shall have an accuracy of 0.50% with a goal of 0.25%. The "high" ranges of bands 31 and 32 shall have an accuracy of 10%.

d. Calibration relative to the Sun using the solar diffuser plate and solar diffuser stability monitor.

Passbands for each of the 36 spectral bands must conform to specific spectral shape requirements, including center wavelength and bandwidth (see Table B-4). After launch, spectral response must be both stable and measurable.

Geometrically, the instrument must meet specific field of view and pointing requirements. Depending on the spectral band, Instantaneous Fields of View (s) of 250, 500 and 1000 meters are specified. Different bands within a pixel must be coregistered to within +/- 20% of an IFOV. Pointing accuracy must be within 60 arc seconds with pointing knowledge better than 30 arc seconds.

Other requirements also affect radiometric uncertainty. The specification contains sections addressing polarization sensitivity, minimum MTF requirements, detector crosstalk, stray light, and transient response. These effects will all be characterized individually and their effect on radiometric uncertainty evaluated.

2.3 Instrument Characteristics

Those readers not familiar with the overall MODIS instrument design and the characteristics and operating modes of the on-board calibrators can refer to a summary of the relevant aspects of instrument performance in Appendix C.

2.4 Calibration Strategy

The basic MCST approach to calibration is "success-based", i.e., the null hypothesis that the instrument meets specifications and functions correctly is assumed at launch. The basis of the calibration strategy is to utilize all available information sources to test the null hypothesis and institute alternative procedures to maintain the required calibration accuracy over the life of the mission. Statistical characterization of the multiple calibration sources will produce confidence intervals for the predicted calibration coefficients. New coefficients are applied when sufficient change occurs in the intervals to drive coefficients outside bounds.

A similar paradigm is used to mitigate noise and exceptional conditions which are observed. Statistical characterization of noise, striping, failing detector, etc. will be used to produce decision thresholds which are used to invoke or not invoke application of filtering algorithms to mitigate the condition.

Appendix D contains a more detailed discussion of the calibration strategy and includes a discussion of lunar processing conditions and the data transformation approach which creates a standard calibrated data dynamic range.

Chapter 3

Theoretical Basis for the MODIS Characterization and Calibration Algorithm

The algorithms that will be used for MODIS calibration processing are in a very preliminary stage of development and decisions on actual calculations that will be used have not been made. The material provided in this document is representative of techniques that are being studied and this material is provided for review at the current state of algorithm development. Studies of alternative calibration approaches and algorithms are on-going and, in many cases, the algorithm descriptions provided in this document are incomplete. Some of the potential techniques have been implemented in the past and MODIS calibration can build on the heritage of these past implementations. Other techniques discussed here are extensions of previously implemented algorithms, or are entirely new techniques.

The algorithm discussed here is the proposed baseline Operational Phase algorithm; it thus assumes that initial conditions, such as the tests which are done during the A&E Phase to establish the operational schedule of the OBCs, are complete. Pre-launch test analysis, on-orbit A&E special testing, and exception handling will all be developed in detail at a later date. The overall algorithm control flow is shown in Figure 3.0-1. This section sequentially discusses each of the processes shown in this flow. It explains the processes involved, assigns a priority to the development of each process and presents a theoretical basis for the techniques being considered for implementation. A detailed control flow diagram, with illustrative equations, is given in Section 3.10. Additional information on the techniques is presented in Appendix D, Calibration Strategy.

3.1 Geolocation

Each pixel will be geolocated before its radiance is determined. Geolocated data are needed for the Utility Mask, the Image-derived Characterization techniques and for generation of the Quality Assurance Metadata. With review from MCST, the MODIS Science Data Support Team (SDST) is responsible for developing and implementing the MODIS Geolocation Algorithm. A synopsis of the algorithm follows. This algorithm must be available at launch. Specific detailed information on the current algorithm for geolocation is presented in Appendix E.

Geolocation begins with the determination of pixel viewing vectors (look vectors) in an instrument-referenced coordinate system. The look vectors are transformed through three intermediate coordinate systems (spacecraft, orbital, and Earth Centered Inertial) before the intersection of the look vectors with a suitable Earth reference ellipsoid (probably WGS84) is determined in an Earth Centered Rotating

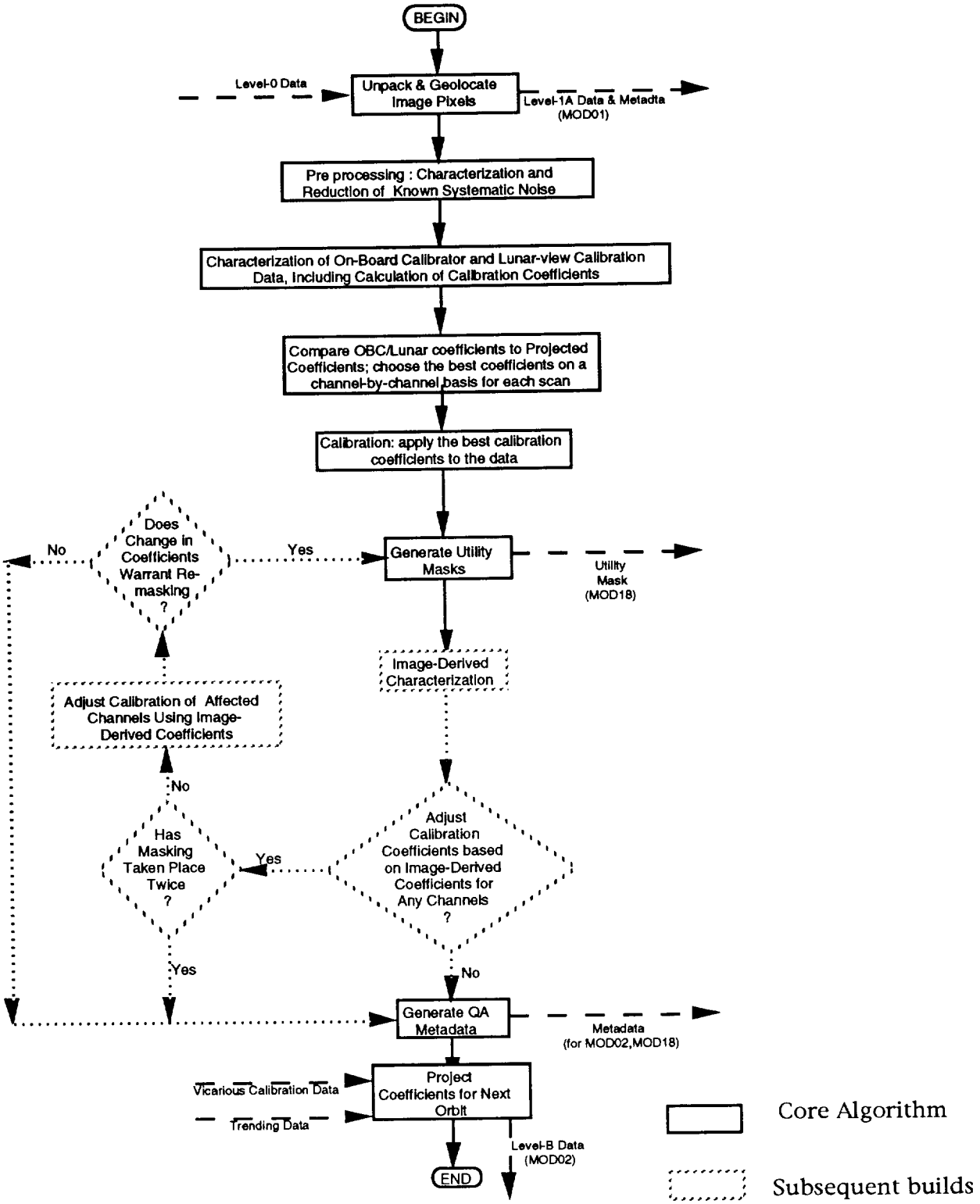

Figure 3.0-1. Level-1 Control Flow Diagram

coordinate system. Intersection points with the reference ellipsoid are then transformed to the desired geodetic coordinates.

The final phase of the computation corrects for shifts in pixel location that occur because of terrain altitude deviations from the reference ellipsoid. Because the look vector might intersect the Earth surface in several locations at high look angles, an iterative procedure is used to determine the first (highest) intersection of the look vector with the surface. The procedure can be computationally intensive, and a special coordinate system [Space Oblique Mercator (SOM)] is being considered for use with Earth digital elevation data. Use of this coordinate system may simplify the interpolation needed to determine pixel locations that are situated between originally supplied digital elevation reference points. Besides computations concerned with determining pixel geodetic latitude, geodetic longitude, and height above the Earth ellipsoid, other portions of the algorithm determine satellite zenith angle, satellite azimuth, range to the satellite, the solar zenith angle, and the solar azimuth.

3.2 Pre-Processing: Characterization and Reduction of Known Systematic Noise

Pre-launch laboratory tests will establish the magnitude of some systematic noises, such as ghosting, stray light and crosstalk. The calibration precision, and the theoretically attainable accuracy, will improve if known systematic noise is reduced as far as feasible through pre-processing the data before calibration. Prioritization of pre-launch development of pre-processing algorithms will be based on the results of the laboratory tests. Reduction of any systematic noise which threatens the ability to calibrate to the levels listed in Table 2.2-1 will be given very high priority, while algorithms for reduction of lower-magnitude noise will be developed as resources are available.

Noise pre-processing will depend on three conditions:

(1) Demonstration that a particular type of systematic noise (i.e., image ghosting) is present in the MODIS data.
(2) Characterization of the noise thoroughly enough that it can be reduced or removed via ground processing.
(3) MODIS Science Team approval of its reduction/removal.

If all three of these conditions are met then the raw data will be analyzed for that particular type of systematic noise each orbit and, if it is present, it will be reduced before the data is calibrated.

Systematic noise analysis will employ time and frequency domain techniques to identify unusual conditions in and characterize the quality of the MODIS data. The techniques range from statistical analysis of variance and covariance to one-dimensional, two-dimensional, and possibly higher-order Fourier and other transforms. These techniques have a heritage from the Thematic Mapper LIDQA program (Barker and Markham, 1985), which was the first comprehensive, science

team based characterization of a satellite sensor. The basic operations for MODIS noise analysis are listed below. These operations are presented in generalized form here and are not intended for direct use in generating computer code. Definitions of the variables can be found in the Glossary in Appendix F.

Sample Mean: $$\mu = \frac{1}{N}\sum_{i=1}^{N} Qi$$

Sample Standard Deviation: $$\sigma = \left[\frac{1}{N}\sum_{i=1}^{N}\left(Q_i - \mu\right)^2\right]^{\frac{1}{2}}$$

Sample Correlation: $$P_{12} = \left[\frac{1}{N}\sum_{i=1}^{N}\left(Q_i^1 - \mu_1\right)\left(Q_i^2 - \mu_2\right)\right]^{\frac{1}{2}}$$

One-Dimensional Discrete Fourier Transform: $$F_k = \sum_{i=1}^{M} Q_i e^{\frac{-\sqrt{-1}\ 2\pi i k}{M}}$$

Two-Dimensional Discrete Fourier Transform: $$F_{kl} = \sum_{i=1}^{M}\sum_{j=1}^{N} Q_{ij} e^{\frac{-\sqrt{-1}\ 2\pi(ik+jl)}{MN}}$$

Histogram of Quantized Data: H_i = Count of Q occurrence in bin i

One-Dimensional Convolution: $$R_k = \sum_{i=1}^{N} Q_i\, Q_{i-k}$$

Two-Dimensional Convolution: $$R_{kl} = \sum_{i=1}^{N}\sum_{j=1}^{M} Q_{ij} Q_{i-k,j-l}$$

Least Squares Fit: choose $c_0, c_1, \ldots c_n$ such that $$min \sum_{i=1}^{N}\sum_{j=1}^{N}\left(f\left(i,j,c_0,c_1,\cdots c_n\right) - Q_{ij}\right)^2$$

Many more advanced measures are available for characterizing data quality such as information theory measures (Entropy) and nonlinear transforms, such as Hadamard, which represent step-like signals more efficiently. Spectral transforms such as Greenness (Kauth, 1976), Brightness (Crist, 1984), and Tasseled Cap from scene classification disciplines may be useful in quantifying MODIS data characteristics. These will be selected and employed as required in the post-launch evaluation phase.

The most basic systematic noise analysis will involve techniques such as running zero level standard deviations of all 470 detector channel noise levels and frequency spectrums for all the channels. These two measures provide knowledge of the SNR performance and location of any coherent components contributing to the noise

variance. Correlation measures can indicate relationships between particular noise components in different channels and histogram analysis can detect A/D problems and nonlinearities in the overall system transfer function.

Once a decision is made that the systematic noise is present reduction techniques such as, 1-D & 2-D Fourier notch filtering and Kalman filtering may be used.

The output of this processing phase is a Level-1A' set of data. This data set is an interim set internal to the calibration algorithm and will not be archived. The original, archived Level-1A data is not changed. The type and magnitude of noise found in the data and the filter used to remove it, if any, will be stored as metadata.

3.3 Characterization of On-Board Calibrator and Lunar-View Calibration Data, Including Calculation of Calibration Coefficients

The dataset from each calibrator is characterized and evaluated individually. Then, the coefficients for the reflective bands are calculated, followed by the coefficients for the emissive bands. The coefficients for the reflective bands are expected to be stable over many scans, and possibly over many orbits; the coefficients for the emissive bands are expected to vary on a scan-by-scan basis. The rest of this sub-section addresses the proposed processing for each of the OBCs, and how the data will be used to calculate potential calibration coefficients. These characterizations are the highest development priority. The algorithm provided will draw on the OBC algorithms provided by SBRC in accordance with Specification ¶(3.1.4.1).

3.3.1 The Solar Diffuser

The Solar Diffuser (SD) panel is positioned to be illuminated by the sun whenever MODIS is over the north pole and the opaque solar diffuser door is open. If that door is open the Solar Diffuser data is available for 30 frames of data per scan for approximately 30 scans. The data may be taken with an unobstructed entrance aperture or with a perforated screen in place to reduce the illumination intensity so as not to saturate bands with lower L_{max} values. Only one of these modes is available on any given orbit.

Whenever the Solar Diffuser is used the Solar Diffuser Stability Monitor (SDSM), which measures the stability of the Solar Diffuser plate by ratioing the value from the sun with the value from the Solar Diffuser, is also active.

The SDSM signal when viewing the solar diffuser panel is

$$Q_{SD}(\lambda,t) = R'(\lambda)\, f(\lambda,\theta,\phi,\theta',\phi',t)\, S(\lambda)$$

and when viewing the sun directly it is

$Q_S(\lambda,t) = R'(\lambda)\, K(\lambda)\, S(\lambda)$

Where

$R'(\lambda)$ is the spectral response of the SDSM,

$f(\lambda,\theta,\phi,\theta',\phi',t)$ is the measured Bidirectional Reflectance Distribution Function (BRDF) of the SDSM,

$S(\lambda)$ is the solar irradiance, and

K is a constant for a given λ.

These two equations may be used to solve for K in terms of measured quantities:

$$K(\lambda) = \frac{Q_S(\lambda,t_0) f(\lambda,\theta,\phi,\theta',\phi',t_0)}{Q_{SD}(\lambda,t_0)}$$

Applying this same equation after launch (at time t_1) at the specific angles $(\theta_1,\phi_1,\theta_1',\phi_1')$ yields

$$f(\lambda,\theta_1,\phi_1,\theta_1',\phi_1',t_1) = \frac{K(\lambda) Q_{SD}(\lambda,t_1)}{Q_S(\lambda,t_1)}$$

Where $Q_S(\lambda,t_1)$ and $Q_{SD}(\lambda,t_1)$ are SDSM measurements of the direct Sun and illuminated solar diffuser panel after launch at time t_1. Because $f(\lambda,\theta,\phi,\theta',\phi',t_0)$ was measured over the full range of angles before launch (at time t_0) and the last equation given the Bidirectional Reflectance Distribution Function (BRDF) after launch at specific angles, a degradation ratio C is computed from:

$$C = \frac{f(\lambda,\theta_1,\phi_1,\theta_1',\phi_1',t_1)}{f(\lambda,\theta_1,\phi_1,\theta_1',\phi_1',t_0)}$$

A degradation constant ($<C(\lambda)>$) may be determined by averaging the degradation ratio across one orbit (~900 frames of data)

$$<C(\lambda)> = \frac{1}{n}\sum_{i=1}^{n} C(\lambda)_i$$; where n=number of frames of data (~900).

The Bidirectional Reflectance Distribution FunctionBRDF when MODIS is viewing the solar diffuser plate is:

$$f(\theta_1,\phi_1,\theta'_2,\phi'_2,t_1) = <C(\lambda)>\, f(\theta_1,\phi_1,\theta'_2,\phi'_2,t_0)$$

where the angles θ_2',ϕ_2', define the MODIS line of sight to the solar diffuser.

For a single detector channel and one frame of data, the spectral radiance into the sensor aperture from the Solar Diffuser, $L(\lambda)$, is:

$$L(\lambda) = \langle C(\lambda) \rangle \, f(\lambda, \theta_1, \phi_1, \theta'_2, \phi'_2, t_0) \, S(\lambda)$$

where:

- $\langle C(\lambda) \rangle$ is the degradation constant for this region. The spectral bandpasses of the MODIS channels are narrower than those of the SDSM; therefore multiple bands will have the same degradation constant.
- $f(\lambda, \theta_1, \phi_1, \theta'_2, \phi'_2, t_0)$ is the Bidirectional Reflectance Distribution FunctionBRDF of the SD pre-launch, where $\theta_1, \phi_1, \theta'_2, \phi'_2$ are the incident and scattered angles which are fixed and known.
- $S(\lambda)$ is the solar spectral irradiance.

The value used to calculate the calibration coefficients will be the average radiance for this orbit; the error estimate will be its standard deviation:

$$\langle L(\lambda) \rangle = \frac{1}{n} \sum_{i=1}^{n} L(\lambda)_i \text{ ; where n=number of frames of data (~900).}$$

3.3.2 Electronic Calibration

The electronics between the detector and the signal output can also affect the data, as can the linearity of the A/D converters. Each channel has a dedicated A/D converter. Accordingly, the Specification (see Appendix B) requires MODIS to be able to calibrate (characterize, according to this document's usage) each channel's electronics. The electronics characterization procedure varies slightly between the photovoltaic and photoconductive channels. The photovoltaic electronic calibration is done on each scan that the Solar Diffuser is not illuminated and the data replaces the Solar Diffuser data in the datastream. The photoconductor electronic characterization is done during the Space View on any scan specified by ground command. These procedures are described below.

The signal for the photovoltaic (PV) bands 1-30 leaves the detectors, feeds into a capacitance transimpedance amplifier (CTIA), a multiplexer selecting the channel, an integrator on the input to the Analog Electronics Module (AEM) to remove the multiplexer transient effects, a programmable gain and offset, and then a 12 bit Analog to Digital Converter (A/D). Normally the CTIA is reset after each multiplexer readout to prepare for the next IFOV. For electronic calibration, the instrument electronically inserts a programmed amount of charge into the CTIA rather than reading the detector input. At the end of the multiplexer readout interval, the CTIA is not reset, which results in the next IFOV time having an increase in charge. The result is a stair-step output. SBRC currently plans to record 25 steps in increments of 4% of full scale. These would be inserted into data packets

taken in the Solar Diffuser data sector at times when the Solar Diffuser door is closed. The offset and size of the steps are adjustable if finer resolution is needed.

The signal for the photoconductive detectors (PC) 31-36 is read out directly by the off-focal plane electronics (no CTIA) and then travels a similar path to the PV's. As a result, it is not possible to disconnect the detectors from the following electronics. SBRC's solution is to inject charge in addition to the detector output. This is done only when looking at the Space View, in order to use the full range of the electronic calibration. The lower number of available data frames restrict the electronic calibration to 10 steps (10%) increments. The offset is adjustable, which would allow finer resolution if needed.

Electronic Characterization in both cases consists of analyzing the counts out as a function of the charge inserted in order to establish the linearity of the electronics, and specifically the linearity of the A/D converters. This characterization will begin with a linearity test, such as the Coefficient of Determination calculation (a statistical test). If that test passes the A/D response will be taken to be linear; if it fails then further characterization of the non-linearity of the data will be conducted. Any change in A/D response on-orbit may require revision of the functional form of the calibration equation for the affected channel; such revision would be subject to Configuration Control Board review.

3.3.3 The Spectroradiometric Calibration Assembly (SRCA)

The SRCA has three distinct and mutually exclusive operating modes, each of which will be treated separately here.

3.3.3.1 SRCA Radiometric Mode

The SRCA Radiometric mode simulates the integrating sphere test performed on the ground and is used to provide radiometric calibration points for the VIS/NIR and SWIR bands. Since the Solar Diffuser can only be used once an orbit, the SRCA will provide a way to characterize intra-orbit variations in the calibration of the data. Of the SRCA modes, this one is the default mode, with the intention of keeping one 1 W bulb lit continuously.

Prior to launch, the SRCA radiance will be correlated with the full aperture ground based integrating sphere. The SRCA uses various combinations of the three 10 W and one 1 W lamps (with a backup of each) to provide the required radiances. The stability of these lamps is monitored by self-calibration diode (SCD) readings. If there is a change in the lamps, this change can be factored out using the SCD data. If the change is uniform across all wavelengths it can be handled as a single multiplier on the pre-launch lamp values. If it has spectral shape then that shape can be determined from the SRCA Spectral mode, and will be implemented as a band-dependent multiplicative constant on the pre-launch lamp values.

$L(\lambda)_{SRCA,\ Post\text{-}launch} = C(\lambda)\ L(\lambda)_{SRCA,\ Pre\text{-}launch}$

3.3.3.2 SRCA Geometric Mode

In the SRCA spatial characterization mode, an IR source and the SIS will be combined with a beamsplitter. Two spatial reticles in the exit plane of the monochromator will be scanned across the SRCA aperture. One reticle is used to characterize the along-track registration, the other to characterize across-track. For a given reticle position, the response of the detectors is recorded. By comparing this to pre-launch measurements, any shifts in registration can be characterized. This characterization will be included in the metadata.

Across-track band-to-band registration can be adjusted via ground command to bring any single band on one focal plane into registration with any single band on another focal plane to approximately 25 meters. This adjustment is accomplished by changing the detector read-out timing, and is therefore only available in the across-track direction.

3.3.3.3 SRCA Spectral Mode

The spectral response measurements for the VIS/NIR/SWIR regions as measured by the SRCA will be compared with the full aperture measurements taken before launch. These will allow the determination of the center wavelength to an accuracy of 1 nm with a precision of 0.5 nm. This will allow the characterization of any shift in the center wavelength of a band after launch.

3.3.4 Blackbody

The blackbody target provides a defined source of thermal radiation. As such, it is used to provide one of the two required calibration points for the thermal bands. Its radiance depends upon its geometry, surface emissivity, and temperature. The geometry and emissivity will be characterized prior to launch. The blackbody (BB) has 12 temperature sensors embedded in it. Using these values, the mean temperature, <T>, observed by an will be calculated each scan by a thermal model provided by SBRC. Given the mean temperature, the radiance from the Black Body (BB) for a frame of data is then given by:

$$L_{BB}(\lambda) = \varepsilon(\lambda) c_1\ \pi^{-1}\lambda^{-5}[\exp(c_2/\ \lambda\langle T\rangle) - 1]^{-1}$$

with constants:

$c_1 = 3.74 \times 10^4$ W-cm-2-um 4

$c_2 = 1.44 \times 10^4$ um-K

The Black Body radiance value used for the scan is the average of the 30 frames of Black Body data:

$$\langle L_{BB}(\lambda)\rangle = \frac{1}{30}\sum_{i=1}^{30} L_{BB}(\lambda)_i$$

3.3.5 Space Viewport

The Space Viewport (SV) provides a radiance source that is nominally zero and is observed every scan. As such, it has several uses on orbit. The Space View provides an opportunity for passive lunar characterization (see Lunar View Processing, below). Electronic Calibration of the PC bands (31-36) is done while viewing it (see 3.3.1.3) and image ghosting can be characterized by looking at the edge of the port. Most importantly, it provides one of the points necessary for deriving calibration coefficients for all bands. This last function requires both that the moon is not in the viewport and that electronic calibration is not being conducted.

3.3.6 Earth Scan Characterization/Calibration Data

For those earth-scans devoted to looking at the moon, at free space, or at the dark earth in the reflective bands, the data are more logically viewed as characterization/calibration data than as image data and are therefore treated here.

3.3.6.1 Lunar View Characterization

The Moon offers a stable, solar-based source for calibration. The Moon has several unique properties: it is within the dynamic range of most imaging instruments, it is surrounded by a black field in both the reflective and emissive bands, and its surface brightness distribution can be well known. Although the moon's photometric properties are thought to be intrinsically constant over long time scales (natural rate of change estimated at 10^{-9} percent per year [Kieffer, 1985]), the effects due to the variation of illumination conditions and observation geometry must be considered. These in turn are related primarily to the lunar photometric function and the lunar libration. There will be two types of Lunar observations, those taken when the moon is in the Space Viewport (passive lunar looks) and those when the spacecraft is positioned to look at the moon (active lunar looks). The lunar processing algorithm will be the same in either case. However, the accuracy of the results will be greater for the active lunar looks both because the active looks will be chosen to view a full moon and because they will provide more frames of data for analysis.

Lunar processing will begin by predicting the position of the moon with respect to MODIS. When data from the predicted event is available, the presence and position of the moon will be verified, and any difference between the predicted and actual position of the moon will be used to update the prediction generation routine.

A table of expected radiances is generated based on the lunar profile, that is, what features of the moon are visible from MODIS at the time of the observation, the brightness and the viewing angle. These radiances are then mapped onto the MODIS focal planes to predict the detector-specific at-aperature radiance, $L(\lambda)$, necessary for calibration.

3.3.6.2 Noise Characterization

While known systematic noise which has been approved for reduction was addressed in the pre-processing stage, it is still of interest to characterize the residual noise, and to distinguish between random noise and residual systematic noise. Random noise cannot be removed, but its characterization is important to validation of the calibration. Systematic noise which is detected at this step is a candidate for future approval for reduction in the pre-processing.

Systematic noise detection on-orbit will involve characterization of both dark image data and OBC data. Fourier transforms of dark image data will probably be the basis of systematic noise detection. Taking dark image data in the reflective bands, instead of relying solely on the dark data from the Space View, is important to give the Fourier transform routine enough consecutive data to detect various frequencies of noise and minimize aliasing. Some dark data will be available every orbit for the reflective bands, provided the MODIS day/night modes are triggered according to the following two-orbit cyclic pattern:

> Begin day $mode_1$ at point 1 (see Figure 3.3-1) which is 5% of the orbit before crossing the terminator into daylight, i.e., spend 5% of the orbit taking dark data in the day mode.
>
> End day $mode_1$ and begin night $mode_1$ at point 2, which is 5% of the orbit before crossing the terminator into darkness.
>
> End night $mode_1$ and begin day $mode_2$ at point 3, which is 5% of the orbit into daylight.
>
> End day $mode_2$ and begin night $mode_2$ at point 4, which is 5% of the orbit into darkness
>
> End night $mode_2$ and begin day $mode_1$ of the next 2 orbit cycle at point 1.

This operational pattern preserves the 50% day mode/50% night mode split on average, and therefore does not affect the overall data rate. It should not affect MODIS global coverage since the daylight data lost will be over the poles where successive orbits provide largely overlapping data. Systematic noise present in the dark data from both orbits 1 and 3 is probably present at all points in-between and is a candidate for removal.

Noise in all bands (reflective and emissive) can be characterized by analysis of those frames of data during the active lunar look which do not contain the moon and are therefore frames of empty space. The advantage of these over the Space View is the much larger number available in active lunar look mode.

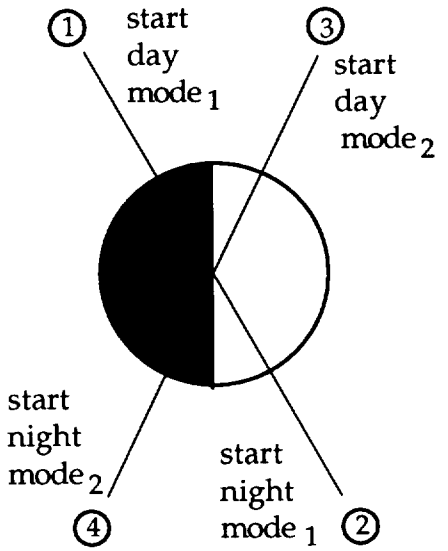

Figure 3.3-1 Day/Night Mode Two-Orbit Cycle

3.3.7 Calculation of Radiometric Calibration Coefficients in the Reflective Bands

For each reflective detector, use the most recent values for the Solar Diffuser, the SRCA in Radiometric Mode, the lunar view and the Space View, each weighted appropriately according to its radiometric accuracy, to curve-fit a curve of the same functional form as the calibration curve determined for that detector pre-launch. The result will be a parameterized curve, with error estimates on the parameters. The parameters are the OBC/Lunar-derived radiometric calibration coefficients in the reflective bands.

3.3.8 Calculation of Radiometric Calibration Coefficients in the Emissive Bands

For each emissive detector, use the most recent values from the Blackbody and the Space View to parameterize a line; the slope and intercept of that line are the OBC calibration coefficients.

3.4 Compare OBC/Lunar coefficients to Projected Coefficients; choose the best coefficients on a channel-by-channel basis for each scan.

Each channel will be calibrated individually for each scan. Compare the values of the OBC/Lunar coefficients with the Projected Coefficients which were generated the previous orbit. If the average value and the entire (2σ) error bars of the projected coefficients are within the (2σ) error bars of the OBC/Lunar coefficients then accept the projected coefficients for that channel and scan. Otherwise, accept the OBC/Lunar coefficients. In either case, document the choice, and the 'losing' coefficients, in the metadata.

3.5 Calibration: apply the best calibration coefficients to the data.

The functional form of the calibration equation for a given detector channel is assumed constant and determined pre-launch. The coefficients for use in that equation are determined by the processing discussed in section 3.4 above. Actual application of the coefficients is a linear or polynomial function evaluation. The general high order case is:

$$Q_{Cal} = C_0 + C_1 Q + C_2 Q^2 + \ldots$$

The calibration step is the application of the calibration equation with the chosen coefficients to the data. The result is Level-1B data. For convenience of computer processing, the proposed algorithm leaves the calibrated data in integer format, i.e., it provides a 16-bit integer, Q_{Cal}, which is linearly related to L (a 32-bit real number). The conversation table to transform from Q_{Cal} to L (or back) will be supplied. For further discussion, see Appendix D.

3.6 Generate Utility Masks

The Utility Mask (Standard Product MOD18) will consist of three masks, registered to all 36 bands of Level-1 and Level-2 imagery. There will be one mask for the 250 m bands, one for the 500 m bands, and one for the 1000 m bands. Each pixel's mask will be 64 bits wide. Some bits will represent binary masks, i.e., a '1' means the condition is true and a '0' means it is false, while others will be grouped into 3-bit (8 level) fractional masks to represent the estimated level of a class present in the pixel. Binary masks will be used for classes such as dead detector (yes/no), glint (present/absent), definitely opaque cloud, definitely not opaque cloud, spectral outlier, spatial center/edge, and day/night terminator line. Fractional masks will be used for classes such as water, land, snow, cloud, and cloud shadow. There will be different discipline-dependent masks for some of theses classes and there will be different algorithms for daytime and nighttime imagery. Each mask will also contain information on the last cloud-free classification of the pixel.

3.6.1 Dead/Failing Detector Elements

The MODIS Specification (Goddard Space Flight Center, 1993) allows up to two dead detector elements per focal plane, with not more than one dead detector per spectral

band. To support those members of the user community to whom the exact data from the missing channel is not critical, MODIS characterization processing will provide an approximation to the missing data based on a weighted average of the surrounding pixels. The Dead Detector bit of the Utility Mask will indicate whether a given detector channel is dead or not. Those products which do not require the approximated data can ignore it by masking it out. There will also be a Noisy/Failing Detector Mask because the uncertainty in the calibration of such channels will be higher than that for other channels in the same band, which may affect the error estimates on any Level-2 or higher products produced from their data. Quantitative estimates of the calibration uncertainty for each channel will be in the metadata.

3.6.2 Classification Masking Algorithm Basis Overview

The classification mask is still in the early stages of development and no specific algorithm has been chosen. Accurate, automated image classification is still a challenging problem. Rather than engage in basic research in this area, MCST has begun by developing a classification mask evaluation tool which we will use to evaluate the results of published techniques. There are a variety of promising new classification techniques such as texture mapping, neural network classifiers, and wavelet transforms which may complement older techniques such as thresholding.

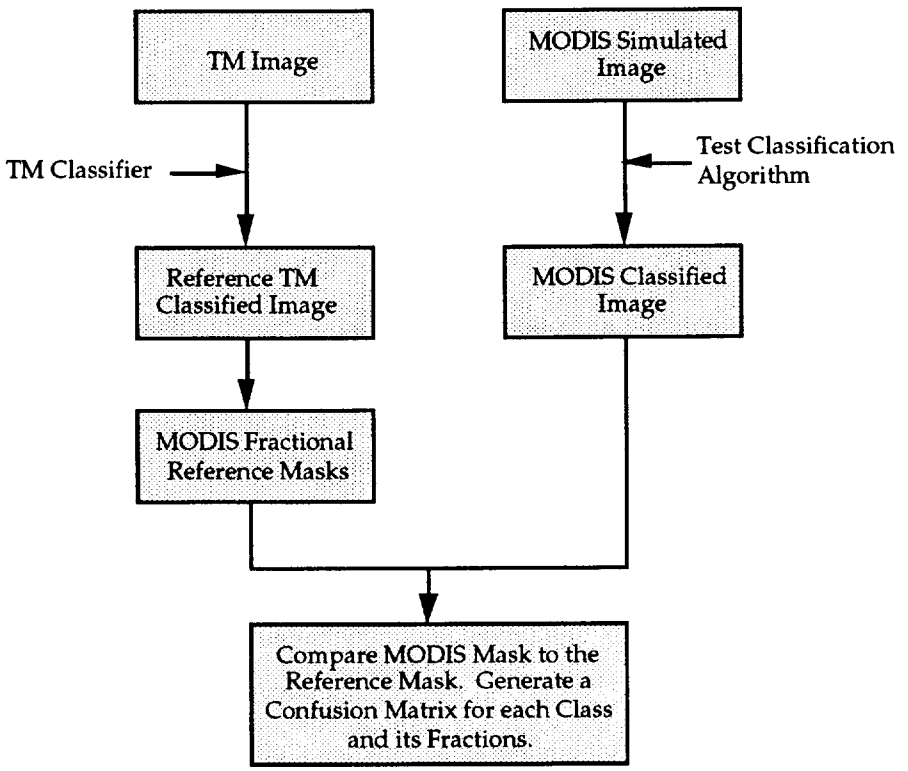

Figure 3.6-1 Masking Algorithm Evaluation Tool

MCST will use the mask evaluation tools to investigate existing algorithms. Many classification techniques work well on a limited set of scene types; the tool will allow MCST to identify a given techniques' strengths and weaknesses. The final Utility Mask algorithm may automatically choose among several classifiers depending on scene type. In addition, classification becomes more tractable when an *a priori* classification of a pixel, based either on map data or on previous classifications, is used to influence the classification probabilities for the pixel's current classification. MCST will therefore use a database of previous cloud-free classifications to aid in masking.

A schematic of the Classification Mask Evaluation Tool is shown in figure 3.6-1. The tool begins with a reference image from another sensor of relatively high resolution. MCST uses TM data since TM has 30 m resolution and TM bands 1-7 roughly correspond to MODIS bands 1-4, 6-7, and 31.

The TM image is classified using the maximum likelihood classification methodology; this classification is taken to be "truth". The tool's sensitivity to TM classification method is currently being evaluated. Then, for each possible class, a mask is created at the MODIS pixel size which gives the fraction of the MODIS-sized pixel occupied by that class. So, if a MODIS pixel is 8 x 8 (=64) TM pixels, and 16 of those TM pixels are classified as water, the MODIS water fractional reference mask pixel would have a value of 16. These fractional reference masks give the 'actual' class composition of a MODIS pixel.

The original TM image is also transformed into a simulated MODIS image (Barker, et al, 1992). This MODIS image is then classified using whatever classification algorithm is being evaluated. The resulting classified image is compared to the MODIS fractional reference masks generated above. A confusion matrix for each class allows quantitative evaluation of the classification effectiveness. Because many classification techniques are useful in some scene types but not on others, MCST is in the process of building a library of different TM reference scene types for mask evaluation. An example of a classified/reference comparison and its confusion matrix is shown in Figure 3.6-2.

3.7 Image-Derived Characterization, Including Calculation of Potential Calibration Coefficients

The MODIS image data will contain information about instrument performance; extracting and validating that information will allow evaluation of the calibration and, potentially, improvement of it.

There are two broad classes of image-derived characterization techniques, those which utilize all the image data and those which use only a subset. The first type are techniques which use statistical analysis of the data to characterize (and potentially compensate for) instrument performance artifacts such as channel-to-channel within-band striping. The second type use scene-specific information to characterize

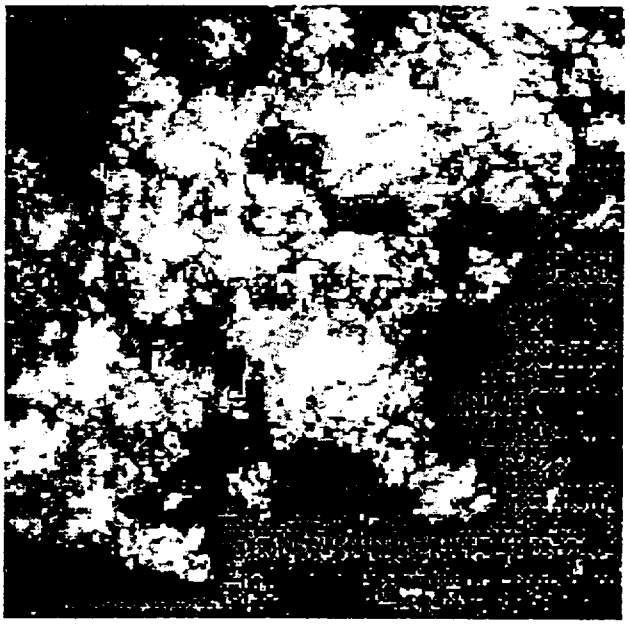

Segmented Bahama Cloud

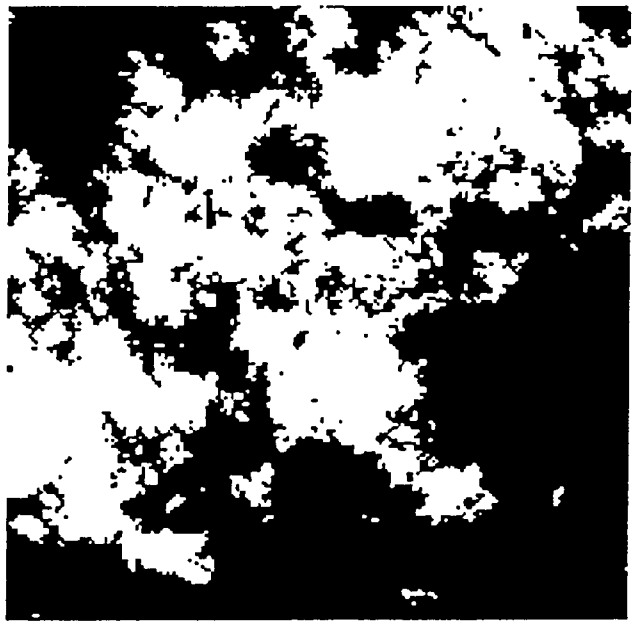

Reference Bahama Cloud Mask

Image Segmentation of TM2

Feature vector size = 1

The number of clusters = 10

% of cloud correctly classified 99.1428

Confusion Matrix

0	0	1
1	55006	0
2	56131	335
3	7274	9210
4	638	12541
5	261	10193
6	245	11249
7	19	11961
8	1	9565
9	0	9276
10	0	8595

Figure 3.6-2 Sample Output From Classification Mask Evaluation Tool

instrument performance. Several illustrative examples of image-derived techniques follow.

3.7.1 Histogram Equalization

Historically, most images from sensors having multiple detectors for each band have demonstrated striping. This is due to slight variations in the detector signal caused by noise. One bit striping may occur even when the detector variations are within the range allowed by the MODIS specification (Goddard Space Flight Center,

The basis for the correction of striping is the observation that, although each detector in a scan sees a different area in any specific scene, over a sufficiently large region each detector will encounter the same distribution of radiances. Therefore, the probability density functions for each detector output can be considered equal. The histograms of observed radiance levels for the large sample should then be equal for two detector channels with identical characteristics. Thus, dissimilar histograms indicate unequal detector channel responses and histogram equalization can be employed to remove or reduce striping. The roughly factor of 2 growth in pixel size as view angle varies from nadir to 55° leads to a 'bowtie' effect at the edges of the scans shown schematically in Figure 3.7-1.

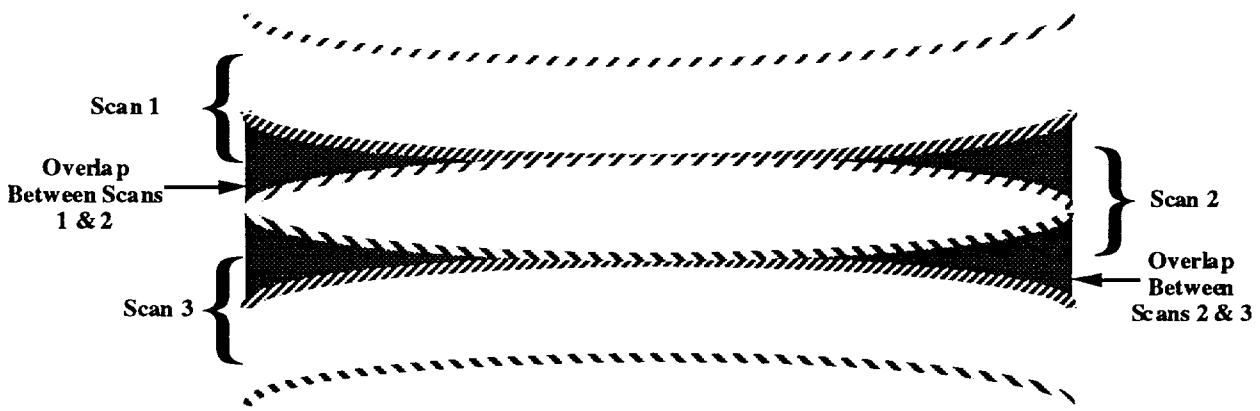

Figure 3.7-1 Schematic of Overlap in MODIS Scans

The result is that approximately 45% of the MODIS pixels overlap. This overlap supports the assumption that the MODIS detectors, on average, see the same distribution of radiances.

The general approach to histogram equalization uses the cumulative probability-distribution function by creating a look-up table which has the normalized total of all pixels having that radiance or less in each bin. Historically, a linear two-parameter approximation has been used for this on the Landsat MSS and TM ground processing systems.

There are two standard methods for two-parameter destriping:

Method 1-Normalization with respect to one channel
In this method, one channel is designated and all the histograms of the other channels are modified so that they match the designated channel's histogram. This is achieved by means of an inversion function represented by a look-up table. This method has been used for MSS imagery (Irons, 1983), and GOES imagery (Weinreb, 1989).

Method 2-Relative normalization

All channel biases and gains are averaged by an iterative process: The bias and the gain are modified by the means and the standard deviations of the raw data. Two iterations are required. This method has been used for TM imagery (Irons, 1983) and is the one chosen for MODIS destriping.

Between-Band Normalization

The basis of between-band normalization is analogous to the within-band histogram discussed above, in that small errors in calibration can be detected using a large relative reference sample (i.e., scene histogram) that is not observed and removed by the primary absolute calibration reference. For the within-band case, the reflectance distribution from a large sample will be invariant from detector channel to detector channel, i.e., scan-line to scan-line. For the between-band case, no simple relationship exists because the bands view different spectral regions; however, spectral correlation can be observed and exploited in certain cases. Three sources of coherent spectral information are available on MODIS:

1. Highly (100%) correlated scene samples
2. Solar Diffuser data
3. SRCA lamp data

The Solar Diffuser source is exploited in the current algorithm. Samples from each of the reflective bands are curve-fit to a solar spectral irradiance curve. A least squares fit produces error bands for a chosen level of confidence. Each band will be analyzed for its fit to the model and gain and bias adjustments derived similarly to the within-band case. This operation is intended to provide greater band-to-band consistency than what can be obtained with absolute calibration alone.

3.7.2 Automated Calibration-Site-Based Radiometric Rectification by Relative Multiband Normalization

A technique referred to as radiometric rectification has been included in the suite of MODIS calibration capabilities since it offers a means of normalizing the data from the same or multiple sensors without use of calibration sources or instrumented scene sites. The method is described by Hall, et. al. (1991) and is based on an earlier article by Hall and Badhwar (1987). The technique can normalize multiple acquisitions at the same time and over time if the reference sites are invariant over the time scales of EOS/MODIS. The method can also be used to cross normalize other EOS instruments with the six MODIS instruments.

The method has two key elements:

1. Control Set Selection:

The radiometric control sites must have nearly constant reflectance over time. Factors such as precipitation, weathering, vegetation growth on initially non-

vegetated surfaces, or for water glint and changes in sediment level introduce error in the method. The rectification algorithm uses the KT greenness-brightness (Kauth and Thomas, 1976) transformation to identify non-vegetated pixels suitable for reference. These tests will result in 2000 or more sites being defined over the Earth which will be used routinely for rectification

2. Rectification Transformation Generation:

The method adjusts the band-by-band average digital counts of the multiple sensor data sets based on the a selected reference. A set of linear transformations is generated using means derived from dark and light pixels selected from the control sites in all data sets. Solution of the equations relating the means of the reference and to-be-adjusted data sets results in the coefficients for the transformations. The transformation and the coefficients are given as:

$T_i(x_i) = m_i x_i + b_i$, i=1...n (band index)

$m_i = (BR_i - DR_i)/(BS_i - DS_i)$

$b_i = (DR_i\ BS_i - DS_i\ BR_i)/(BS_i - DS_i)$

The T represents the transformation of the to-be-adjusted (subject) image data to the reference and the x_i is the subject data value for band i. The coefficients are m_i and b_i and are given as functions of the dark, D, and bright, B, counts for the reference and subject images.

Results by Hall indicate normalization accuracies of 1% for the visible and near infrared bands from TM. Performance was not as good for the mid-infrared bands. The method is considered experimental and will be pursued as a means of normalizing all the EOS data to enable inter comparison at an accuracy level significantly greater than that achievable for absolute calibration.

3.7.3 Modulation Transfer Function (MTF) Correction

MTF effects are not a noise source, but are treated here in the context of normalization and correction. The effect of the overall MODIS system MTF on the observed scene radiance is to blur radiance from scanned surrounding pixels into the central pixel. The MTF describes the transfer of signal through the sensor system as a function of spatial frequency. The point spread function describes the distribution of energy on the focal plane and is the inverse Fourier transform of the MTF.

The basis for MTF correction is the inverse filter which compensates for the high frequency attenuation effect of the MTF. This process in effect boosts the high frequency gain of the sensor. Many mathematical and physical problems arise when

compensation is attempted and extensive research has been conducted on this subject. A solution due to Riemer (1977) is applied to the MODIS case. The realization of the restriction filter is a 7 x 7 (Riemer) hence which is convolved with each band of the MODIS data stream. The resulting characterization of the MTF effect on each pixel is stored as metadata. If desired, it could be used to invert the MTF effect.

3.7.4 Calculation of Potential Calibration Coefficients

Any of the image-derived characterization methodologies which generate Q, $L(\lambda)$ pairs are candidates for use in checking the calibration. The weighted Q, $L(\lambda)$ pairs will be combined just as the various OBC sources were, i.e., used as the basis for a regression fit to the calibration function for a given band, with the suggested calibration coefficients being the regression coefficients. Image-derived calibration coefficients and noise characterizations will be included in the metadata; in addition, if the coefficients can be used to improve the calibration then they may be applied. If applied, then the utility masks may need to be updated and the image-derived characterizations done again. In order to avoid an endless loop through this process, it is arbitrarily truncated with two passes through the masking.

3.8 Generate Quality Assurance Metadata

Metadata includes all data about the data which is stored. The results of all characterizations done throughout the processing are stored as metadata.

In addition, quality assurance characterizations are done on the final, calibrated data. Quantitative estimates of the calibration uncertainty for each channel will be in the metadata. Illustrative types of A.A metadata are discussed below.

Means and variances for all calibration sources will be obtained from the characterization process and standard statistical tests will be applied to determine if the means and/or variances have undergone significant change. Any such change would imply that MCST should re-evaluate the accuracy of that calibration source.

Trend analysis will also be done as part of the metadata generation process: tracking the change of channel calibration values provides information on detector/channel health and expected life. All parameters which were trended in the course of characterization processing will be analyzed for Outliers, which would indicate a potential significant change in instrument behavior. Also, all residuals calculated during curve fitting will be analyzed for randomness; non-random residuals indicate a possible lack of congruence between the data and the function form to which the data were fit. This would, for example, suggest that the functional form of a channel's calibration equation may need to be updated.

3.9 Project Calibration Coefficients for the next orbit

Use trending techniques on all data up to & including this orbit, and any available Vicarious calibration information, to project a complete set (including orbit location dependence) of calibration coefficients for each channel for the next orbit. The equations to implement the weighted combination of these information sources have not yet been determined.

3.10 Level-1 Algorithm Detailed Control Flow Diagram, with Illustrative Equations

The following figures, 3.10-1 through 3.10-8 depict the Level-1 Algorithm Control Flow.

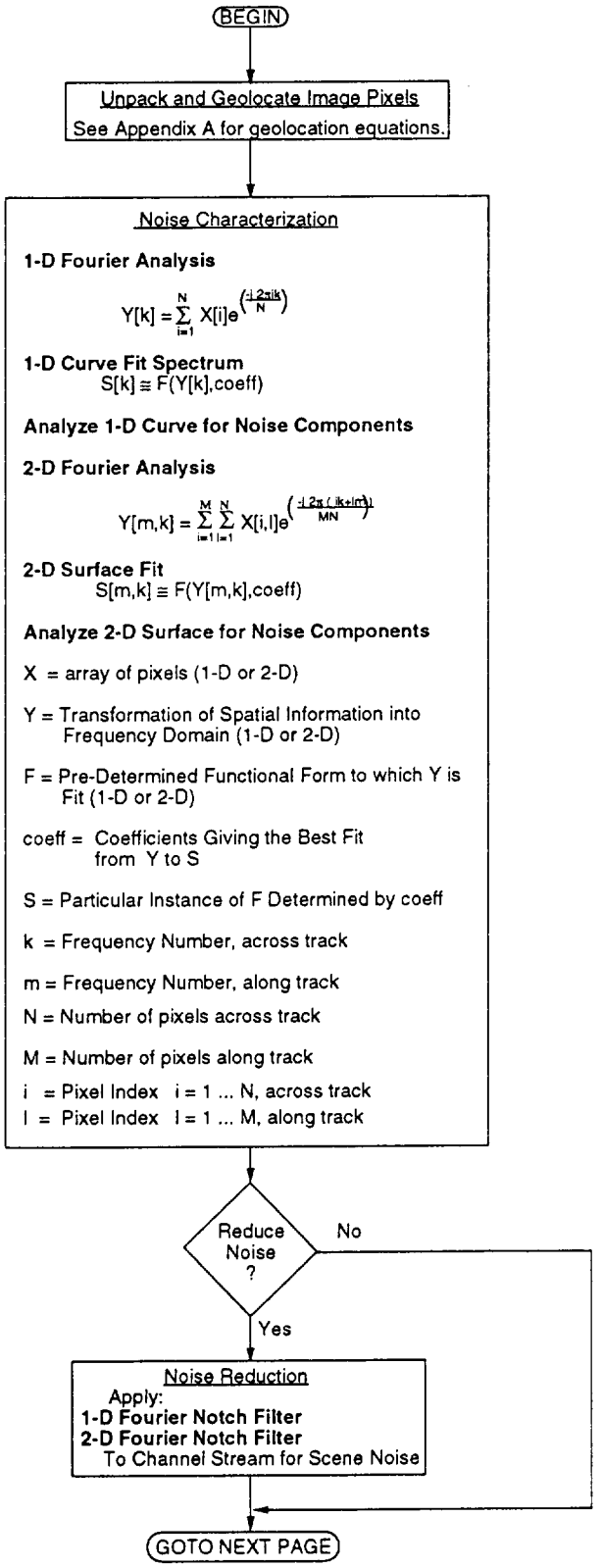

Figure 3.10-1. Level-1 Algorithm Detailed Control Flow Diagram

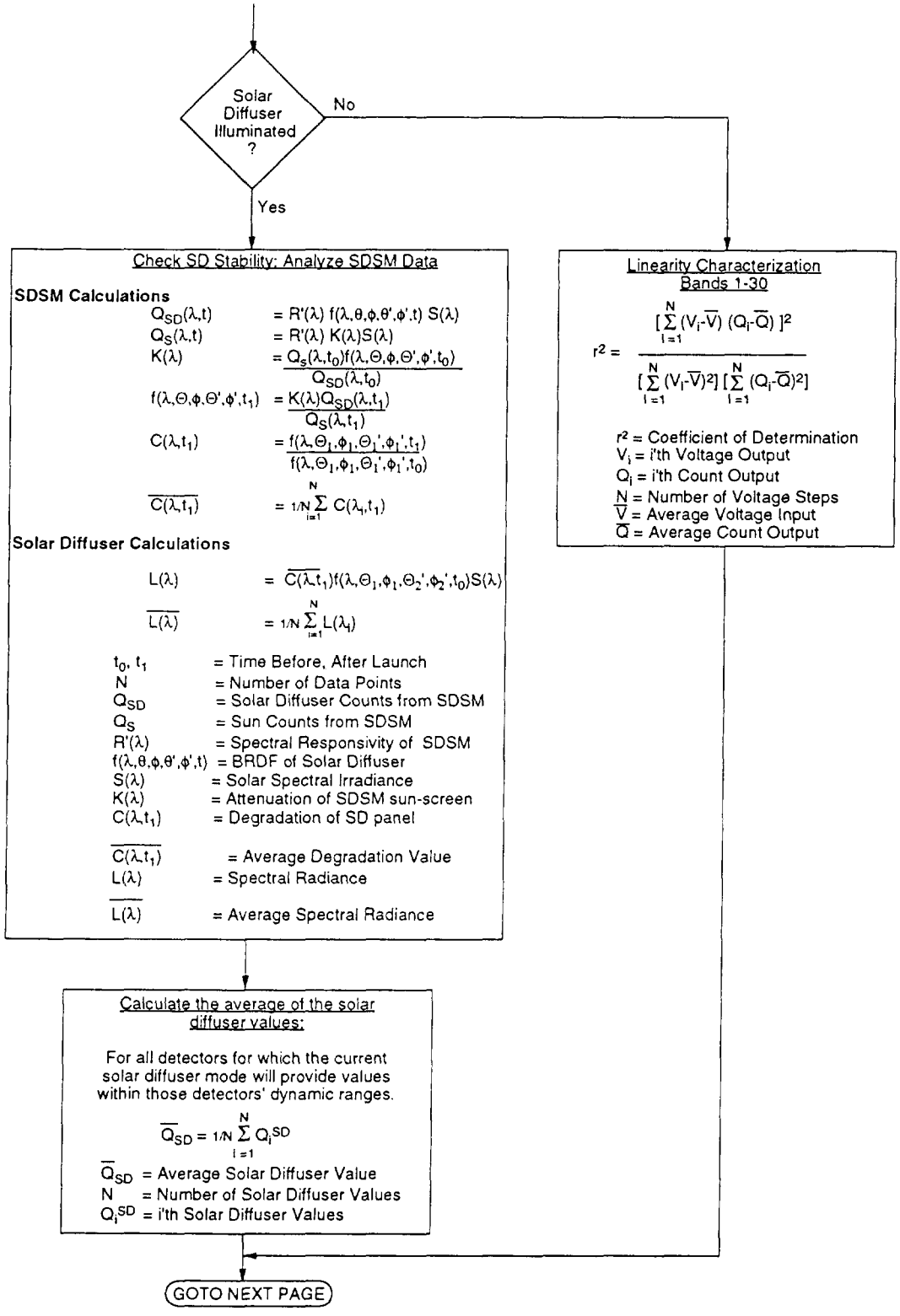

Figure 3.10-2. Level-1 Algorithm Detailed Control Flow Diagram (cont.)

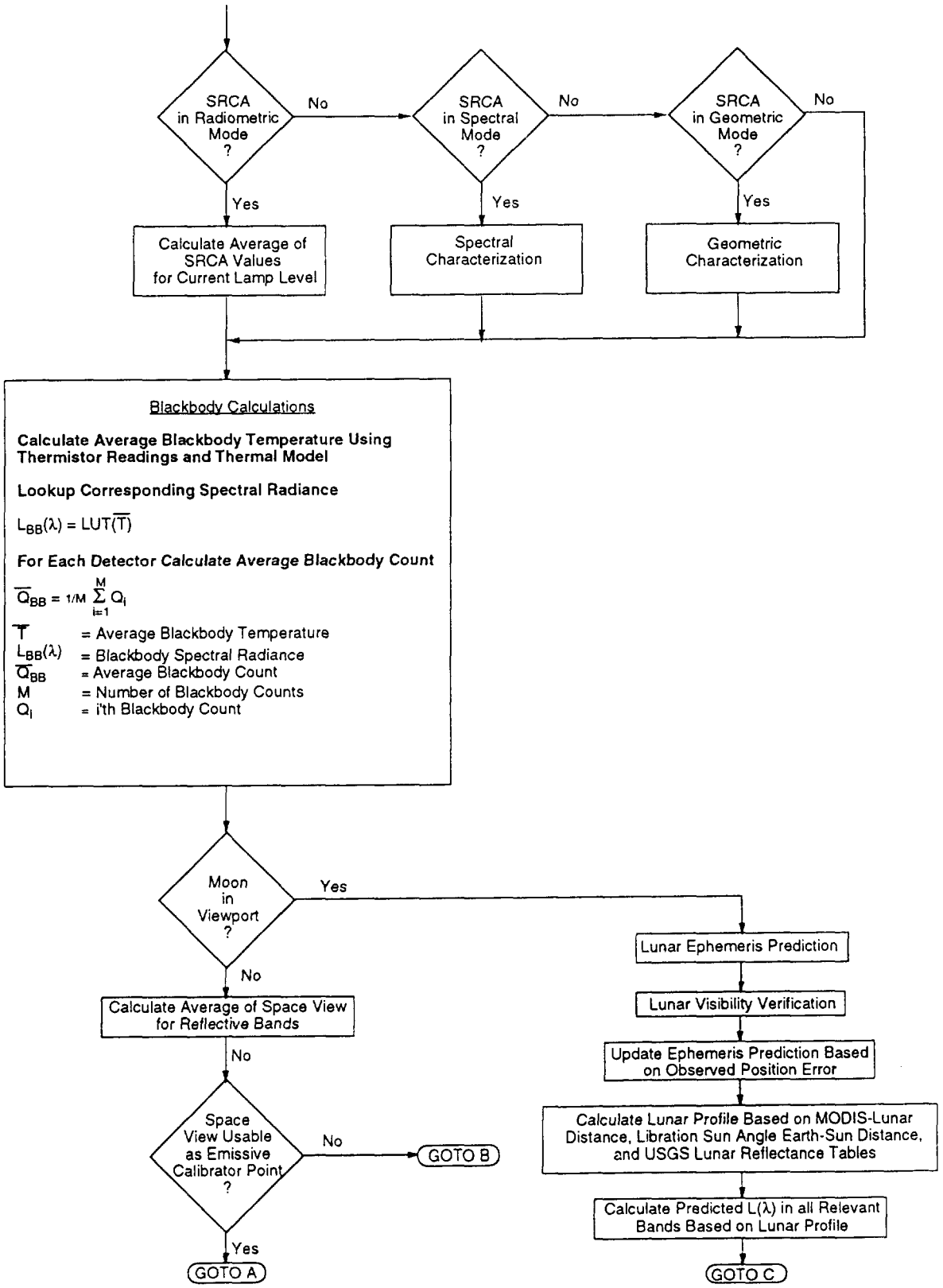

Figure 3.10-3. Level-1 Algorithm Detailed Control Flow Diagram (cont.)

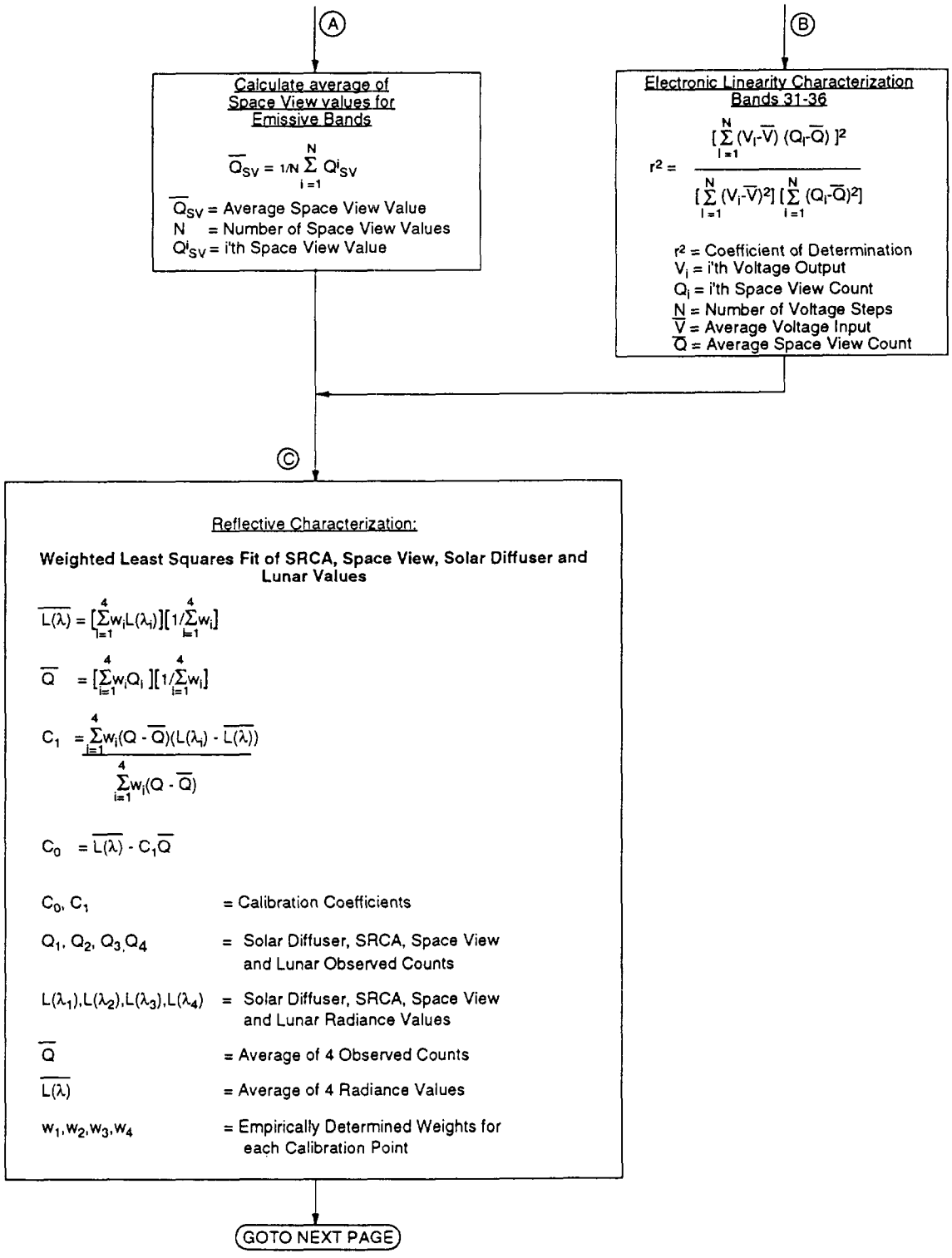

Figure 3.10-4. Level-1 Algorithm Detailed Control Flow Diagram (cont.)

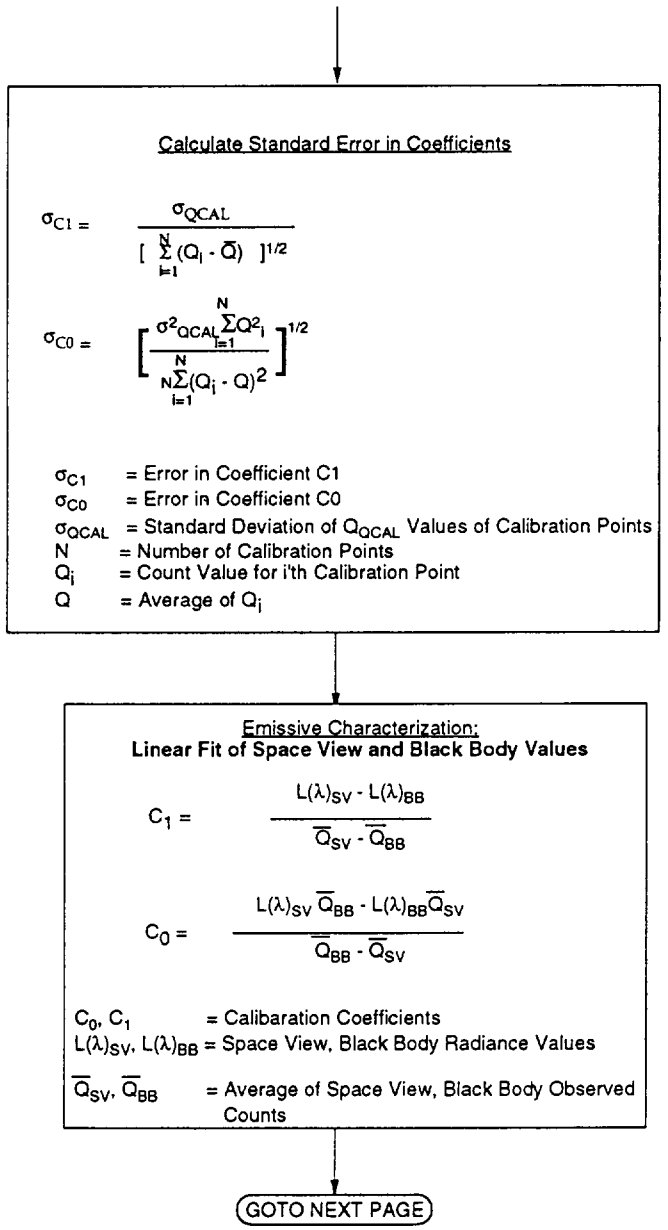

Figure 3.10-5. Level-1 Algorithm Detailed Control Flow Diagram (cont.)

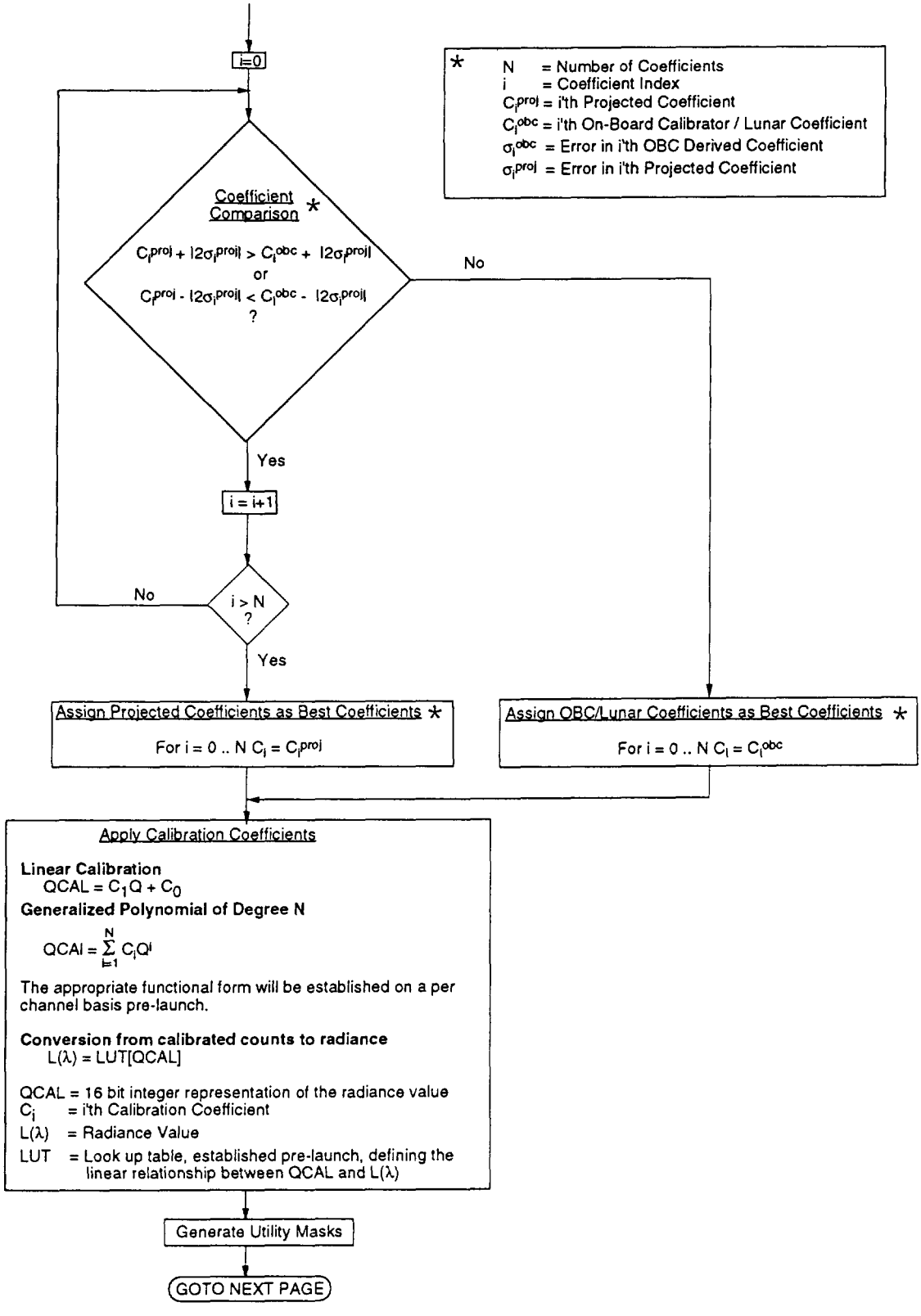

Figure 3.10-6. Level-1 Algorithm Detailed Control Flow Diagram (cont.)

<u>Image Derived Characterization:</u>
Example : Histogram Equalization (Irons, 1982)
(Performed on a Band-by-Band Basis)

Compute Average and Standard Deviation for Each Channel

$$\overline{X}^i_\alpha = 1/N \sum_{j=1}^{N} X^i_j$$

$$\sigma^i_\alpha = \sqrt{1/N \sum_{j=1}^{N} (X^i_j - \overline{X}^i_\alpha)^2}$$

Compute Adjusted Average and Standard Deviation for Each Channel

$$\overline{X}^i_{\alpha+1} = (\overline{X}^i_\alpha - C0^i_\alpha) / C1^i_\alpha$$

$$\sigma^i_{\alpha+1} = \sigma^i_\alpha / C1^i_\alpha$$

Average Adjusted Values for All Channels in Band

$$\overline{X}_{\alpha+1} = 1/M \sum_{i=1}^{M} \overline{X}^i_{\alpha+1}$$

$$\overline{\sigma}_{\alpha+1} = 1/M \sum_{i=1}^{M} \sigma^i_{\alpha+1}$$

Compute Adjusted Calibration Coefficients

$$C1^i_{\alpha+1} = C1^i_\alpha \sigma^i_{\alpha+1} / \overline{\sigma}_{\alpha+1}$$

$$C0^i_{\alpha+1} = C0^i_\alpha + C1^i_\alpha (\overline{X}^i_\alpha - (\sigma_{\alpha+1} \overline{X}_{\alpha+1} / \sigma^i_{\alpha+1}))$$

This process may be iterated by setting X^i_α to $X^i_{\alpha+1}$ and σ^i_α to $\sigma^i_{\alpha+1}$ and repeating the calculations, if iteration is found to produce further significant adjustments to C0 and C1.

$\overline{X}^i_\alpha$ = Average Value for Channel i

$\overline{\sigma}_\alpha$ = Standard Deviation of Values for Channel i

$\overline{X}^i_{\alpha+1}$ = Adjusted Average for Channel i

$\overline{\sigma}^i_{\alpha+1}$ = Adjusted Standard Deviation for Channel i

$\overline{X}_{\alpha+1}$ = Average of Adjusted Averages for All Channels in a Band

$\sigma_{\alpha+1}$ = Average of Adjusted Standard Deviations for All Channels in a Band

$C0^i_\alpha$, $C1^i_\alpha$ = Initial Calibration Coefficients for Channel i

$C0^i_{\alpha+1}$, $C1^i_{\alpha+1}$ = Adjusted Calibration Coefficients for Channel i

M = Number of Channels in Band

N = Number of Pixels in Scan

GOTO NEXT PAGE

Figure 3.10-7. Level-1 Algorithm Detailed Control Flow Diagram (cont.)

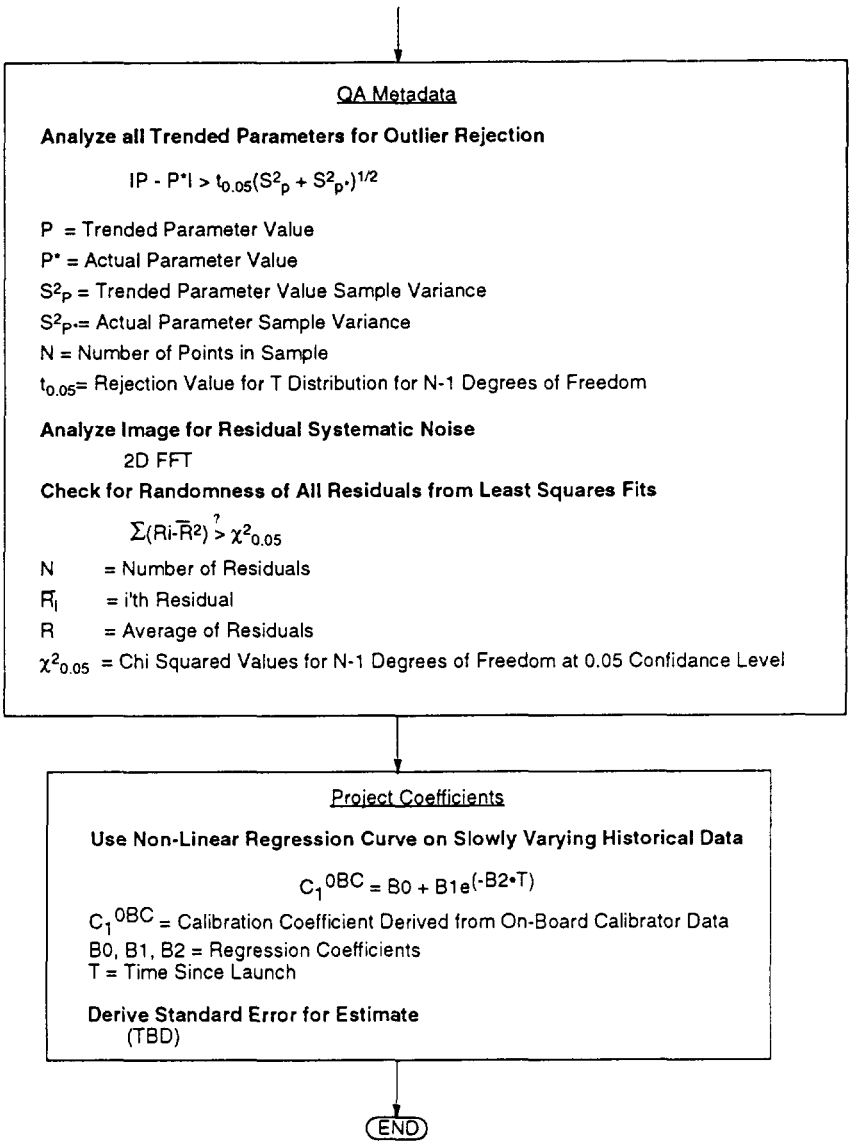

Figure 3.10-8. Level-1 Algorithm Detailed Control Flow Diagram (cont.)

Chapter 4

Error Budgets

An error budget for the characterization and calibration algorithm will accompany the final decisions on the specific numerical algorithms to be used to implement various sections of the algorithm. As the permissible error in calibration is given in the MODIS Instrument Specification (MODIS Spec., 1993), this section addresses the ability of SBRC to meet that calibration with their current error budgets.

SBRC is already conducting much of the analysis of the uncertainties in calibrating the instrument. As shown in Table 4.1, SBRC currently predicts that it will have little difficulty in meeting the accuracy requirements of the Specification.

Table 4.1
MODIS Calibration Requirements

Parameter	Phase C/D Requirement	Predicted	
		Preflight	On-Orbit
Radiometric Calibration			
Below 3000 nm	5%	4%	3%**
Above 3000 nm	1%	1%	1%**
Reflectance	2%	4%	2%
Spectral Band-to-Band Stability	0.5% FS 1.0% HS	0.5% FS 1.0% HS	0.5% FS
Spectral Characterization (Knowledge)			
Center Wavelength	0.5 nm preflight 1.0 nm on-orbit	0.5 nm	1.0 nm*
Geometric Characterization			
Band-to-Band Registration	0.2 (0.1) IFOV	0.1 IFOV	0.15 IFOV
Diffuser BRDF			
<2.0 µm	1.0%		
2.0 to 2.5 µm	1.5%		

FS = Full Scale HS = Half Scale

* Dependent on good correlation with full aperture ground measurement and SRCA subaperture measurements

** Multiple calibration methodologies are required

Radiometrically, the Specification (MODIS Spec., 1993) requires the Radiometric Math Model to determine absolute and relative calibration accuracies, assess instrument performance in terms of Signal to Noise Ratio (SNR) and Noise Equivalent differential Temperature (NEdT), and identify major error contributors. The results of Radiometric Math Model Version 22 are presented in Figures 4.1 through 4.3. These figures show the twelve main error sources as combined and budgeted by SBRC. Where possible, SBRC uses actual data instead of estimates. Figures 4.1 through 4.3 demonstrate that SBRC is confident that its uncertainties will be within requirements.

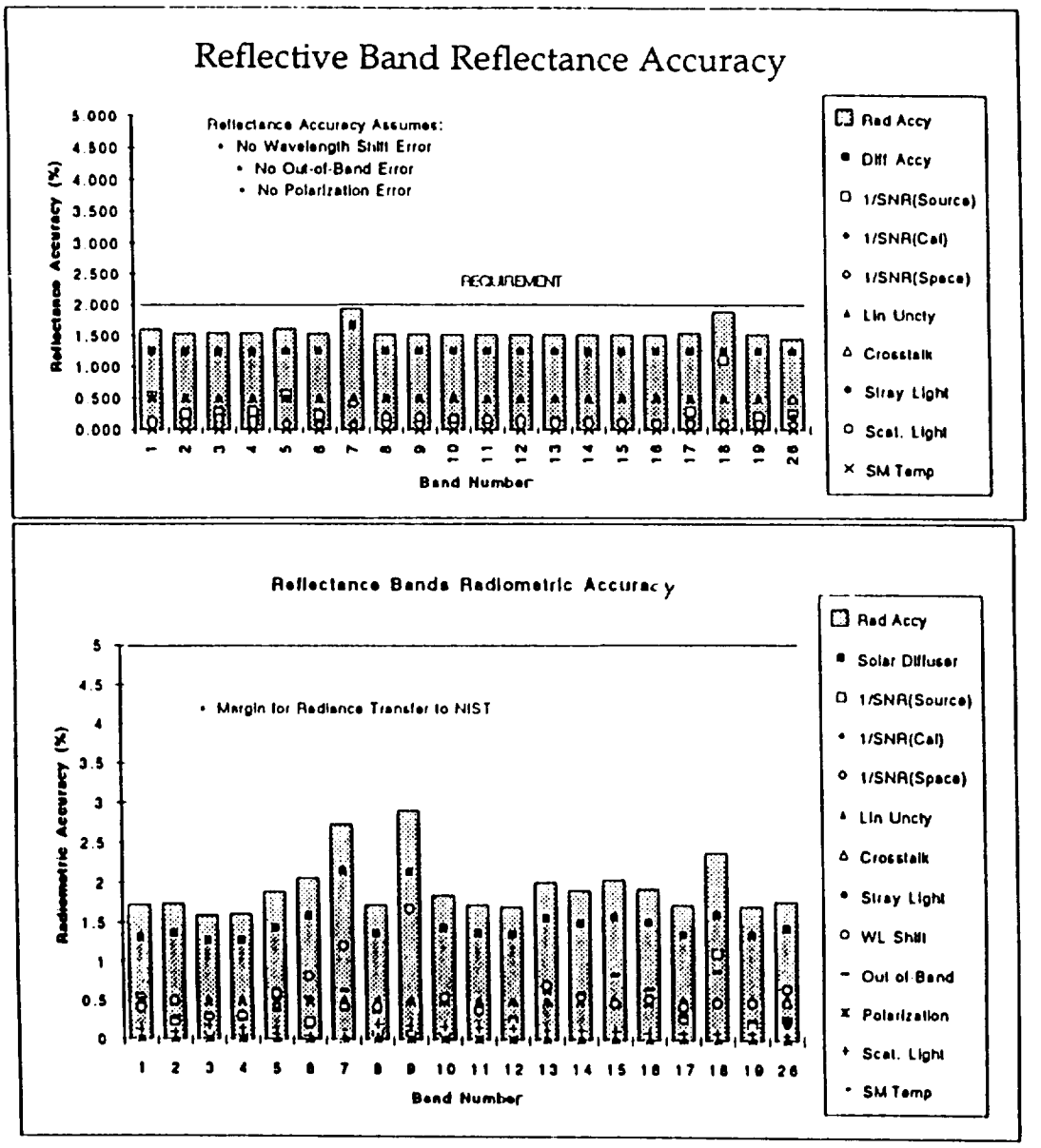

Figure 4.1. Radiometric and Reflectance Accuracies

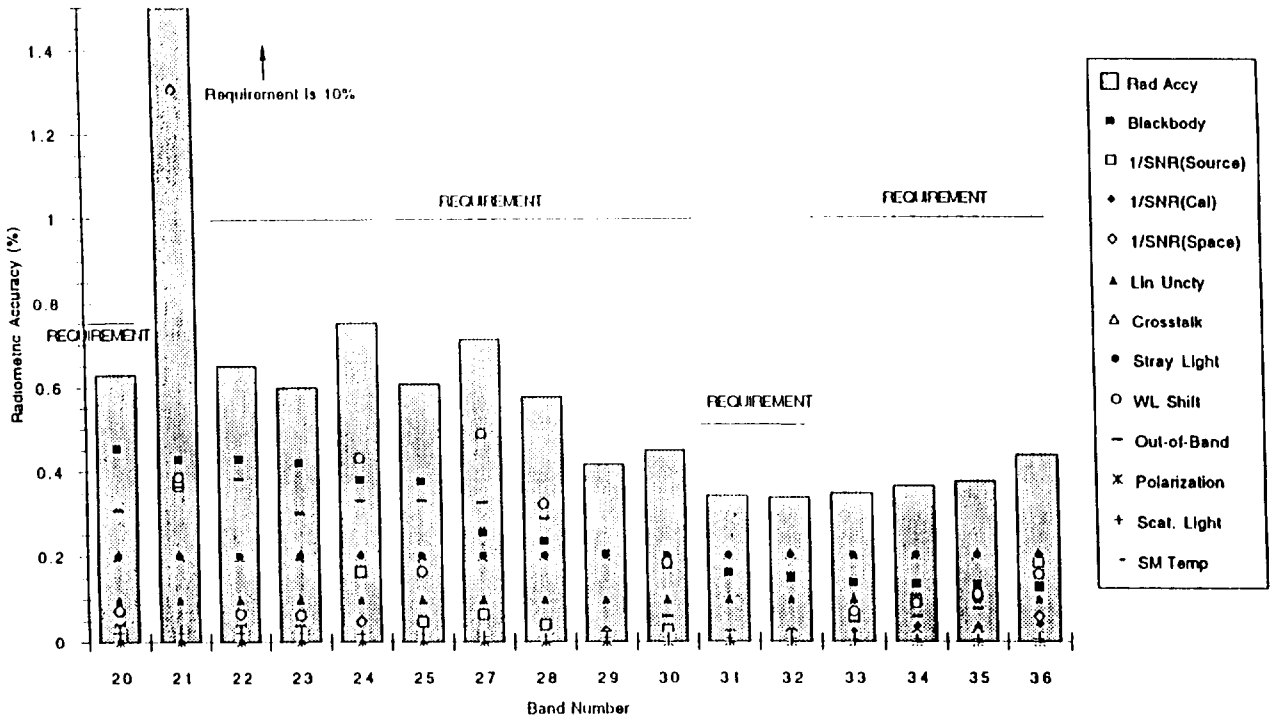

Figure 4.2. Emissive Bands Radiometric Accuracy

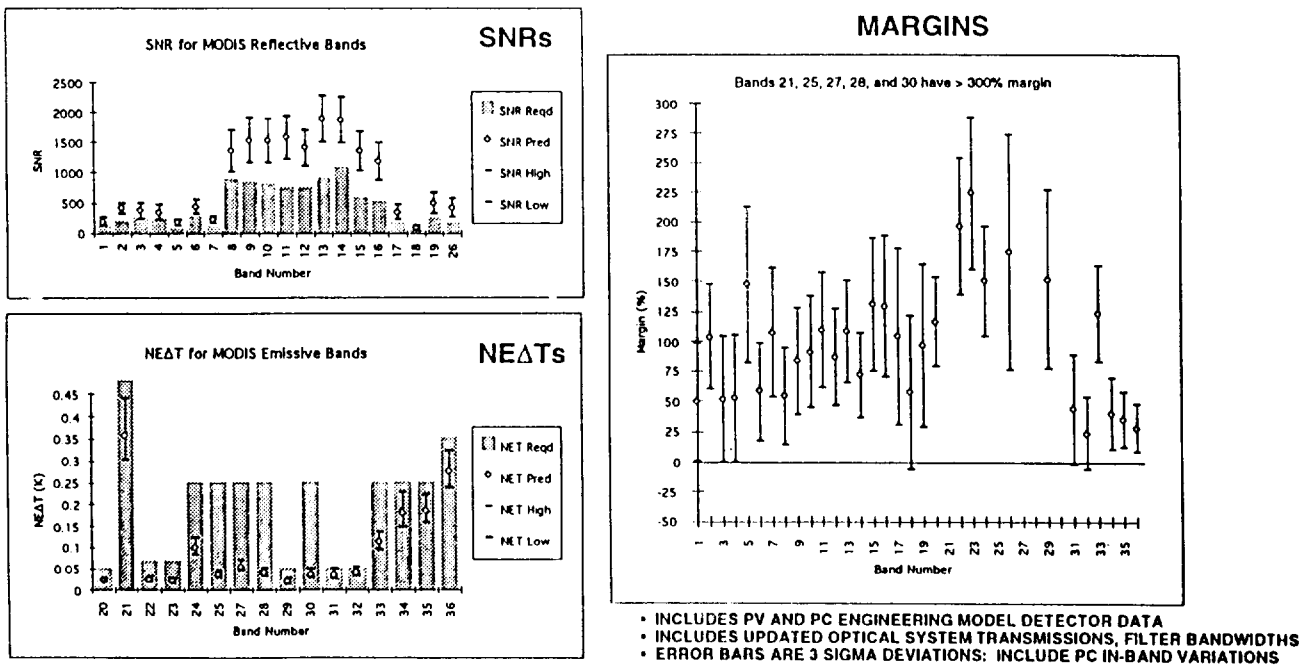

Figure 4.3. SNR, NEdL, and Error Margins

For geometric calibration, SBRC's error analysis is presented in Figures 4.4 and 4.5. Figure 4 includes 14 uncertainty contributors to the geometric coregistration and shows that SBRC expects to meet the 0.2 pixel requirement. Contributors to pointing accuracy are broken into two areas; static uncertainties which could eventually be corrected for, and dynamic uncertainties. Figure 4.5 shows this breakdown and indicates that SBRC is confident they will meet the requirements.

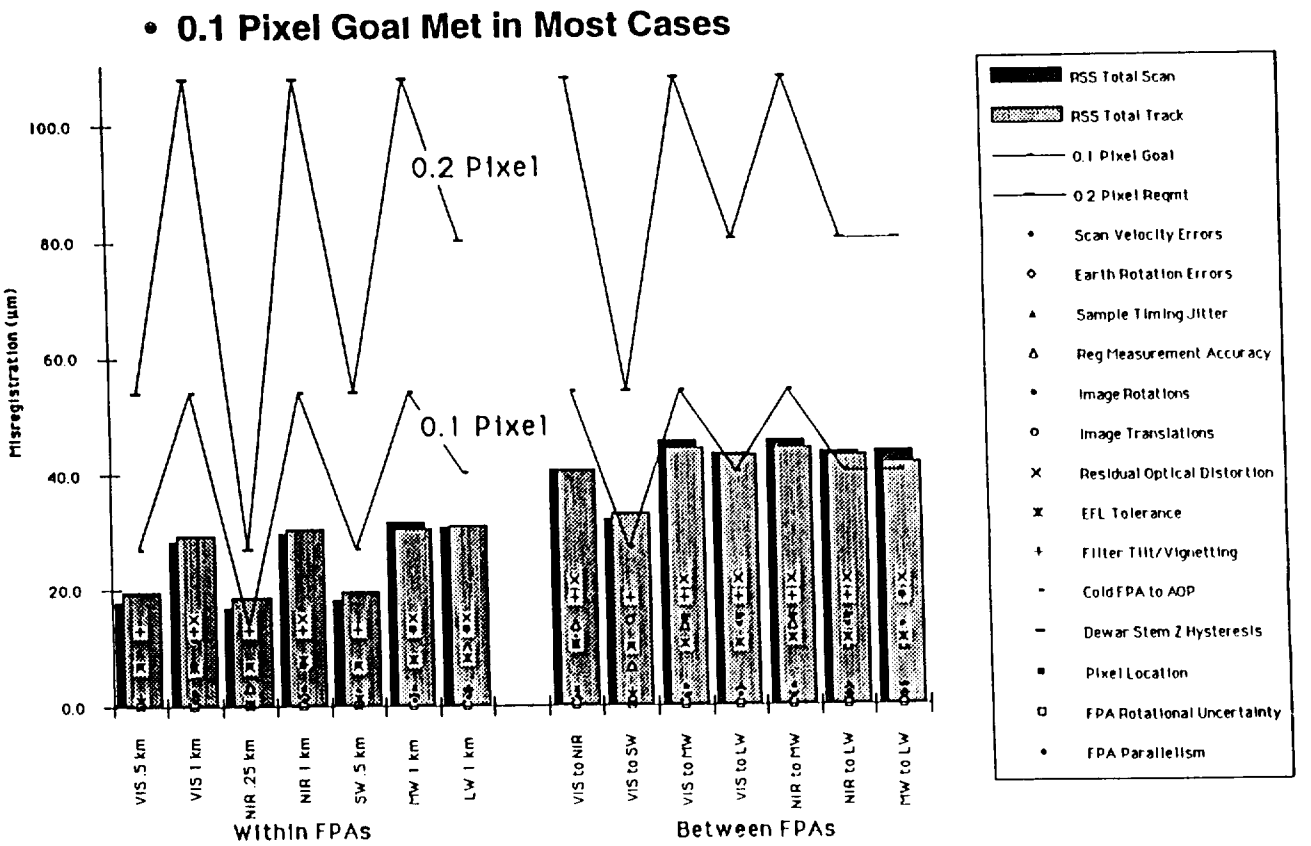

Figure 4.4. Geometric Coregistration

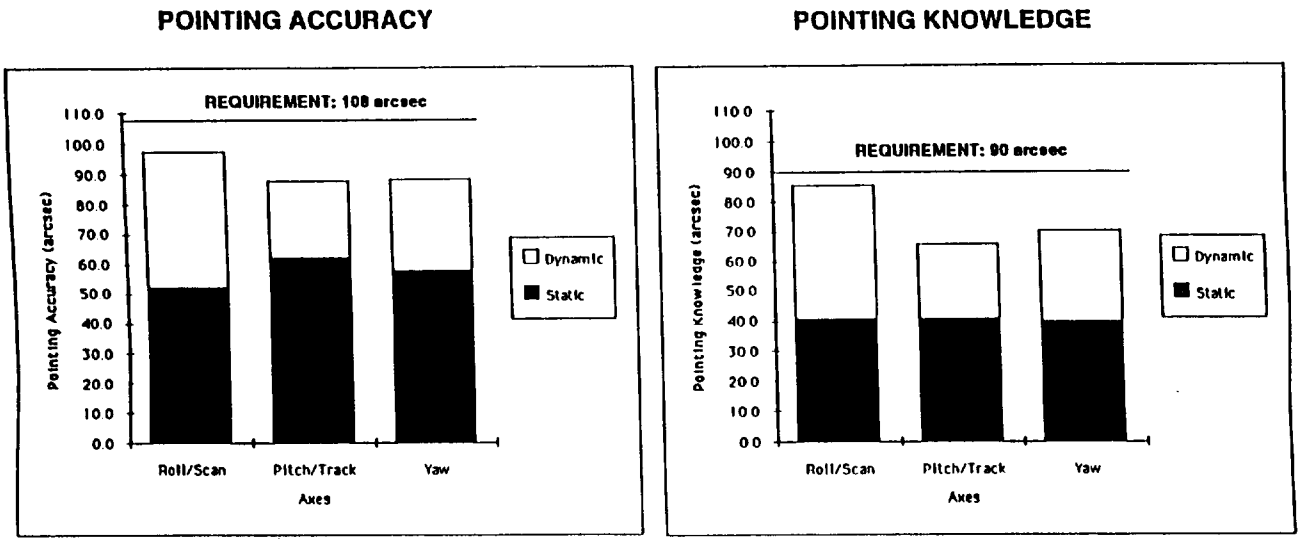

- POINTING KNOWLEDGE LOWER SINCE SEVERAL SYSTEMATIC ERRORS CAN BE MEASURED AND THEREFORE REMOVED

Figure 4.5. Pointing Accuracy and Knowledge

Table 4.2 shows a breakdown of these uncertainties into subsystem components. Two contributors to radiometric accuracies, MTF and polarization, have independent requirements. Accordingly, SBRC has analyzed the MTF and Polarization requirements.

Figure 6 presents the MTF analysis and indicates few problems in meeting the requirements.

Figure 7 shows that the sensitivity to polarization requirement will be met as well.

SBRC anticipates meeting or exceeding the radiometric calibration and spectral and geometric characterization requirements. SBRC is required to deliver a calibration algorithm which meets the Specification's calibration requirements. MCST will adapt and incorporate the SBRC algorithm into the Level-1 software and will take as a minimum requirement that the total Level-1B processing error budget continue to meet the Specification requirements.

Table 4.2
Pointing Budgets Flowed Down to Subsystem

MODIS POINTING BUDGETS: ACCURACY

POINTING ACCURACY	Component Specification	Specification Paragraph	Object Space Angles: Theta X Roll/Scan (arcsec) (3 Sigma)	Theta Y Pitch/Track (arcsec) (3 Sigma)	Theta Z Yaw (arcsec) (3 Sigma)
STATIC					
Mirror Wedge Half Angle	15.0 arcsec	151766/3 6 4 2	0.0	21.2	21.2
Alignment: Wedge Bisector-Axis	10.0 arcsec	151766/3 2 1 2	0.0	14.1	14.1
Thermal/Structural Effects SMA	10.0 arcsec	151766/3 2 3 1	10.0	10.0	10.0
Timing Induced Scan Underlap	76.7 m	151766/3 4 1 1	0.0	22.1	0.0
Registration Error	0.100 Pixels	151758/3 4 6 3	29.2	29.2	29.2
SMA to OBA Alignment	10.0 arcsec	151771/bd	10.0	10.0	10.0
SMA to OBA Measurement	5.0 arcsec	151771/bd	5.0	5.0	5.0
Scan Axis to Mounting Feet Alignment	10.0 arcsec	151771/bd	10.0	10.0	10.0
MF Therm/Str: SMA to S/C Interface*	20.0 arcsec	151765/3 2 2 2	20.0	20.0	20.0
MF Therm/Str: OBA to S/C Interface*	20.0 arcsec	151765/3 2 2 2	20.0	20.0	20.0
OBA Distortions (Telescope)	15.0 arcsec	151772/3 2 1.2	15.0	15.0	15.0
Cube Installation Error	9.0 arcsec	151766/3 8	9.0	9.0	9.0
Cube Angle Measurment Error	5.0 arcsec	151766/3 8	5.0	5.0	5.0
Instr/Spacecraft Mate Error	15.0 arcsec	TBD ICD	15.0	15.0	15.0
Cooler Launch Errors	10.0 µm	151779/3 3 6	7.3	7.3	0.0
Other Static Errors			10.0	10.0	10.0
Static (RSS Total)			**61.9**	**61.9**	**57.8**
DYNAMIC					
Bearings	9.8 arcsec	151766/3 4 1 3	0.0	9.8	19.6
Mirror Control System	90.0 µr	151766/3 4 1 2	37.1	0.0	0.0
Scan Angle Measurement	11.1 arcsec	151766/3 4 1 4	11.1	0.0	0.0
MF Therm/Str: SMA to S/C Interface**	5.0 arcsec	151765/3 2 2 2	5.0	5.0	5.0
MF Therm/Str: OBA to S/C Interface**	5.0 arcsec	151765/3 2 2 2	5.0	5.0	5.0
OBA Distortions (Telescope)	5.0 arcsec	151772/3 2 1 2	5.0	5.0	5.0
Neighboring Instruments	20.0 arcsec	TBD ICD	20.0	20.0	20.0
Other Dynamic Errors			10.0	10.0	10.0
Dynamic (RSS Total)			**45.6**	**25.9**	**31.9**
Dynamic Error Requirement	x1.477s Scan	UID/3 4	1279.1	28.1	1279.1
Total (Static + Dynamic)			**97.4**	**87.8**	**88.3**
Pointing Accuracy Requirement		151759/3 4 6 1	**100.0**	**100.0**	**100.0**

*Thermal/Structural Errors include 1g sag, thermal distortion & hygroscopic effects of Mainframe
**Dynamic Thermal/Structural Errors from in-orbit thermal variations

MODIS POINTING BUDGETS: KNOWLEDGE

POINTING KNOWLEDGE	Component Specification	Specification Paragraph	Object Space Angles: Theta X Roll/Scan (arcsec) (3 Sigma)	Theta Y Pitch/Track (arcsec) (3 Sigma)	Theta Z Yaw (arcsec) (3 Sigma)
STATIC					
Mirror Wedge Half Angle		151766/3 6 4 2	0.0	0.0	0.0
Alignment: Wedge Bisector-Axis		151766/3 2 1 2	0.0	0.0	0.0
Shaft to Motor		151766/3 2 3 1	0.0	0.0	0.0
Timing Induced Scan Underlap		151766/3 4 1 1	0.0	0.0	0.0
Registration Error	0.025 Pixels	151758/3 4 6 3	7.3	7.3	7.3
SMA to OBA Alignment	0.0 arcsec	151771/bd	0.0	0.0	0.0
SMA to OBA Measurement	5.0 arcsec	151771/bd	5.0	5.0	5.0
Scan Axis to Mounting Feet Alignment	10.0 arcsec	151771/bd	10.0	10.0	10.0
MF Therm/Str: SMA to S/C Interface*	20.0 arcsec	151765/3 2 2 2	20.0	20.0	20.0
MF Therm/Str: OBA to S/C Interface*	20.0 arcsec	151765/3 2 2 2	20.0	20.0	20.0
OBA Distortions (Telescope)	15.0 arcsec	151772/3 2 1.2	15.0	15.0	15.0
Cube Installation Error	0.0 arcsec	151766/3 8	0.0	0.0	0.0
Cube Angle Measurment Error	5.0 arcsec	151766/3 8	5.0	5.0	5.0
Instr/Spacecraft Mate Error	15.0 arcsec	TBD ICD	15.0	15.0	15.0
Cooler Launch Errors	10.0 µm	151779/3 3 6	7.3	7.3	0.0
Other Static Errors			10.0	10.0	10.0
Static (RSS Total)			**40.1**	**40.1**	**39.4**
DYNAMIC					
Bearings	9.8 arcsec	151766/3 4 1 3	0.0	9.8	19.6
Mirror Control System	90.0 µr	151766/3 4 1 2	37.1	0.0	0.0
Scan Angle Measurement	11.1 arcsec	151766/3 4 1 4	11.1	0.0	0.0
MF Therm/Str: SMA to S/C Interface**	5.0 arcsec	151765/3 2 2 2	5.0	5.0	5.0
MF Therm/Str: OBA to S/C Interface**	5.0 arcsec	151765/3 2 2 2	5.0	5.0	5.0
OBA Distortions (Telescope)	5.0 arcsec	151772/3 2 1 2	5.0	5.0	5.0
Neighboring Instruments	20.0 arcsec	TBD ICD	20.0	20.0	20.0
Other Dynamic Errors			10.0	10.0	10.0
Dynamic (RSS Total)			**45.6**	**25.9**	**31.9**
Dynamic Error Requirement	x1.477s Scan	UID/3 4	1279.1	28.1	1279.1
Total (Static + Dynamic)			**95.7**	**64.9**	**70.4**
Pointing Knowledge Requirement		151759/3 4 6 1	**90.0**	**90.0**	**90.0**

*Thermal/Structural Errors include 1g sag, thermal distortion & hygroscopic effects of Mainframe
**Dynamic Thermal/Structural Errors from in-orbit thermal variations

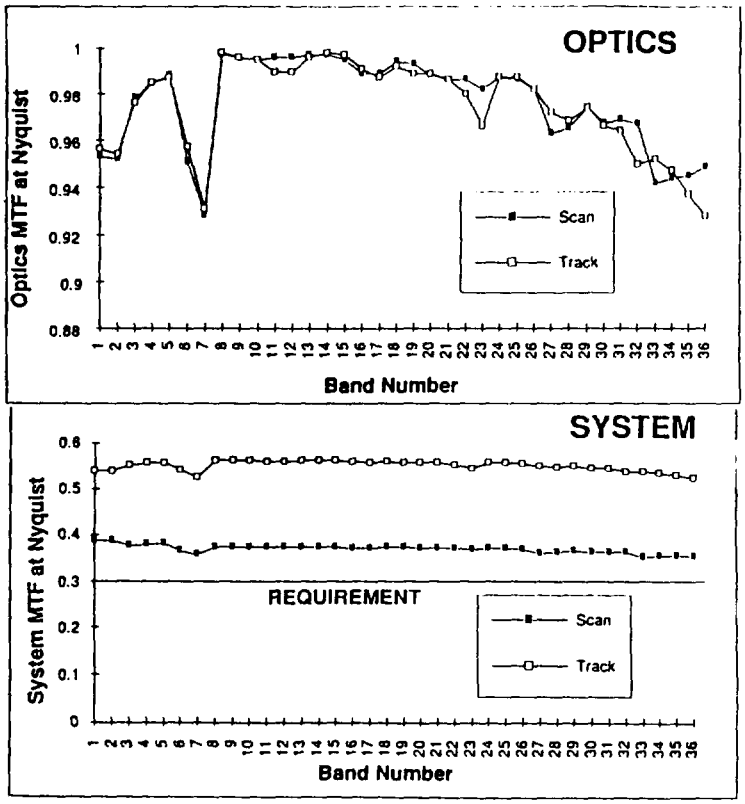

Figure 4.6. MTF Requirements

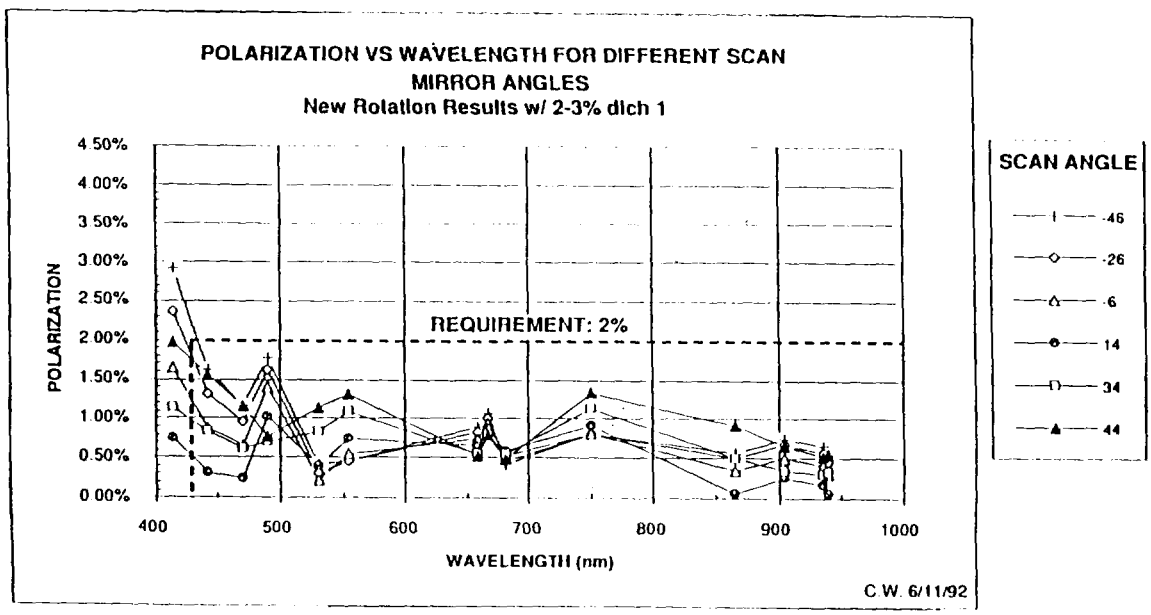

Figure 4.7. Polarization Sensitivity for MODIS

Chapter 5

Summary

The baseline characterization and calibration algorithm outlined in this document works on one orbit of MODIS data at a time (with a small amount dark data from the previous orbit for noise characterization verification). Calibration is applied on a per-channel, per-scan basis. The functional form (linear, quadratic, ogive, etc.) of the calibration equation for each channel is determined pre-launch and will be subject to Configuration Control. The most appropriate calibration coefficients are determined on a scan-by-scan basis.

For the Reflective bands the solar diffuser, the spectroradiometric calibration assembly, the space view and lunar looks each provide a Q, QCAL pair for each channel. These four pairs are curve-fit to the channel's calibration function; the parameters of the curve fit are the calibration coefficients for that channel.

For the Emissive bands the blackbody and the space view each provide a Q, QCAL pair for each channel, which are then curve-fit to obtain the calibration coefficients for that channel.

The calibration coefficients derived from the on-board calibrators and lunar looks are then compared to the projected coefficients which were calculated at the end of the previous orbit's processing. The projected coefficients are based on a combination of data sources, including trending of previous calibration coefficients and any available vicarious calibration data. Over time, if the channel is stable, the error estimates associated with the projected coefficients should become small compared to the errors associated with any single calculated calibration coefficient. For a given channel and scan, if the projected coefficients and their associated error bars lie entirely within the on-board calibrator-based coefficients' error bars then the projected coefficients will be used. Otherwise, the on-board calibrator-based coefficients will be used. In either case, the chosen coefficients are applied to the data to create a calibrated dataset.

The calibrated data is then processed through the Utility Masking algorithm, which generates classified images for characterization. Image-based characterization techniques are used to detect residual instrument signatures; these characterizations are stored in the metadata, along with any suggested signature removal techniques. Some of these techniques may be used to alter the calibration (subject to MODIS Science Team approval); if this is done, the adjusted dataset is re-masked and re-characterized.

The final Level-1 dataset is run through quality assurance tests, the results of which are stored as metadata. The final step in the baseline algorithm is updating the calibration trending and calculating the projected coefficients for the next orbit.

Appendix A

MODIS Level-1A Earth Location Algorithm Theoretical Basis Document, Version 1.0

Produced by:

Jim Storey
Hughes, STX

Dr. Albert Fleig
Edward Masuoka
Science Data Support Team (SDST)
Goddard Space Flight Center/NASA

1.0 Introduction

This document describes version 1.0 of the MODIS Level 1A Earth Location algorithm. This algorithm will be implemented as part of the MODIS Level 1A processing software in order to include Earth location and related spatial information in the Level 1A MODIS data products. The Earth location algorithm uses Earth ellipsoid and terrain surface information in conjunction with spacecraft ephemeris and attitude data, and knowledge of the MODIS instrument geometry to compute the geodetic position (latitude, longitude, and height), ground to satellite direction and range, and sun direction for each MODIS spatial element (one kilometer nadir ground field of view). The heart of the algorithm is a mathematical procedure that intersects the MODIS instrument's line of sight with the Earth's terrain surface.

The term "spatial element" is used throughout this document to refer to the ground field of view of a single detector sample from one of the 1000 meter nadir resolution MODIS bands. A single spatial element is associated with one detector sample from each of the 1000 meter bands, four samples from the 500 meter bands, and sixteen samples from the 250 meter bands. The Earth location information generated for each MODIS spatial element is stored in eight data fields added to the MODIS scan data during Level 1A processing. These fields include: 1) geodetic latitude, 2) geodetic longitude, 3) height above the Earth ellipsoid, 4) satellite zenith angle, 5) satellite azimuth, 6) range to the satellite, 7) solar zenith angle, and 8) solar azimuth. This document describes the algorithm used to generate these eight Earth location

related fields and briefly discusses the supporting data preparation and validation processes.

Other applicable documents include:

1. MODIS Technical Description Document (Preliminary), prepared for NASA Goddard Space Flight Center by Hughes Santa Barbara Research Center, document number DM VJ50-0073, dated September 1992.

2. An Analysis of MODIS Earth Location Error, Version 1.0, by Paul A. Hubanks and Albert J. Fleig, MODIS Science Data Support Team, dated March 1993.

3. MODIS Level 1A System Requirements Document (Draft), prepared by the MODIS Science Data Support Team, dated April 1993.

4. Unique Instrument Interface Document (UIID), Moderate-Resolution Imaging Spectroradiometer (MODIS) Instrument, Revision A, EOS-AM Project, Goddard Space Flight Center, dated November 6, 1992.

5. Earth Observing System General Instrument Interface Specification (GIIS) for the EOS Observatory, Revision A, prepared for NASA Goddard Space Flight Center by General Electric Company Astro Space Division, document number GSFC 420-03-02, dated December 1, 1992.

6. DMA TR 8350.2-A, DMA Technical Report, Supplement to Department of Defense World Geodetic System 1984 Technical Report, prepared by the Defense Mapping Agency WGS84 Development Committee, dated December 1, 1987.

7. Snyder, John P., Map Projections - A Working Manual, United States Geological Survey Professional Paper 1395, U. S. Government Printing Office, Washington, 1987.

8. Topographic Data Requirements for EOS Global Change Research (Draft), prepared by the U. S. Geological Survey EROS Data Center, dated April 30, 1993.

2.0 Overview and Background Information

The MODIS Earth location algorithm will operate as part of the Level 1 processing system for MODIS data from the EOS AM and PM satellites. Level 1 processing is divided into two phases termed Level 1A and Level 1B. Level 1A processing involves unpacking and verifying Level 0 MODIS data received from the EOS Data and Operations System (EDOS), organizing these data into MODIS scan oriented data structures, generating the Earth location data, adding associated ancillary information and the metadata required to describe the data set, and producing a data product in an EOS standard format. Level 1Bprocessing applies radiometric

calibration to the raw detector output contained in the Level 0 data and passed through to the Level 1A data product. This calibrated data is used in subsequent Level 2 science algorithm processing. In both Level 1 and Level 2 processing the MODIS science data is geometrically raw in the sense that no resampling has taken place. In this context the Earth location data fields are treated as additional attributes of the spatial elements that contain the MODIS science data, explicitly describing each spatial element's ground location.

The MODIS instrument contains thirty-six spectral bands at three different spatial resolutions with nominal ground fields of view of 250 meters, 500 meters, and 1000 meters. The detectors from the different bands are nominally aligned to form spatial elements each with 81 data channels (one from each of the twenty-nine 1000 meter resolution bands, four from each of the five 500 meter resolution bands, and sixteen from each of the two 250 meter resolution bands). The Level 1A Earth location algorithm provides a single Earth reference for each spatial element. A table of sub-pixel corrections for each detector in each band will be included in the data product to capture the effects of band to band and detector to detector offsets.

2.1 Experimental Objective

The eight Earth location data fields include geodetic latitude and longitude, height above the Earth ellipsoid, satellite zenith angle, satellite azimuth, range to the satellite, solar zenith angle, and solar azimuth. These data will be used in Level 1B, Level 2, and especially in Level 3 processing where spatial resampling is carried out, as well as by the end users of all product levels. The MODIS Land Team has a requirement for Earth location knowledge accurate to 0.1 pixels to support image registration for change detection. This accuracy requirement guides the design of the Earth location algorithm.

The Earth location latitude and longitude reference is needed to relate the MODIS science data to other spatially referenced data sets, including other MODIS data, and to provide a uniform, worldwide spatial reference system for all data products. Earth locations are provided at each spatial element to incorporate the effects of terrain relief which introduce high spatial frequency variations in the positions of off-nadir spatial elements. Without compensating for this effect, data sets acquired with different viewing geometry could be misaligned by tens of kilometers in areas of high relief. Earth location refinement for higher resolution bands and/or to incorporate sub-pixel band/detector misalignment can be accomplished by interpolating between spatial element Earth locations.

The Earth location height and satellite viewing angles are included to allow subsequent processes to apply higher resolution terrain data corrections to the interpolated Earth locations for higher resolution image bands. This would be done by moving along the vector from the ground point to the satellite, defined by the viewing angles, until the height correction indicated by the higher resolution terrain data was achieved. The ground point height and satellite zenith angle are

measured with respect to the local ellipsoid normal and the satellite azimuth is relative to local geodetic north.

The solar angles (as well as the satellite angles) are provided as an Earth location by-product, for use in MODIS Level 2 processing, such as atmospheric correction. The solar angles are defined with respect to the same coordinate axes as the satellite angles.

2.2 Historical Perspective

Similar Earth location algorithms are widely used in modeling and geometrically correcting satellite image data from the Landsat MSS, Landsat TM, SPOT, and AVHRR missions. In each case the fundamental problem is to compute the point at which the sensor line of sight intersects the Earth ellipsoid and/or terrain surface, leading to much commonalty among these algorithms. Experience with SPOT and AVHRR data in particular has demonstrated the importance of compensating for the effects of terrain relief when geolocating off-nadir satellite imagery.

In the MODIS Level 1A processing system the Earth location algorithm is used to tag each spatial element with its locational "attributes". This information contributes to the subsequent Level 1B and Level 2 processing prior to being used to perform spatial resampling during Level 3 processing. In most Landsat and SPOT applications the Earth location data is used immediately to resample the instrument detector output to an Earth referenced grid, prior to data analysis. This difference in philosophy leads to data processing and data storage considerations which are somewhat unusual for the MODIS Earth location algorithm. Two places where this is particularly relevant are the density at which Earth locations must be stored to capture the high spatial frequency variations due to terrain relief and the need to defer band and detector alignment resampling until Level 3 processing.

2.3 Instrument Characteristics

Although the basic outline of the Earth location algorithm has much in common with other instruments there are particular characteristics of the MODIS instrument and science data stream that have special relevance to Earth location. Of primary significance is the geometry of the multiple detectors (ten each for the 1000 meter bands, twenty each for the 500 meter bands, and forty each for the 250 meter bands), from the multiple bands (36), which are themselves distributed over four focal planes. These bands and detectors are nominally aligned into coincident spatial elements (10 per data frame) which correspond to a particular 1000 meter equivalent ground field of view. Sub-pixel misalignments will be measured pre-flight at the Santa Barbara Research Center, monitored in-flight by the MODIS Spectroradiometric Calibration Assembly (SRCA) and through image data analysis, and adjusted in-flight (focal plane to focal plane) through sample timing adjustments. The best estimates of the sub-pixel offsets from nominal locations for

each detector in each band will be included with the Level 1A data products for use in subsequent processing (e.g. Level 3 resampling).

The second characteristic of the MODIS instrument of particular importance for Earth location is the behavior of the cross-track scanning mirror. The double-sided scan mirror sweeps out a 110 degree Earth field of view in each scan, effectively moving the instrument's ten spatial elements over a swath of the Earth which is 10 kilometers wide at nadir. This scan width increases to 20 kilometers at scan angles of +/- 55 degrees due to the panoramic "bow tie" effect. This effect leads to scan to scan overlap at scan angles greater than 25 degrees. The scanning mirror motion is measured and downlinked in the instrument data stream. These mirror measurements will be used by the Earth location algorithm to determine the instrument pointing (rather than assuming mirror linearity).

A copy of the spacecraft ancillary data message containing spacecraft ephemeris and attitude information is included in the MODIS instrument data stream. This data will be included in the Level 0 data set used as input to the Level 1A process. Under normal operating conditions the ephemeris and attitude information contained in the Level 0 data will be used to provide the spacecraft knowledge required by the Earth location algorithm. A description of this data message and additional information on spacecraft characteristics can be found in references 2 and 5.

2.4 Ancillary Input Data

Several important ancillary input data sets are used by the MODIS Earth location algorithm. These include digital elevation data used to describe the Earth's terrain surface, instrument constants used to describe the internal geometry of the MODIS instrument, and ground control points used to validate the accuracy of the Earth location data.

The digital elevation model (DEM) used by the MODIS Earth location algorithm will be derived from the best available global database of terrain information provided by the EOS Project. The EOS-wide requirements for terrain data are described in reference 8. The relationship between the accuracy of this ancillary data set and the resulting accuracy of the MODIS Earth location data is discussed in reference 2. The terrain data will be preprocessed into orbit oriented units, as described in section 3.2.2 below, for processing efficiency and also to control the spatial frequency characteristics of the data. This preprocessing will also convert the input elevation data from height above the geoid to ellipsoid height if necessary.

Three types of instrument constants are required for MODIS Earth location processing. Although the term "constants" is used here it is understood that the values of these parameters may be intentionally adjusted, or change with time, or may be updated as better knowledge of their true values becomes available. They are constants when generating a particular data product.

The first type of instrument constants includes the focal plane, band, and detector offsets. These will be stored in the MODIS data product as a table of offsets which describe the sub-pixel corrections to be applied to each detector (channel) in a spatial element. The second type may be classified as optics parameters. This includes the relationship between the optical axis and instrument alignment axes as a function of scan angle, and possibly the focal lengths of the aft optics. The relationship between the optical axis and the instrument alignment axes is needed to convert a spatial element number and mirror angle to a viewing vector. The requirement for the aft optics focal lengths depends on the way the band and detector offsets are represented. If they are provided as coordinates in micrometers in the focal plane, for example, then focal length knowledge will be required. The third type of instrument constant required is the instrument to spacecraft alignment matrix. This matrix describes the spatial relationship between the MODIS instrument alignment axes and the EOS spacecraft. This relationship may have a time varying component that can be detected and modeled over time, but will be assumed to be static at launch.

The ground control points used to validate the MODIS Earth location algorithm's performance are image windows containing well defined features with known ground locations. These control points will be collected from a variety of sources prior to launch. Complete global coverage is not necessary since the current MODIS operational concept includes the use of control with a subset of MODIS Level 1A products only. This is based on the idea that it will be more effective to concentrate the acquisition of high quality ground control along a few orbits so that one product in ten, for example, has abundant control rather than all having minimal control.

3.0 Algorithm Description

This section presents the underlying theory and mathematical development of the MODIS Earth location algorithm in section 3.1. It addresses implementation and operational considerations in section 3.2.

3.1 Theoretical Description

The supporting theoretical concepts and mathematics of the MODIS Earth location algorithm are presented in the following subsections. Section 3.1.1 addresses the coordinate systems used by the algorithm and the relationships between them, citing references where appropriate. Section 3.1.2 presents a review of the MODIS viewing geometry to put the subsequent discussion in context. Section 3.1.3 is the heart of this document, presenting the mathematical development of, and solution procedure for the Earth location algorithm. Section 3.1.4 briefly discusses estimates of uncertainty and product accuracy issues. This last topic is treated in more detail in reference 2.

3.1.1 Coordinate Systems

There are seven basic coordinate systems used by the MODIS Earth location algorithm. These coordinate systems and the transformations between them are referred to frequently in the remainder of this document and are defined here. They are presented in the logical order in which a spatial element number and mirror angle would be transformed into a geodetic position.

1. Instrument Coordinate System

The instrument coordinate system is the coordinate system in which a spatial element number (1 through 10) and mirror angle is converted to a viewing vector. It is based on the MODIS reference axes defined by the MODIS alignment cube. The relationship between the MODIS instrument axis (boresight) and the alignment cube will be measured as a function of scan mirror position during pre-flight optical alignment. This relationship will be monitored in flight by analyzing pointing errors as functions of scan angle.

2. Spacecraft Coordinate System

The spacecraft coordinate system is fixed to the EOS spacecraft with its origin at the spacecraft center of mass. The coordinate axes are defined by the spacecraft attitude control system. It is the orientation of this coordinate system relative to the orbital coordinate system that is captured in the spacecraft attitude data.

3. Orbital Coordinate System

The orbital coordinate system is centered on the satellite, and its orientation is based on the spacecraft position in inertial space. The origin is the spacecraft center of mass, with the Z axis pointing from the spacecraft center of mass to the Earth center of mass. The Y axis is the normalized cross product of the Z axis and the instantaneous (inertial) velocity vector, and corresponds to the negative of the instantaneous angular momentum vector direction. The X axis is the cross product of the Y and Z axes. This coordinate system is defined in the MODIS UIID (reference 4).

4. Earth Centered Inertial (ECI) Coordinate System

The ECI coordinate system is space fixed with its origin at the Earth's center of mass. The Z axis corresponds to the mean north celestial pole of epoch J2000.0. The X axis is based on the mean vernal equinox of epoch J2000.0. The Y axis is the cross product of the Z and X axes. This coordinate system is described in detail in reference 6. Data in the ECI coordinate system will be present in the MODIS Level 1A product in the form of ephemeris data contained in the spacecraft ancillary data message.

5. Earth Centered Rotating (ECR) Coordinate System

The ECR coordinate system is Earth fixed with its origin at the center of mass of the Earth. It corresponds to the Conventional Terrestrial System defined by the Bureau International de l'Heure (BIH) which is the same as the U. S. Department of Defense World Geodetic System 1984 (WGS84) geocentric reference system. This coordinate system is exhaustively described in reference 6.

6. Geodetic Coordinate System

The geodetic coordinate system is based on the WGS84 reference frame with coordinates expressed in latitude, longitude, and height above the reference Earth ellipsoid. No ellipsoid is required by the definition of the ECR coordinate system but the geodetic coordinate system depends on the selection of an Earth ellipsoid. Latitude and longitude are defined as the angle between the ellipsoid normal and its projection onto the equator, and the angle between the local meridian and the Greenwich meridian, respectively. The Earth location data fields in the MODIS Level 1A product will be expressed in the geodetic coordinate system.

7. Space Oblique Mercator (SOM) Coordinate System

The SOM system is an orbit oriented map projection, based on the Oblique Mercator projection, which nominally follows the satellite ground track. It provides a mapping from latitude and longitude to a plane coordinate system that is approximately aligned with the MODIS data. It is used here for convenience as a method of storing the digital elevation data in an Earth referenced grid that closely matches the MODIS data geometry. The SOM projection is described in reference 7. The use of SOM versus other reference systems that achieve the same objective is still being studied.

Coordinate Transformations

1. Instrument to Spacecraft

The relationship between the instrument and spacecraft coordinate systems is described by the instrument alignment matrix. This relationship will be measure pre-flight and refined in-flight as described in section 3.2.3. The transformation from instrument coordinates to spacecraft coordinates is a three dimensional affine transformation implemented as a matrix multiplication. An affine transformation rather than a simple rotation matrix is recommended to account for possible non-orthogonality in the instrument coordinate axes. The transformation matrix will initially be defined to be fixed. Subsequent analysis may detect repeatable variations with time that can be effectively modeled, making this a (slowly) time varying transformation.

2. Spacecraft to Orbital

The relationship between the spacecraft and orbital coordinate systems is defined by the spacecraft attitude. This transformation is a three dimensional rotation matrix with the components of the rotation matrix being functions of the spacecraft roll, pitch, and yaw attitude angles. The nature of the functions of roll, pitch, and yaw depends on the exact definition of these angles (i.e. how they are generated by the attitude control system). Since the spacecraft attitude is constantly changing this transformation is time varying.

3. Orbital to ECI

The relationship between the orbital and ECI coordinate systems is based on the spacecraft's instantaneous ECI position and velocity vectors. The rotation matrix to convert from orbital to ECI can be constructed by forming the orbital coordinate system axes in ECI coordinates:

$\mathbf{P}$ = spacecraft position vector
$\mathbf{V}$ = spacecraft velocity vector
$\mathbf{T}_{eci/orb}$ = rotation matrix from orbital to ECI

$\mathbf{b}_3 = -\mathbf{P}/|\mathbf{P}|$ (nadir vector direction)
$\mathbf{b}_2 = \mathbf{b}_3 \times \mathbf{V}/|\mathbf{b}_3 \times \mathbf{V}|$ (negative of angular momentum vector direction)
$\mathbf{b}_1 = \mathbf{b}_2 \times \mathbf{b}_3$ (circular velocity vector direction)

$$\mathbf{T}_{eci/orb} = [\mathbf{b}_1 \quad \mathbf{b}_2 \quad \mathbf{b}_3]$$

4. ECI to ECR

The transformation from ECI to ECR coordinates is a time varying rotation due, primarily, to Earth rotation but also containing more slowly varying terms for precession, astronomic nutation, and polar wander. The ECI to ECR rotation matrix can be expressed as a composite of these transformations:

$$\mathbf{T}_{ecr/eci} = \mathbf{ABCD}$$

A = Polar Motion
B = Sidereal Time
C = Astronomic Nutation
D = Precession

Each of these transformation terms is described in detail in reference 6.

5. ECR to Geodetic

The relationship between ECR and geodetic coordinates can be expressed simply in its direct form:

$$X = (N + h)\cos(lat)\cos(lon)$$

$$Y = (N + h)\cos(lat)\sin(lon)$$

$$Z = \left(N\left(1 - e^2\right) + h\right)\sin(lat)$$

where (X, Y, Z) are the ECR coordinates, (lat, lon, h) are the geodetic coordinates, N is the ellipsoid radius of curvature in the prime vertical, and e^2 is the ellipsoid eccentricity squared. Unfortunately, there is no closed form solution for the inverse problem (which is the problem of interest here). Latitude and height must be solved iteratively for points that do not lie on the ellipsoid surface.

6. Geodetic to SOM

The transformation from geodetic coordinates to the SOM map projection is extremely complex. The mathematics of this transformation are described in reference 7.

3.1.2 MODIS Viewing Geometry

The MODIS instrument detectors are aligned in parallel rows on four separate focal planes. Each focal plane has its own aft optics assembly that illuminates the detectors on that focal plane. The detector placement geometry and aft optics focal length define the internal geometry of each focal plane relative to the instrument optical axis. The rows of detectors from each band are separated on the focal plane in the along-scan (cross-track) direction. The different bands are aligned into corresponding spatial elements on-board by delaying the samples from each band to account for the slight along-scan motion needed to view the same target point. These delays are fixed within each focal plane but the relative delays between focal planes can be adjusted in flight.

The instrument's 110 degree field of view is swept over the four focal planes by the double-sided rotating scan mirror. The pre-flight optical alignment tests of the MODIS instrument should document any differences in the scanning geometry of the two mirror sides. The scan mirror rotates at a rate of 20.3 revolutions per minute. With each mirror rotation capturing two scans (one for each mirror side) the scan period is 1.477 seconds. Of this time, approximately 0.451 seconds is devoted to the Earth view portion of the scan with detector samples being taken every 333.33 microseconds (for the 1000 meter resolution bands). Significant

spacecraft motion and Earth rotation takes place during this long scan period. More detailed information on the MODIS instrument's construction, operation, and pre-flight testing is provided in reference 1.

The 110 degree-wide instrument field of view sweeps out a ground swath approximately 2330 kilometers in width. This swath is sampled 1354 times by the MODIS spatial elements. Since ten spatial elements are sampled in each data frame, the nominal scan width is 10 kilometers at nadir. The wide ground swath made possible by the +/- 55 degree viewing angles exhibits significant Earth curvature effects. The apparent Earth zenith angle of a line of sight at a 55 degree scan angle is increased to approximately 65 degrees by Earth curvature. This effect, along with the increasing target range, also contributes to the growth of the projected ground spatial element as a function of scan angle. A 1000 meter (nadir) resolution spatial element at a 55 degree scan angle has ground dimensions of approximately 4800 meters cross-track by 2000 meters along-track. A graph depicting the growth of the spatial element ground field of view with scan angle is contained in reference 2. The center of the spatial element (nominal detector) will be used when computing spatial element lines of sight. It should be noted that this does not necessarily correspond to the centroid of the ground projected field of view for off-nadir pixels.

3.1.3 Mathematical Description of Algorithm

As the scan mirror sweeps across the Earth view the MODIS detectors are sampled and nominally aligned into spatial elements in sets of ten. Each set of ten spatial elements will be referred to as a data frame in the subsequent discussion. The MODIS Earth location algorithm proceeds as follows:

1. Compute the sampling time for a frame of 10 spatial elements:

    Use the frame time code converted to spacecraft time
    Apply any MODIS frame sampling delay
    Apply the spacecraft clock offset and convert to UTC

2. Interpolate the mirror scan angle based on sampling time:

    Use the 78 scan mirror encoder time measurements in the engineering data
    Use two point (TBD) Lagrange interpolation to compute the mirror scan angle
    [Various interpolation and mirror position estimation techniques for using the mirror data will be evaluated during the prototyping phase of the Level 1A processing system development, including the use of a Kalman filter which models the behavior of the mirror control system.]

3. Construct an array of look vectors in the instrument coordinate system for the 10 spatial elements assuming ideal detector placement and using the interpolated mirror scan angle.

4. Compute the required coordinate transformations:

[Construct the instrument to spacecraft alignment matrix based on the sampling time if a time varying model is needed (baseline is fixed matrix)] ($\mathbf{T}_{sc/inst}$)
Interpolate the spacecraft attitude from the sampling time and construct the spacecraft to orbital coordinate transformation matrix ($\mathbf{T}_{orb/sc}$)
Interpolate the ECI spacecraft position and velocity from the sampling time and construct the orbital to ECI transformation matrix ($\mathbf{T}_{eci/orb}$).
Construct the ECI to ECR rotation matrix from the sampling time ($\mathbf{T}_{ecr/eci}$)
Construct the composite transformation matrix:

$$\mathbf{T}_{ecr/inst} = \mathbf{T}_{ecr/eci}\mathbf{T}_{eci/orb}\mathbf{T}_{orb/sc}\mathbf{T}_{sc/inst}$$

5. Transform the look vectors, spacecraft position vector, and solar vector to ECR:

Rotate the look vectors to the ECR coordinate system:

$$\mathbf{U}_{ecr} = \mathbf{T}_{ecr/inst}\,\mathbf{U}_{inst}$$

Rotate the spacecraft position vector to the ECR coordinate system:

$$\mathbf{P}_{ecr} = \mathbf{T}_{ecr/eci}\,\mathbf{P}_{eci}$$

Retrieve the ECI solar vector based on the sampling time (PGS Toolkit call or extracted from the spacecraft ancillary data message and converted to ECI)

Rotate the solar vector to the ECR coordinate system:

$$\mathbf{S}_{ecr} = \mathbf{T}_{ecr/eci}\,\mathbf{S}_{eci}$$

6. Intersect the ECR look vectors with the WGS84 (or other EOSDIS standard) Earth ellipsoid:

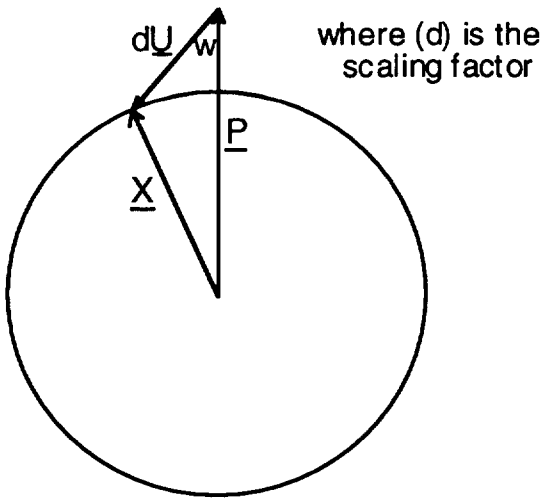

Figure 1: Ellipsoidal Look Vector Intersection

Rescale the look vector and satellite vector using the ellipsoid semi-major (a) and semi-minor (b) axis dimensions (a, a, b):

$$\mathbf{U}' = \begin{bmatrix} u_1 / a \\ u_2 / a \\ u_3 / b \end{bmatrix} \qquad \mathbf{P}' = \begin{bmatrix} p_1 / a \\ p_2 / a \\ p_3 / b \end{bmatrix}$$

Note:

$$\mathbf{X}' = \begin{bmatrix} x_1 / a \\ x_2 / a \\ x_3 / b \end{bmatrix} = \text{the unknown ground point vector (rescaled)}$$

Solve for the scaling (d) of $\mathbf{U}'$ which intersects the unit sphere:

From the law of cosines:

$$|\mathbf{X}'|^2 = |d\,\mathbf{U}'|^2 + |\mathbf{P}'|^2 - 2\,|d\,\mathbf{U}'|\,|\mathbf{P}'|\cos(w)$$

$$\cos(w) = -(\mathbf{U}' \bullet \mathbf{P}')/(|\mathbf{U}'|\,|\mathbf{P}'|) \quad \text{Note that } (\mathbf{U}' \bullet \mathbf{P}') \text{ is negative}$$

By definition $|\mathbf{X}'| = 1$ so:

$$1 = d^2|\mathbf{U}'|^2 + |\mathbf{P}'|^2 + 2d|\mathbf{U}'|\,|\mathbf{P}'|(\mathbf{U}' \bullet \mathbf{P}')/(|\mathbf{U}'|\,|\mathbf{P}'|)$$

Simplifying and rearranging:

$$d^2|\mathbf{U}'|^2 + 2d(\mathbf{U}' \bullet \mathbf{P}') + |\mathbf{P}'|^2 - 1 = 0$$

This can be solved for d using the quadratic formula:

$$d = \left| \frac{-2(\mathbf{U}' \bullet \mathbf{P}') - \sqrt{4(\mathbf{U}' \bullet \mathbf{P}')^2 - 4|\mathbf{U}'|^2(|\mathbf{P}'|^2 - 1)}}{2|\mathbf{U}'|^2} \right|$$

Use d to compute $\mathbf{X}'$ and $\mathbf{X}$:

$$\mathbf{X}' = \mathbf{P}' + d\mathbf{U}'$$

$$\mathbf{X} = \begin{bmatrix} x'_1 a \\ x'_2 a \\ x'_3 b \end{bmatrix} = \begin{bmatrix} (p'_1 + du'_1)a \\ (p'_2 + du'_2)a \\ (p'_3 + du'_3)b \end{bmatrix} = \begin{bmatrix} p'_1 a + du'_1 a \\ p'_2 a + du'_2 a \\ p'_3 b + du'_3 b \end{bmatrix}$$

$$\mathbf{X} = \mathbf{P} + d\mathbf{U}$$

7. Convert the ECR ellipsoid pierce points to geodetic coordinates (special case direct solution):

$$lon = \tan^{-1}\left(\frac{x_2}{x_1}\right)$$

$$lat = \tan^{-1}\left(\frac{x_3/(1-e^2)}{\sqrt{x_1^2 + x_2^2}}\right)$$

$$h = 0$$

8. Compute the local ellipsoid normal unit vector from the geodetic latitude and longitude:

$$\mathbf{n} = \begin{bmatrix} \cos(lat)\cos(lon) \\ \cos(lat)\sin(lon) \\ \sin(lat) \end{bmatrix}$$

9. Compute the ECR unit vector from the ground point to the satellite:

$$\mathbf{u} = -\frac{\mathbf{U}}{|\mathbf{U}|}$$

10. Compute the component of the satellite vector which is in the local vertical direction:

$$v = \mathbf{u} \bullet \mathbf{n}$$

11. Compute the distance along the satellite vector (D_{max}) we must move to achieve a height of H_{max} where H_{max} is a pre-computed value representing the highest local terrain height:

$$D_{max} = \frac{H_{max}}{v}$$

12. Compute the ECR coordinates of the point along the look vector that corresponds to H_{max}:

$$\mathbf{X}_{max} = \mathbf{X} + D_{max}\mathbf{u}$$

13. Compute the distance along the satellite vector (D_{min}) we must move to achieve a height of H_{min} where H_{min} is a pre-computed value representing the lowest local terrain height:

$$D_{min} = \frac{H_{min}}{v}$$

14. Compute the ECR coordinates of the point along the look vector that corresponds to H_{min}:

$$\mathbf{X}_{min} = \mathbf{X} + D_{min}\mathbf{u}$$

15. Convert $\mathbf{X}_{max}$ and $\mathbf{X}_{min}$ to geodetic coordinates (iterative general solution)

16. Convert the geodetic coordinates to DEM map projection coordinates (SOM) $\mathbf{x}_{min}$ and $\mathbf{x}_{max}$

17. Construct and normalize the SOM search vector:

$$\mathbf{S} = \mathbf{x}_{min} - \mathbf{x}_{max}$$

$$\mathbf{s} = \frac{\mathbf{S}}{|\mathbf{S}|}$$

18. Perform terrain intersection iterations:

$$\mathbf{x}_0 = \mathbf{x}_{max}$$
$$h_0 = \mathrm{DEM}(\mathbf{x}_0)$$
$$h'_0 = H_{max}$$

$ds =$ DEM grid resolution (nominally 1000 meters)

$$dh = \frac{ds(H_{min} - H_{max})}{|\mathbf{S}|}$$

do until $(h_i \geq h'_i)$

$$\mathbf{x}_i = \mathbf{x}_{i-1} + ds\,\mathbf{s}$$
$$h_i = \mathrm{DEM}(\mathbf{x}_i)$$
$$h'_i = h'_{i-1} + dh$$

end do

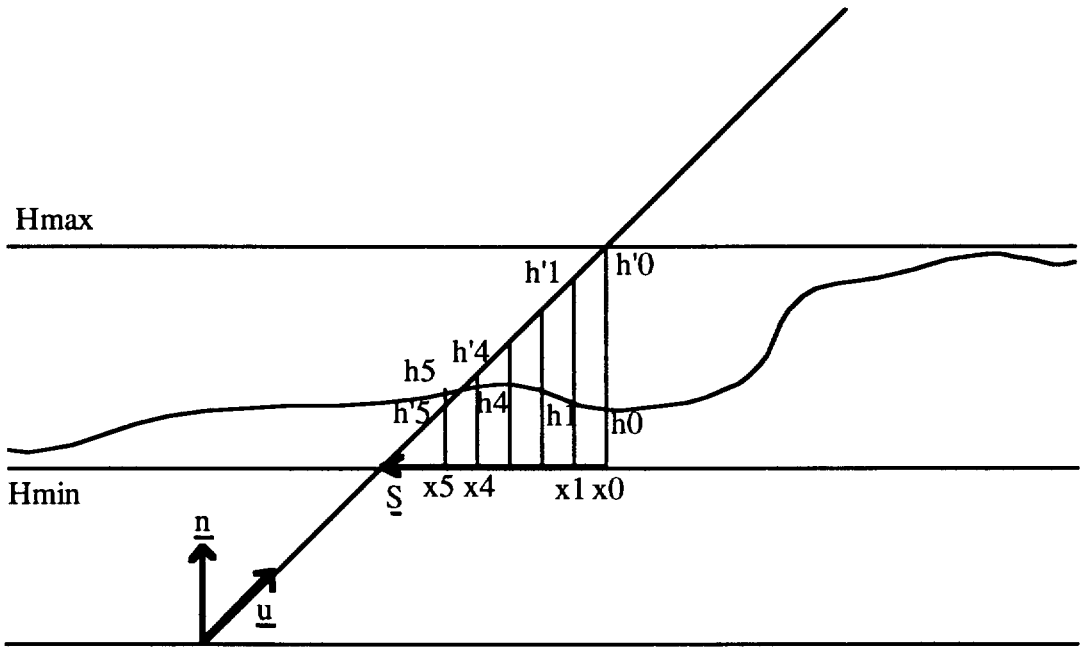

Figure 2. Terrain Intersection Search Geometry

19. Compute the precise terrain intersection from the last two iterations:

The final terrain intersection height can be expressed:

$$h_{final} = \alpha h_i + (1-\alpha) h_{i-1} = \alpha h'_i + (1-\alpha) h'_{i-1}$$

Solving for the weights:

$$\alpha = \frac{h'_{i-1} - h_{i-1}}{h_i - h_{i-1} - dh}$$
$$1-\alpha = \frac{h_i - h'_i}{h_i - h_{i-1} - dh}$$

The final (SOM) position is:

$$\mathbf{x}_{final} = \alpha\,\mathbf{x}_i + (1-\alpha)\,\mathbf{x}_{i-1}$$
$$h_{final} = \alpha h_i + (1-\alpha) h_{i-1}$$

20. Convert the SOM precise intersection to geodetic coordinates.

21. Compute the normal vector at the final geodetic position.

$$\mathbf{n}_{final} = \begin{bmatrix} \cos(lat_{final})\cos(lon_{final}) \\ \cos(lat_{final})\sin(lon_{final}) \\ \sin(lat_{final}) \end{bmatrix}$$

22. Convert the geodetic ground point to ECR.

23. Compute the satellite zenith angle, azimuth, and range from the final ground point, the satellite position, and the normal vector.

24. Compute the sun zenith angle and azimuth from the ECR solar vector, $\underline{S}_{ecr}$ and the normal vector.

3.1.4 Variance or uncertainty estimates

The fundamental measure of uncertainty of interest for the MODIS Earth location algorithm is the positional accuracy of the geodetic coordinates computed for each spatial element. This accuracy is limited by the uncertainty in the spacecraft, instrument, and ancillary elevation data provided to the algorithm.

A complete analysis of MODIS Earth location error is presented in "An Analysis of MODIS Earth Location Error" (reference 2). That document presents a detailed breakdown of the anticipated sources of error in the EOS AM spacecraft ephemeris and attitude knowledge, and in the MODIS instrument pointing knowledge, and demonstrates the effects these errors and errors in the ancillary digital elevation data have on the resulting data product geolocation accuracy. The current best estimates of the contributing errors, provided by the spacecraft and instrument builders, as well as the spacecraft and instrument specification requirements were used in that analysis. What follows is extracted from that report.

Spacecraft position error, spacecraft attitude knowledge error, and instrument pointing knowledge error were analyzed separately with all contributing errors classified as either static or dynamic. Static errors are unknown constant offsets caused by imprecise knowledge of the instrument or spacecraft geometry or by geometric distortions occurring during or after launch. These error components, though initially unknown, should not change with time, after launch. Estimates of these constant offsets will be computed using the product validation and geometric parameter estimation procedures described in section 3.2.3. The dynamic error components are time varying and cannot be easily modeled. Tables detailing the various error sources and their expected magnitudes are presented in the MODIS Earth location error report.

The sensitivity of the output product accuracy to the uncertainty in the input data varies with scan angle. Plots depicting this sensitivity for spacecraft position errors and for spacecraft/instrument pointing errors are presented in reference 2. The variation with scan angle is summarized in the following tables. Only spacecraft position and attitude tables are shown because the propagation of the instrument pointing errors parallels the spacecraft pointing errors. The numbers used are from the spacecraft specifications and are two sigma values. These are used to demonstrate the sensitivity to scan angle and the relative effects of position and pointing errors only, not as true estimates of the expected product accuracy. A similar error propagation using the current best estimates of the input errors is contained in reference 2.

Table 1:
Geolocation Impact of Two Sigma Spacecraft Position Errors

Spacecraft Position	**X-Axis** Position Error	Corresponding **Along-Track** Earth Location Error		**Y-Axis** Position Error	Corresponding **Cross-Track** Earth Location Error		**Z-Axis** Position Error	Corresponding **Cross-Track** Earth Location Error	
		0 deg.	55 deg.		0 deg.	55 deg.		0 deg.	55 deg.
Current Spec.	100.0 m	90.0 m	88.5 m	100.0 m	90.0 m	90.0 m	100.0 m	0.0 m	197.3 m

Table 2
Geolocation Impact of Two Sigma Attitude Knowledge Errors

Spacecraft Attitude	**Roll** Pointing Error	Corresponding **Cross-Track** Earth Location Error		**Pitch** Pointing Error	Corresponding **Along-Track** Earth Location Error		**Yaw** Pointing Error	Corresponding **Along-Track** Earth Location Error	
		0 deg.	55 deg.		0 deg.	55 deg.		0 deg.	55 deg.
Current Spec.	60.0 arcsec	205.1 m	990.5 m	60.0 arcsec	205.1 m	235.9 m	60.0 arcsec	0.0 m	336.9 m

The accuracy impact of the digital elevation data is also a function of scan angle with no effect on Earth location at nadir and a greater than one-to-one correspondence between height and position errors at high scan angles. In the context of image to image registration the displacement due to terrain errors is self canceling if the two data sets are taken from approximately the same viewing geometry but are arithmetically added if the views are from different directions. The effect of the input elevation model on the product accuracy is further complicated by the

relationship between elevation accuracy and terrain roughness. In rugged areas, elevation variations of hundreds of meters can occur within a single MODIS spatial element. Assigning a single geodetic coordinate to such a spatial element using a representative elevation, masks the true complexity of the terrain and the real differences in what is being viewed from different directions.

3.2 Practical Considerations

The following sections discuss practical implementation and operational considerations including numerical stability, computational efficiency, automated and interactive product validation, automated quality control and metadata generation, and possible processing exception conditions.

3.2.1 Numerical Computation Considerations

The MODIS Earth location algorithm incorporates two iterative procedures which must be implemented carefully to ensure convergence. The first of these is the general iterative conversion from ECR to geodetic coordinates. This procedure is straightforward and robust and although it converges relatively slowly at mid-latitudes, can be driven to any desired precision through iteration. Some computational efficiency gain may be achieved, if necessary, by relaxing the convergence criterion on this procedure but this will not be attempted initially.

The second iterative procedure is the detection of the MODIS line of sight intersection with the terrain. Simple approaches to implementing this algorithm break down at high off-nadir angles due to the possibility of multiple intersections of the line of sight with the terrain surface. Under these conditions care must be taken to ensure that the algorithm converges to the correct terrain intersection point (i.e. the intersection closest to the satellite). This is achieved here by searching from above to find the first (highest) terrain intersection. The iteration proceeds monotonically down until the look vector is below the terrain surface so convergence is not a problem. The precision of the final terrain intersection determination is a function of the local relief due to the use of local linear approximations in the algorithm (the look vector is treated as linear in the local SOM space). The degree to which this approximation breaks down is a function of the height range searched and the satellite look angle. These statistics will be monitored for quality control purposes as described in section 3.2.4.

3.2.2 Programming/Procedural Considerations

Computational Load

The computational burden imposed by the MODIS Earth location algorithm arises primarily from the terrain intersection computation. Current estimates indicate that approximately 80% of the Earth location processing load is used by the terrain

correction step. Within this procedure there are two computations which consume the bulk of the processing: the conversion from ECR to geodetic coordinates and the conversion from geodetic to SOM.

The ECR to geodetic conversion was mentioned in the previous section as a place where computational savings might be possible but the SOM conversion, in addition to being the more computationally intensive of the two, provides more interesting possibilities for computational efficiency. One possibility is to compute the SOM projection rigorously for only the first and last spatial elements in each data frame, interpolating the other eight. Since the SOM projection is approximately aligned with the MODIS orbit it should be very regular over a single data frame as should the spatial element locations themselves (since they are based on ideal detector placement). This possible simplifying approximation requires further analysis to evaluate its full effect. Another possibility is to adopt some other orbit oriented map projection which is less computationally burdensome than SOM. Toward this end, other candidate projections are currently being studied in conjunction with the MISR team who have a similar requirement.

In both the ECR to geodetic conversion and the SOM projection the main computational driver is the number of trigonometric functions which must be performed. One way to achieve efficiency in these computations is to carefully apply small angle approximations and Taylor series expansions when the angles involved change very little between invocations. Another approach is to implement the standard sine and cosine functions as look-up tables pre-computed based on the required precision of the calling routine.

Development Approach

Whatever approximations are deemed to be possible or desirable for efficiency purposes, the initial version of the MODIS Earth location algorithm will be implemented with no efficiency oriented approximations. This "brute force" method of terrain intersection searching will operate completely in ECR coordinates to avoid the SOM search vector linearization approximation mentioned in section 3.2.1. The computational price to be paid for this comes in the need to convert from ECR to geodetic to SOM to interpolate a terrain height at each step in the iteration. This computationally intensive version will be developed first to serve as a baseline for validating the accuracy of subsequent approximations adopted for computational efficiency.

Other Related Processing

Significant preprocessing effort is required to put the digital elevation data into a form that is convenient for the Earth location algorithm. This involves resampling the EOS Project supplied digital elevation data into a 1000 meter spacing grid in the orbit-oriented SOM projection. Using an orbit oriented grid ensures that the line of sight search direction will be primarily along the DEM grid line direction. Since the

SOM coordinate system is unique for each satellite path there will be 233 different preprocessed DEMs, one for each possible EOS orbital path. Depending on the spatial resolution (spatial frequency content) of the original digital elevation data, spatial filtering may also be necessary during DEM preprocessing. To avoid aliasing artifacts in the geodetic positions assigned to the MODIS spatial elements, it is necessary to remove spatial frequencies that cannot be captured by the MODIS sampling interval, from the DEM data. This filtering will be a complex process based on the MODIS scanning geometry which leads to a ground sample spacing that varies with scan angle.

Preprocessing will also be required to prepare the control point data used for product validation. The control data image chips will be preprocessed to simulate the effects of the MODIS viewing geometry so that they can be more efficiently matched to the real 250 meter resolution image data. Each control point will be processed based on all of the EOS orbital paths from which it may be seen by the MODIS instrument. These control points will then be assembled into sets based on the orbital paths. The use of control points is discussed in more detail in the next section.

3.2.3 Product Validation and Geometric Parameter Estimation

The accuracy of the MODIS Earth location data is validated using automated control point correlation methods coupled with off-line analysis. Control point validation will be built into the MODIS Level 1A production system but operationally will only be applied to a subset of the Level 1A products based on control availability, cloud cover, and processing load considerations. The Level 1A production system will use the control points to collect the raw validation data (in the form of control point residual errors) automatically. This data will then be analyzed off-line at the MODIS Team Leader Science Computing Facility (TLCF). The automatically extracted validation data and off-line analysis approach will also be used to monitor the stability of and estimate refinements to the instrument geometric parameters described in section 2.3. These product validation and geometric parameter estimation activities are described in more detail in the following sections.

3.2.3.1 Product Validation

The 250 meter resolution MODIS bands will be used in conjunction with pre-assembled sets of ground control points to validate the accuracy of the MODIS Earth location data. The control point image chips will be preprocessed as described in section 3.2.2 to simulate the MODIS viewing geometry. This will include applying the MODIS modulation transfer function (MTF) to the higher resolution control chips.

The known position of the control point can be used to extract an image neighborhood from the new MODIS data at the location predicted by the Earth location data. Nominal radiometric calibration parameters will be applied to the MODIS neighborhood to remove radiometric artifacts. A simple cloud detection

algorithm (e.g. thresholding) will also be used to identify areas that are not suitable for image correlation. The control point image chip can then be correlated with the MODIS neighborhood to measure the (hopefully sub-pixel) displacement between its predicted and observed locations. This measured image distortion, along with the control point chips and extracted MODIS neighborhoods, will then be passed to the MODIS TLCF for off-line analysis. The control chips and neighborhoods will be used to verify the performance of the control point mensuration procedure itself while the measured distortions will be used in anomaly detection, trend analysis, and to build up a statistical record of Earth location performance.

There are a number of possible control point correlation techniques that can be applied to the problem of measuring the sub-pixel misregistration of the control points with the MODIS neighborhoods. Some of these include normalized cross correlation with a correlation surface fit to estimate the sub-pixel maximum, phase correlation with a linear fit to estimate the sub-pixel phase shift, and correlation (normalized cross correlation or least squares correlation) with an oversampled control chip with correlation coefficients computed at sub-pixel increments. Various methods will be tested and analyzed in the Earth location software prototype environment. The Earth location prototyping effort will also investigate various potential sources of control including Landsat images and vector shoreline data.

3.2.3.2 Geometric Parameter Estimation

Corrections to some of the instrument geometric parameters mentioned in section 2.4 will be estimated on the ground using the data generated by the automated Earth location validation procedure. For example, the static errors in the EOS spacecraft attitude knowledge and the MODIS instrument pointing knowledge will be modeled as refinements to the pre-launch knowledge of the instrument to spacecraft alignment matrix. Refined alignment matrices will be estimated off-line on the MODIS TLCF using control point data from multiple Level 1A products. Multi-band MODIS image data and the SRCA calibration data can also be used to estimate refinements to the pre-launch focal plane alignment and band/detector location parameters. This would be done by using the SRCA reticule patterns, or well defined image features that appear in multiple bands, to measure the sub-pixel misregistration of bands from the same and different focal planes. Other residual instrument geometric misalignments could also be investigated but will require additional information from the instrument builder to develop the appropriate models.

The off-line geometric analysis and parameter estimation effort will grow more ambitious with time as more data becomes available. This will make it possible to compare the control point validation data and the MODIS image data itself from the same and different orbital passes under varying conditions to detect constant offsets and slowly varying trends. A list of intended analysis tasks ranging from those that can be undertaken immediately after launch (analogous to at-launch science

products) to those that will require the accumulation of a longer data record (analogous to post-launch science products) includes the following:

- Verify the performance of the automatic correlation procedure through interactive control point mensuration.
- Estimate the systematic biases in the instrument alignment matrix by detecting trends in the automatically extracted control point results.
- Validate the image internal geometric accuracy by correlating multiple MODIS products from the same orbital path (including looking for even/odd scan artifacts due to differences in the two scan mirror sides).
- Validate the terrain correction accuracy and identify areas of poor DEM data by measuring tie points between overlapping MODIS products
- Detect and model repeatable within-orbit thermal variations in the geometric parameters using control point and image to image data by correlating the distortion with the position in orbit relative to the sun.

This list represents the current concept of the types of geometric analysis envisioned for the MODIS Level 1A data. The post-launch conduct of this activity will be guided by the characteristics of the real MODIS data.

3.2.4 Quality Control and Diagnostics

The MODIS Earth location procedure will accumulate performance indicators during the normal course of processing for inclusion in the Level 1A product metadata as quality control information. Numeric performance indicators include the number of suspect ephemeris points replaced, the number of suspect attitude points replaced, the convergence criterion for the iterative ECR to geodetic conversion, the maximum horizontal range searched during the terrain intersection iteration and where in the product it occurred, and the most acute angle of look vector/terrain slope intersection and where in the product it occurred. Other quality control fields include quality information taken from the ancillary input data sets such as the DEM and possibly the ephemeris and attitude data if it came from a source other than the Level 0 data itself.

These quality control fields will be included in the Level 1A product metadata along with other descriptive data such as a record of the ancillary data lineage (e.g. data set version number and date, preprocessing history) and a parametric geolocation model which provides an approximate mapping from geodetic coordinates to Level 1A spatial elements, in the metadata. The requirement for a method of spatially indexing into the Level 1A product given only the metadata has been expressed by the MODIS Ocean team and also an implied requirement of the EOSDIS Information Management System (IMS). The accuracy required for this parametric geolocation is not known at this time and no particular model has been adopted. Candidates include a method to be specified or recommended by the IMS developers, and the method developed by the SeaWiFS project.

3.2.5 Exception Handling

The Earth location algorithm will provide mechanisms for gracefully handling the following three known exception conditions: 1) missing ephemeris or attitude data, 2) missing DEM data, and 3) the instrument line of sight does not intersect the Earth (e.g. during a lunar view).

The input ephemeris and attitude data will be checked for consistency and completeness by the Level 1A processing software. If either is completely missing or deemed to be unusable an error message will be generated and no Earth location data will be produced. If gaps exist they will be filled by interpolation (using PGS Toolkit routines, if provided) with appropriate quality control information entered into the product metadata. In the case of missing input DEM data the Earth location will proceed using the Earth ellipsoid as the reference terrain surface. A warning message will be generated and an appropriate notation added to the product metadata. If the line of sight intersection algorithm detects a look vector that does not intersect the Earth ellipsoid the geodetic position fields will be populated with the ECI look vector (to be used to determine which pixels viewed the moon), a null value will be placed in the other Earth location data fields, a warning message will be generated, and a notation will be added to the product metadata.

4.0 Constraints, Limitations, Assumptions

Several simplifying assumptions were made in the development of the MODIS Earth location algorithm. These assumptions and their justifications are as follows:

- Ignore atmospheric refraction of the line of sight - Analysis conducted by the MODIS Characterization Support Team has indicated that this effect is, at most, on the order of a few meters; much smaller than a MODIS pixel.
- Ignore light travel time - The maximum range to a terrestrial target seen by MODIS is about 1414 kilometers. This corresponds to a light travel time of 4.7 milliseconds and an Earth rotation of about 2 meters which is much smaller than a MODIS pixel.
- Ignore the instrument primary mirror offset from the spacecraft center of mass - The ephemeris position represents the spacecraft center of mass rather than the instrument optical origin, but this offset is at most a few meters which is less than the accuracy of the ephemeris data and much less than a MODIS pixel.

The error analysis presented in section 3.1.4 is based on reference 2 which assumed that the individual contributors to the overall MODIS Earth location error were independent zero-mean Gaussian distributed random variables. This assumption is implicit in this document as well. In addition, the Earth location algorithm was developed under the assumption that the nature and magnitudes of the errors documented in reference 2 are essentially correct. The quality of the available DEM

data is assumed to conform to the characteristics specified in reference 8 although this does not affect the algorithm itself, only its final performance.

The implementation of the MODIS Earth location algorithm described above is based on the final assumption that the output product data structure will be sufficiently flexible to permit the addition of eight new Earth location data fields for each spatial element and to allow the efficient extraction of control point neighborhoods from the 250 meter image bands for automated product validation.

Appendix B

Instrument Specification

B.1 Introduction

The MODIS Instrument Specification (Goddard Space Flight Center, 1993) sets forth the performance, testing, calibration and assurance requirements for MODIS. The instrument must meet these requirements upon delivery. The Specification therefore identifies the minimum characterization and calibration that must be done by the contractor.

This appendix presents a detailed discussion of the Specification as it relates to characterization and calibration. The intention is to be both comprehensive and sufficiently detailed enough so that the driving requirements for the calibration algorithm from the instrument become clear. To do so, it is divided into sections based on calibration requirements. Section B.2 presents a summary of the physical instrument requirements. The radiometric, spectral, and geometric requirements are presented in sections B.3, B.4, and B.5 respectively. Other important performance requirements are presented in section B.6. Finally, section B.7 summarizes the remaining Specification requirements.

It should be noted that other existing documents also cover MODIS operating requirements. These are cited in section ¶2.0 of the Specification (hereafter Specification references:¶ are denoted simply by section number). However, these do not directly relate to characterization and calibration and so are not discussed here.

B.2 Physical Instrument Requirements

The instrument must meet several basic physical requirements for operability. Table B-1 presents a summary of these parameters and cites the relevant Specification sections. Additionally, the lifetime and survivability requirements are addressed below.

One key requirement for the success of MODIS is that it be operable over its entire five year lifetime. The Specification (¶3.2.3) defines failure of the instrument to be the loss of 25% or more of the 36 spectral bands or more than 50% of the bands in any one spectral region (i.e., VIS, NIR, SWIR, MWIR, or LWIR). A band is considered as failed if the response in more than 25% of its detector elements falls 50% or more below the pre-launch response, or if its detector elements cannot be calibrated to perform within specification. Upon delivery, the instrument may have a maximum of one dead element per band and no more than two per focal plane (¶3.4.5.3.2).

While the lifetime of the MODIS instrument is intended to be five years in orbit, the Specification (¶3.2.3) requires it to be operable after delivery, without servicing, for six

Table B-1.Physical Requirements

Parameter	Requirement	Specification Section
Volume (Length x Width X Height)	1 x 1.6 x 1 m	3.6.2.2
Max. Appendage Length (external to Volume)	1 m	3.6.2.2
Mass	< 250 kg	3.6.2.2
Power	<225 W ave., <275 W peak	3.6.2.1
Ground View	120° cross-track 5° along-track	3.6.2.4.1
Sun View	allowed, no size requirement	3.6.2.4.2
Space View	allowed, no size requirement	3.6.2.4.3
Altitude	705.3 km	3.1.1
Equatorial Crossing Time		
AM Platform	10:30 AM +/- 15 min descending	3.2.1
PM Platform	1:30 PM +/- 15 min ascending	3.2.1
Lifetime	85% prob., 95% goal of being 5+ years	3.2.3
Radiation Recovery	unaffected by ambient	3.2.4.1
	< 5 km, < 5 data words for particles <20 MeV	3.2.4.2
Solar Recovery	< 10 orbits after 30 s direct view	3.4.10.4

months before launch as well as the five years in orbit. This follows a maximum period of eight years in storage plus two years of Integration and Test. If the storage period exceeds one year, the instrument will be thoroughly tested and recalibrated prior to integration on the spacecraft. The probability of meeting the five year lifetime is required to be 85% with a goal of 95% as determined by test experience and analytical assessment.

For survivability, the instrument is expected to operate within specification despite background radiation or unplanned scans through the sun. The instrument will pass through the South Atlantic Magnetic Anomaly; it may be unreasonable to expect to shield electronic parts from all possible particles. Therefore, the Specification (¶3.2.4.2) requires that a single event caused by particles having energy less than 20 MeV shall affect no more than 3 contiguous bands per focal plane, and 5 contiguous pixels per band. These pixels shall recover after 5 contiguous 1000 m pixel readout times (5 km) from the inception of the event. If the event affects the electronics following the focal planes, no more than 5 data words leaving the memory buffer may be degraded.

Under certain unplanned spacecraft attitudes, MODIS may scan through the sun. Therefore, the instrument shall be capable of scanning direct solar input in its 110-degree-wide FOV for 30 seconds per event, up to a total of 5 minutes in five years, without detectable performance degradation or lifetime reduction. Any radiative cooler must meet these same requirements for direct solar input. After any 30 second exposure, the instrument shall return to its calibrated condition within 10 orbits. Normal, expected solar inputs shall not degrade the instrument's performance for any portion of the orbit. Meeting these survivability and lifetime requirements is vital to the success of the MODIS mission.

B.3 Radiometric Requirements

One major goal of the MODIS program is to provide high radiometric accuracy for all of its spectral bands. Each of these bands is designed to address at least one specific scientific goal and thus has specific dynamic range requirements. Tables B-2a and B-2b summarize these requirements.

The instrument is expected to measure radiances from the noise equivalent differential spectral radiance (NEdL) up to the maximum spectral radiance (L_{max}) given for each band (¶3.4.1). L_{max} is the expected maximum value of Earth surface reflectance plus atmospheric effects for a solar zenith angle of 22.5 degrees (¶3.3.4.1). $L_{typical}$ (or L_{typ}), the expected spectral radiance needed for a given band for a solar zenith angle of 70 degrees (¶3.3.4.1), defines the reference radiance for many other specification requirements. Some specification requirements are concerned with the effects of radiance from clouds (L_{cloud}), which can be significantly different than L_{max}, so these values are also included in Tables B-2a and B-2b. L_{cloud} is defined as the spectral radiance of a 100% reflecting Lambertian surface illuminated at a solar zenith angle of 22.5 degrees (¶3.3.3.3). The given signal to noise ratio (SNR) must be met at $L_{typical}$ and exceeded for radiances above L_{typ} (¶3.4.1). Additionally, the sensitivity goal for each band shall surpass the tabulated requirements by 36% (¶3.3.4).

Table B-2a
Radiometric Requirements for MODIS Reflective Bands

Band	Center Wavelngth	Noise Equiv. Spectral Radiance	Spectral Radiance	Max Spectral Radiance	L_{cloud}	Signal to Noise Ratio
N	λ	NEdL	($L_{typical}$)	L_{Max}		SNR
	[nm]	(*)	(*)	(*)	(*)	[unitless]
1	645	0.169	21.8	685	457	128
2	858	0.123	24.7	285	293	201
3	469	0.145	35.3	593	570	243
4	555	0.127	29.0	518	559	228
5	1240	0.073	5.4	110	138	74
6	1640	0.027	7.3	70	68	275
7	2130	0.009	1.0	22	27	110
8	412	0.051	44.9	175	573	880
9	443	0.050	41.9	133	585	838
10	488	0.040	32.1	101	539	802
11	531	0.037	27.9	82	538	754
12	551	0.028	21.0	64	528	750
13	667	0.0104	9.5	32	471	910
14	678	0.008	8.7	31	440	1087
15	748	0.017	10.2	26	373	586
16	869	0.012	6.2	16	286	516
17	905	0.060	10.0	185	252	167
18	936	0.063	3.6	256	267	57
19	940	0.060	15.0	189	244	250
26	1375	0.04	6.0	89.9	113	150

* $\frac{W}{m^2 - sr - \mu m}$

Table B-2b
Radiometric Requirements for MODIS Emissive Bands

Band	Center Wavelength	Noise Equivalent Spectral Radiance	Spectral Radiance	Max. Spectral Radiance	L_{cloud}	Required NEdT	Typical Scene Temp	Max Temp
N	λ	NEdL	($L_{typical}$)	L_{Max}		(K)	T_{typ}	T_{Max}
	[nm]	(*)	(*)	(*)	(*)		(K)	[K]
20	3750	0.000957	0.45	1.71	0.45	0.05	300	335
21	3959	0.150	2.38	86.00	0.67	2.00	335	500
22	3959	0.00190	0.67	1.89	0.67	0.07	300	328
23	4050	0.00217	0.79	2.16	0.79	0.07	300	328
24	4465	0.00218	0.17	0.34	1.44	0.25	250	264
25	4515	0.00620	0.59	0.88	1.53	0.25	275	285
27	6715	0.0108	1.16	3.21	6.87	0.25	240	271
28	7325	0.0172	2.18	4.46	8.10	0.25	250	275
29	8550	0.00899	9.58	14.54	9.58	0.05	300	324
30	9730	0.0219	3.69	6.34	9.92	0.25	250	275
31	11030	0.00701	9.55	13.25	9.55	0.05	300	324
31-hi	11030	0.247	29.1	29.08	9.55	1.00	400	400
32	12020	0.00606	8.94	12.10	8.94	0.05	300	324
32-hi	12020	0.198	25.1	25.07	8.94	1.00	400	400
33	13335	0.0183	4.52	6.56	7.94	0.25	260	285
34	13635	0.0161	3.76	5.02	7.71	0.25	250	268
35	13935	0.0141	3.11	4.42	7.48	0.25	240	261
36	14235	0.0154	2.08	2.96	7.25	0.35	220	238

(*) $\frac{W}{m^2 - sr - \mu m}$

For the thermal bands, the primary concern is temperature. The corresponding noise equivalent temperatures (NEdT), typical scene temperature (T_{typ}), and maximum scene temperatures (T_{max}) are accordingly included in Table B-2b (¶3.3.4.2). Bands 31 and 32 are non-linear and the "high" segments (from 324 K to 400 K) do not carry the same calibration requirements as the lower segments.

The Specification requires that the MODIS band output be quantized (¶3.4.3). The quantization steps must be chosen both to preserve the required signal to noise requirements and so that the quantization is linear to better than 0.5 of the least significant bit.

Given these radiometric performance requirements, the next major specification concern is the radiometric accuracy. Table B-3 presents the absolute radiometric accuracy requirements (¶3.4.5.2).

Table B-3
Radiometric Accuracy Required in the MODIS Specification

Wavelength	Required Accuracy at L_{typ}[a] ($\pm 1\sigma$, %)	Minimum Required Accuracy from $0.3 * L_{typ}$[a] to $0.9 * L_{max}$[a] ($\pm 1\sigma$, %)
< 3 μm	5	6
> 3 μm	1[b]	2
Reflectance Calibration[c]	2	3

a. Based on use of multiple samples of a uniform, extended, non-polarized source.

b. At L_{typ} Band 20 shall have minimum required radiometric accuracy of 0.75% with a goal of 0.50% and Bands 31 and 32 shall have an accuracy of 0.50% with a goal of 0.25%. The "high" ranges of bands 31 and 32 shall have an accuracy of 10%.

c. Calibration relative to the Sun using the solar diffuser plate and solar diffuser stability monitor.

These requirements are based on the use of multiple samples of a uniform, extended, non-polarized source. Spectrally, for bands below 3000 nm, a tungsten lamp-based source may be used for ground tests. For bands above 3000 nm, the source shall have a black-body profile. The Specification mandates measurements at scan angles of 0, +45, and -45 degrees. However, the requirements must be met for all cross-track angles.

The Specification also cites relative radiometric accuracy requirements. When viewing a uniform calibration target, the RMS deviation from the mean of the radiance measurements shall not be greater than the NEdL values in Tables B-2a and B-2b

(¶3.4.5.3.1). For all live channels, the calibrated mean output of each channel shall match every other channel to within the NEdL (¶3.4.5.3.2). This matching requirement does not apply to the "high" segments of the nonlinear bands. For measurement purposes, this matching condition must be met when the instrument views a uniform radiance field at levels of $0.5L_{typ}$, L_{typ}, and $2L_{typ}$ (or L_{max} if $L_{max} < 2L_{typ}$).

Additionally, the Specification requires more than one approach be used to verify calibration accuracy (¶3.4.5.1). All accuracies must be established relative to NIST standards (¶3.4.5.2). Pre-launch, the contractor will conduct an end-to end analysis (¶3.4.5.1) and measure the SNR at a minimum of three equally spaced spectral radiance levels between 0.3 L_{typ} and 0.9 L_{max}, in order to characterize the signal dependence of the system noise (¶3.4.5.5).

B.4 Spectral Band Requirements

The MODIS instrument contains 36 spectral bands spanning regions from 0.4 μm to 14.4 μm. Table B-4 presents a summary of their requirements (¶3.3.3). The Center Wavelength (CW) is defined as the wavelength midway between the 50% response points (50% of the peak spectral response, also called the band edge). Since interference filters are difficult to construct precisely, the Specification allows some tolerance in the actual location of the center wavelength, which is expressed as Center Wavelength Tolerance (CWT) in Table B-4a/b.

The Specification defines the bandwidth (BW), or passband, as the wavelength interval between the 50% response points. It too has an allowed tolerance (BWT) for construction purposes.

Besides the CW and BW, the Specification requires the shape of the spectral bands to conform to certain requirements. The edge range, defined as the wavelength interval between the 5% and 80% response points on a given side, shall not exceed 50% of the bandwidth (¶3.3.3.2). The response between the 80% points shall always exceed 80% of the peak response (¶3.3.3.4). The 1% response points shall be within 1.5 times the bandwidth from the corresponding band edge (¶3.3.3.3). These 1% response points also define the extended bandpass, which is the wavelength interval between them. The out-of-band response is the ratio of the integrated spectral response beyond the extended bandpass to that within the extended bandpass. This ratio includes both the upper and lower response wings and cannot be greater than 0.05 (¶3.3.3.3). Compliance with this out-of-band response requirement shall be determined for a source spectrum equivalent to the sum of L_{cloud} (see B.3) and an extended 300 K blackbody.

Once constructed, the instrument is expected to meet additional characterization and spectral stability requirements. On the ground, all wavelength measurements shall be made with an absolute accuracy of 0.5 nm and a precision of 0.25 nm for wavelengths up to 1 μm, and shall scale linearly with wavelength above 1 μm (¶3.4.7.5). After launch, the center wavelength and bandwidth must be stable to better than 2 nm for the visible bands

Table B-4a
Spectral Requirements for the MODIS Reflective Bands

Band	Center Wavelength	Center Wavelength Tolerance	Bandwidth	Bandwidth Tolerance
N	λ	CWT	BW	BWT
	[nm]	[nm]	[nm]	[nm]
1	645	4	50	4.0
2	858	2.2	35	4.3
3	469	4	20	2.8
4	555	4	20	3.3
5	1240	5	20	7.4
6	1640	7	24.6	9.8
7	2130	8	50	12.8
8	412	2	15	1.5
9	443	1.1	10	1.6
10	488	1.2	10	1.7
11	531	2	10	1.9
12	551	5	10	1.4
13	667	[+1, -2]	10	1.7
14	678	1	10	1.7
15	748	2	10	1.9
16	869	5	15	4.3
17	905	2.3	30	5.4
18	936	2.3	10	5.6
19	940	2.4	50	5.6
26	1375	6	30	8.0

Table B-4b
Spectral Requirements for the MODIS Emissive Bands

Band	Center Wavelength	CW Tolerance	Bandwidth	BW Tolerance
N	λ	CWT	BW	BWT
	[nm]	[nm]	[nm]	[nm]
20	3750	19	180	22.5
21	3959	20	59.4	23.8
22	3959	20	59.4	23.8
23	4050	20	60.8	24.3
24	4465	22	65	26.8
25	4515	22	67	27.1
27	6715	34	360	40.3
28	7325	37	300	44.0
29	8550	43	300	51.3
30	9730	49	300	58.4
31	11030	55	500	66.2
31-hi	11030	55	500	66.2
32	12020	60	500	72.1
32-hi	12020	60	500	72.1
33	13335	67	300	80
34	13635	68	300	81.8
35	13935	70	300	83.6
36	14235	71	300	85.4

and better than 1% of the CW for the other bands (¶3.4.7.4). This includes shifts caused by changes of humidity, temperature, pressure, vibrations, and time.

B.5 Geometric Requirements

In addition to radiometric and spectral requirements, the MODIS Specification mandates specific requirements on the geometry of the earth view. These are primarily IFOV size requirements, coregistration requirements, and pointing knowledge requirements.

The primary geometric requirement is the instantaneous field of view (IFOV). IFOV is the combination of focal length and detector size which results in measuring a predetermined area on the Earth's surface at nadir from the nominal 705 km altitude. This area is measured at the 50% system response points and where the signal is sufficient to meet the SNR requirement (¶3.3.1). Table B-5 gives the along-track IFOV at nadir.

Table B-5
Geometric Requirements

Spectral Band	IFOV
1-2	250 m
3-7	500 m
8-36	1000 m

These are also the Ground Sample Distance (GSD) values, defined as the distance as measured on the ground between adjacent samples. The tolerance is +0/-6% in the along-track direction. In the cross-track direction, the distance traversed by the IFOV during sample integration must equal the GSD. Within a band, each detector must have an IFOV that does not differ from the mean by more than +/- 5% in either dimension (¶3.3.1). Within an , the response in the central 80% of each channel shall not vary by more than +/- 20% of the mean. The contractor is required to measure the system response in the along-track direction to a resolution of at least 10% of its width (¶3.4.5.4).

The Specification mandates close coregistration for corresponding detector elements from different spectral bands. For two elements with the same IFOV, the coregistration shall be within +/- 20% of an IFOV, with +/- 10% of an IFOV as a goal, in both the cross-track and along-track directions (¶3.4.6.3). For spectral bands having different IFOV's, four 500 m pixels and sixteen 250 m pixels shall overlay the corresponding 1000 m pixel at nadir to within 200 m (+/-20% of the 1000 m pixel), with 100 m as a goal. The contractor shall build in a commandable adjustment of the cross-track registration between focal planes, for both ground based and in-orbit registration corrections. The resolution of this adjustment shall be better than 25 meters (¶3.4.6.3). The relative alignment of all spectral bands shall remain within specification following any qualification level testing, launch, and in-orbit operation (¶3.4.6.2).

The instrument shall scan the IFOV +/- 55 degrees cross-track about nadir, using a method which does not introduce any image rotation (¶3.3.2).

To ensure geolocation accuracy (Appendix E), the Specification requires that an alignment reference cube be mounted on the MODIS instrument (¶3.4.6). The alignment of the instrument optical axis with respect to the instrument references and instrument mounting surfaces shall not change by more than 60 arc seconds (¶3.4.6.2). The knowledge of the angular location of each with respect to the reference cube shall be 30 arc seconds (each axis, ±1-sigma) at all scan angles. The contractor will supply an algorithm to relate this knowledge to a cube on the spacecraft mounting structure (¶3.4.6.1). Appendix E discusses pointing requirements and geolocation in greater depth.

B.6 Other Performance Requirements

While the radiometric, spectral, and geometric requirements are the primary concerns for MCST's characterization and calibration activities, several other performance requirements are also significant. Polarization and Modulation Transfer Function (MTF) spreading will both affect the radiometric accuracy. Crosstalk, Stray Light, and the Transient Response not only affect the radiometry, but degrade the imaging ability. This section addresses all five of these performance requirements.

If the instrument polarizes the light before it hits the detectors, interference fringes can result which will introduce noise. The Specification requires MODIS spectral bands 1 to 19 to be insensitive to linear polarization (¶3.3.5). The polarization factor, defined as

$$PF=(Imax - Imin) / (Imax + Imin)$$

shall be less than 0.02 for wavelengths from 0.43 μm to 2.2 μm and over scan angles of +/- 45 degrees. The contractor is required to provide an analytical end-to-end polarization model as part of the radiometric math model (see B-7). The contractor must map the magnitude and direction of the polarization sensitivity for bands 1 to 19 over the full range of angles. This mapping may combine measurements for at least 16 representative bands, including bands 9 through 17, with interpolation for the other bands. The polarization model must account for these measurements.

The Modulation Transfer Function (MTF) characterizes how the instrument resolves structured scenes. High spatial frequencies are attenuated or cut out, resulting in a blurring of the image. This blurring, or spreading, can have strong radiometric implications (light on one side of a bright edge bleeds into the other).

Therefore, the Specification requires the instrument system to satisfy or exceed the MTF requirements (¶3.4.2) presented in Table B-6.

Table B-6
Modulation Transfer Function (MTF) Requirements.

Frequency/Nyquist Frequency	MTF
0.00	1.0
0.25	0.9
0.50	0.7
0.75	0.5
1.00	0.3

The Nyquist frequency has a spatial period equal to two IFOV's on the ground. This MTF shall be met for both the along-track and cross-track directions for a sine wave input. It shall be met for modulations from dark to L_{typ} and dark to L_{max}, and shall be achieved for every channel of every band. The contractor is required to measure the MTF at representative points in the VIS, NIR, SWIR, MWIR, and LWIR regions.

Electronic crosstalk occurs when portions of the signal on one detector show up in the output of others. The Specification (¶3.4.5.3.3) requires that the response of a given detector element (the sender) shall not cause an apparent change in the response of any other detector element (the receiver) that is greater than one least significant bit (1-sigma), when the signal on the sender is equivalent to L_{typ} and the signal on the receiver is zero. This is based upon 12 bits for bands 1 to 32 and 10 bits for bands 33 to 36 (even though current design is 12 bits for all bands). This effect is measured as an increase above the crosstalk associated with photogenerated charge diffusing through the bulk of the detector material. Crosstalk requirements do not apply during transient radiation events. Additionally, other coherent noise mechanisms that lead to structured patterns in the output data (e.g., herringbone or diagonal bars) shall be imperceptible in data taken at the L_{typ} radiance levels for each spectral band. This will be verified by two-dimensional pictorial display tests used on representative bands.

The Specification requires MODIS to reject unwanted scattered and diffracted radiation which affects the radiometric accuracy (¶3.4.8.1). Stray light shall be restricted from entering any of the ports and from causing any degradation in the performance of a radiative cooler. In an operational, nadir-facing attitude, the instrument response to any stray light striking the instrument on any surface outside the FOV, from any angle, shall be less than $0.01L_{typ}$, when the incident radiance is L_{typ}. For compliance testing, the test sources shall have an intensity and view-factor sufficient to yield irradiance levels at any surface equal to the maximum solar irradiance for any spectral interval within the entire MODIS spectral range.

Additionally, the Specification mandates three specific stray light tests for cases within the instrument FOV. The first two, Bright Target (¶3.4.8.2) and Dark Target (¶3.4.8.3), apply to the VIS and NIR bands. The Bright Target test has MODIS viewing a 21 x 21 bright target,

which is surrounded by a dark background. The target is at L_{max} and the background is at L_{typ}. The background is then changed while the center pixel in the target is monitored. When the background is raised to L_{cloud}, the center pixel's radiance shall change by no more than $0.004L_{cloud}$. Figure B-1 demonstrates the geometry of this test.

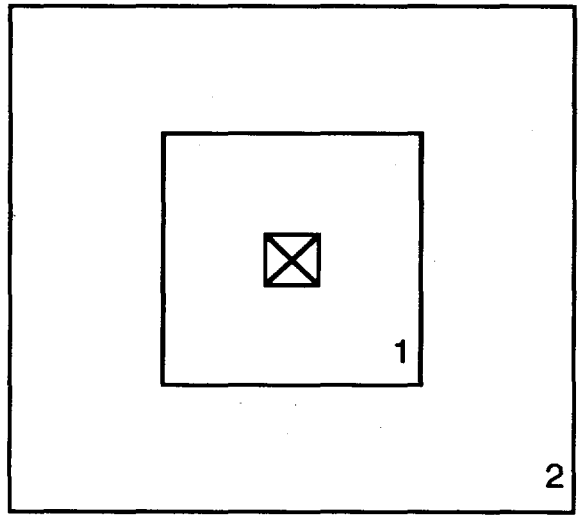

Figure B-1 Stray Light Tests

The target (region 1) is 21 x 21 IFOV for VIS/NIR and 5 x 5 for the Thermal regions. The background (region 2) is changed as the center pixel (the x) is monitored.

The Dark Target test uses the same geometry, with MODIS viewing a 21 x 21 IFOV dark target surrounded by a bright background. This time the target is at L_{typ} and the background is at L_{cloud}. Again, the background is then changed while the center pixel in the target is monitored. When the background is lowered to $0.2L_{max}$, the center pixel's radiance shall change by no more than $0.004L_{cloud}$.

For the thermal bands, the stray light test, Warm Target (¶3.4.8.4), is very similar to the Bright Target test. The test has MODIS view a 5 x 5 IFOV target at L_{typ}, which is surrounded by a background at $0.1L_{typ}$. The center pixel shall change by no more than 1% when the background radiance is increased to L_{typ}.

Finally, the transient response specification (¶3.4.4) sets the requirement for recovery after scanning across a bright target. When the instrument scans across a steep gradient from a maximum radiance of L_{cloud} (L_{max} for the thermal bands), to a minimum of $L_{typical}$, the output signal shall have less than a 1% overshoot and shall settle to within 0.5% of its final value within 2 km. Figure B-2 illustrates the allowed response envelope.

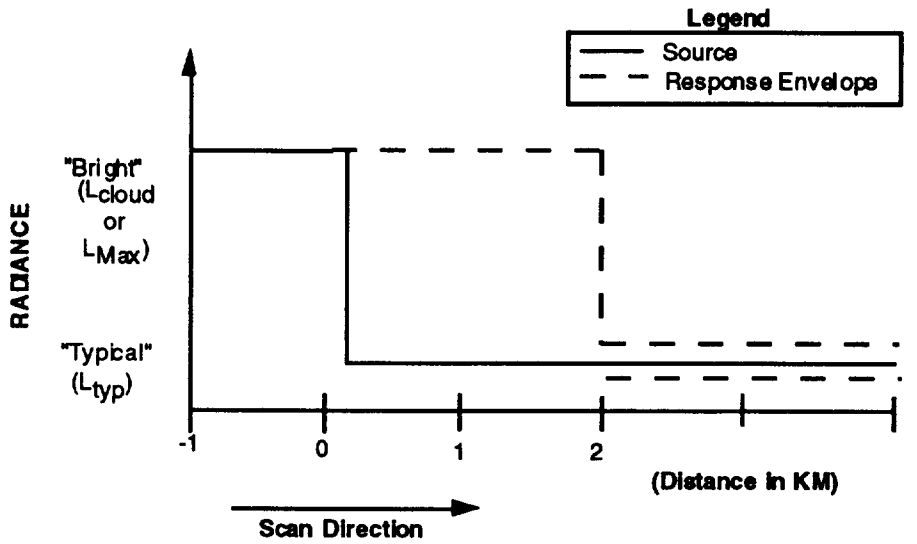

Figure B-2 Transient Response Requirement

The Transient Response Specification requires the instrument to be within +/- 0.005Ltyp of its final value after 2 km. The response envelope shows the allowed radiance values.

B.7 Remaining Specification Requirements

In the interests of completeness, this section presents a summary of the remaining specification requirements. Of relevance to MCST's activities are the In-Flight Calibration requirements, Model requirements, and Pre-Launch Verification and Calibration Requirements. Additionally, the Specification discusses operational modes, communication requirements, software requirements, Ground Support Equipment requirements, and several miscellaneous requirements. These are briefly summarized below--the reader is referred to the Specification if more detail is desired about these items.

The Specification (¶3.4.9) requires an in-flight calibration system, including necessary algorithms. This section therefore drives the design of the On-Board Calibrators. Specifically, the Specification mandates end-to-end calibration, with all absolute radiometric calibration sources filling the aperture. The instrument will provide in-flight radiometric calibration from $0.3L_{typ}$ to $0.9L_{max}$ for all bands (¶3.4.9.1). It shall include a solar diffuser and a solar diffuser monitor for reflectance calibration (¶3.4.9.3). MODIS will carry an in-flight wavelength calibration capability that shall be able to detect a 1 nm shift with a precision of 0.5 nm in its shortest wavelength band. For all wavelengths up to 1 μm, the detectable shifts and measurement precision shall scale with wavelength (¶3.4.9.2). Additionally, provisions shall be made for using the moon for a calibration source (¶3.4.9.4) and for calibrating the electronic response at appropriate points (¶3.4.9.5).

The contractor must deliver several instrument models to NASA (¶3.1.4). Three math models (radiometric, thermal, and structural), must all be maintained and updated (including experimental data when available) throughout the life of the contract. The

radiometric math model (RMM) (¶3.1.4.1) covers the end-to-end radiometric performance of the instrument including sensitivity analyses and error source identification. It will include all on-board and preflight ground laboratory calibration algorithms and data, which are deliverables to GSFC (¶3.1.4.1). The Thermal (¶3.1.4.2) and Structural Math Models (¶3.1.4.3) must similarly be verified before delivery to GSFC. The contractor is also required to build a Structural Model (¶3.1.4.4) and Engineering Model (¶3.1.4.5) for testing purposes. The Protoflight Model (¶3.1.4.6) and two Flight Models (¶3.1.4.7) shall be launched.

The Specification also contains several verification and calibration requirements to be fulfilled before the instrument is accepted (¶5.0). The contractor shall prepare and maintain a Verification Plan (¶5.1.1), Verification Specifications (¶5.1.2) and Verification Procedures (¶5.1.3). These are designed to demonstrate that the Specification requirements and all calibration accuracy requirements are being met (¶5.1). For calibration, a Calibration Management Plan (¶5.1.4) and Calibration Procedures (¶5.1.5) must be submitted for NASA review and approval. All Test and Calibration data (¶5.1.6) will be provided, and the Verification and Calibration Management Plans shall be controlled documents after acceptance (¶5.1.8). Finally, the contractor shall provide and maintain software to monitor critical functions, provide alarms as necessary, and shut down the instrument if the operator does not take corrective action (¶5.1.7).

The Specification provides more detail on specific environmental and calibration test requirements. Testing environments shall include both ambient and vacuum conditions (¶5.2) and shall be performed in accordance with all relevant NASA documents (¶5.3). The MODIS Technical Officer will appoint representatives to oversee all calibration procedures performed by the contractor (¶5.4.1). These calibration tests will include specified sources (¶5.4.2.1), temperature plateaus (¶5.4.2.2), linearity tests (¶5.4.2.3), diffuser spectral calibration (¶5.4.2.4), software (¶5.4.2.5), calibration fixtures (¶5.4.3), and temperature and voltage monitors (¶5.4.4). A history of all test data shall also be supplied (¶5.5).

Several operational modes are defined by the Specification (¶3.2.2). These are listed in Table B-7. The contractor shall recommend the instrument configuration for each of these modes.

The Specification also addresses several communication requirements. The instrument shall accept ground commands via the platform (¶3.5.1) and transmit data back in an appropriately formatted data stream (¶3.5.2). The data rate shall not exceed 10.8 Mbps (¶3.5.2.1). Telemetry data to monitor the instrument health and status will be included in the data stream (¶3.5.3).

The contractor shall provide all software necessary to operate, test, calibrate, design, and analyze the instrument (¶4.1). This includes data processing software (¶4.1.1), instrument-based software/firmware (¶4.1.2), software for operations analysis (¶4.1.3), a command list (¶4.1.4), and instrument ground software (¶4.2).

The Specification requires the contractor to provide and maintain all Ground Support Equipment (GSE) throughout the duration of the contract (¶6.1). This includes the System Test Equipment (STE), which shall be able to operate the instrument during all testing at the contractor's facility and record all received data (¶6.3), equipment for ambient operation (¶6.4) and ancillary equipment (drill template and handling fixtures) (¶6.5).

Finally, the Specification covers several miscellaneous instrument requirements. The contractor must include provisions to decontaminate the radiant cooler (¶3.4.10.1), identify and document sensitive parts and instrument limitations (¶3.4.10.2), and provide witness mirrors to check contamination (¶3.4.10.3). All desired details on these other specification requirements can be found in the Specification itself.

Table B-7
Operational Modes

Operational Mode	Instrument Status
Launch and Orbit Acquisition	monitor health and safety
Outgassing	protect vs. contamination
Activation	turn-on and warm-up
Mission	normal operation
Day Mode	full operating mode
Night Mode	thermal bands only
Solar Calibration	solar diffuser deployed
Lunar Calibration	view moon
Spectral Calibration	SRCA operates
Survival (Emergency Off)	minimum power

B.8 Summary

This Appendix discussed the Specification requirements in detail as they relate to characterization and calibration. Beyond the basic instrument requirements, the primary calibration concerns are radiometric, spectral, and geometric performance and accuracies. Additional performance requirements, such as MTF and stray light, will affect the calibration and so must be met as well. For completeness, this appendix also summarized the remaining specification requirements. These requirements serve as the starting point for MCST's calibration activities.

Appendix C

Instrument Design

The Moderate Resolution Imaging Spectroradiometer (MODIS) is an Earth observation instrument that will be carried on six of the Earth Observing System (EOS) satellite platforms to provide atmospheric, terrestrial, and oceanic observations of the complete Earth during the 15 year lifetime of the EOS program. The spatial resolution of the instrument and the specific spectral bands that the instrument uses for observations were chosen to optimize the scientific returns of

Table C-1
MODIS VIS/NIR/SWIR Spectral Bands

Band	λ (nm)	IFOV (m)	Δλ (nm)	Purpose (Examples)
Land and Cloud Boundaries Bands				
1	648	250	50	Veg Chlorophyll Abs Land Cover Trans.
2	858	250	35	Cloud and Vegetation Land Cover Trans.
Land and Cloud Properties Bands				
3	469	500	20	Soil, Vegetation Differences
4	555	500	20	Green Vegetation
5	1240	500	20	Leaf/Canopy Differences
6	1640	500	24.6	Snow/Cloud Differences
7	2130	500	50	Land and Cloud Properties
Ocean Color Bands				
8	412	1000	15	Chlorophyll
9	443	1000	10	Chlorophyll
10	488	1000	10	Chlorophyll
11	531	1000	10	Chlorophyll
12	551	1000	10	Sediments
13	667	1000	10	Sediments, Atmosphere
14	678	1000	10	Chlorophyll Fluorescence
15	748	1000	10	Aerosol Properties
16	869	1000	15	Aerosol/Atmospheric Properties
Atmosphere/Cloud Bands				
17	905	1000	30	Cloud/Atmospheric Properties
18	936	1000	10	Cloud/Atmospheric Properties
19	940	1000	50	Cloud/Atmospheric Properties

Table C-2
MODIS MWIR/LWIR Spectral Bands

Band	λ (μm)	IFOV (m)	Δλ (nm)	Purpose (Examples)
Thermal Bands				
20	3.75	1000	180	Sea Surface Temperature
21	3,959	1000	59.4	Forest Fires/Volcanoes
22	3,959	1000	59.4	Cloud/Surface Temperature
23	4.05	1000	60.8	Cloud/Surface Temperature
24	4,465	1000	65	Tropospheric Temperature/Cloud Fraction
25	4,515	1000	67	Tropospheric Temperature/Cloud Fraction
26	1,375	1000	30	Tropospheric Temperature/Cloud Fraction
27	6,715	1000	360	Mid-Tropospheric Humidity
28	7,325	1000	300	Upper-Tropospheric Humidity
29	8.55	1000	300	Surface Temperature
30	9.73	1000	300	Total Ozone
31	11.03	1000	500	Cloud/Surface Temperature
32	12.02	1000	500	Cloud Height & Surface Temperature
33	13,335	1000	300	Cloud Height & Fraction
34	13,635	1000	300	Cloud Height & Fraction
35	13,935	1000	300	Cloud Height & Fraction
36	14,235	1000	300	Cloud Height & Fraction

the instrument data. Atmospheric and oceanic phenomena are often not sharply localized in space and an instrument spatial resolution of 1 km was chosen to meet the general needs of atmospheric and oceanic scientists. Certain terrestrial phenomena may be more sharply localized, and instrument resolutions of 500 and 250 m were provided in a few spectral bands to meet the particular needs of terrestrial scientists. Each of the spectral bands used for instrument observations was chosen to meet at least one or more specific scientific measurement objectives. Wavelengths ranging from the middle visible (415 nm) to the longwave infrared (14.24 microns) were chosen; in all, 36 spectral bands were selected. Tables C-1 and C-2 show the spectral band designations, wavelengths, Instantaneous Field of View (-resolution), spectral passband width, and representative scientific applications for the MODIS spectral bands.

The MODIS instrument scans in a cross-track direction (perpendicular to the platform velocity vector) using a rotating, double-sided scanning mirror with constant angular velocity, as depicted schematically in Figure C-1. The afocal telescope assembly and other instrument components at the right of the figure receive and process the image reflected from the scanning mirror. Earth observation data is collected only when the scan is within +/- 55 degrees of nadir. The other components in the mirror scan arc are on-board calibration sources that

are outside the Earth scan limits. On-board calibration sources include a solar diffuser plate illuminated by the sun; a solar diffuser stability monitor (SDSM) that compares reflections from the solar diffuser with attenuated direct solar input in order to monitor potential changes in solar diffuser reflectivity; a spectroradiometric calibration assembly (SRCA) that provides radiometric, spectral, and spatial instrument calibration using internal calibration lamps and an internal infrared source; a calibrated blackbody source of infrared radiation; a direct view of cold space through a Space Viewport; and an occasional view of the Moon when it happens to be visible in the Space Viewport. An external view of the instrument is given in Figure C-2. The physical arrangement of the scanning mirror, the afocal telescope assembly (includes
the fold mirror, the primary mirror, and other components not visible behind the back panel in the figure) and on-board calibration sources in the instrument scan cavity is shown in Figure C-3. The data collection and processing sequence for a half-rotation of the scan mirror is represented schematically in Figure C-4. The number of data frames collected during each portion of the scan is listed in Table C-3.

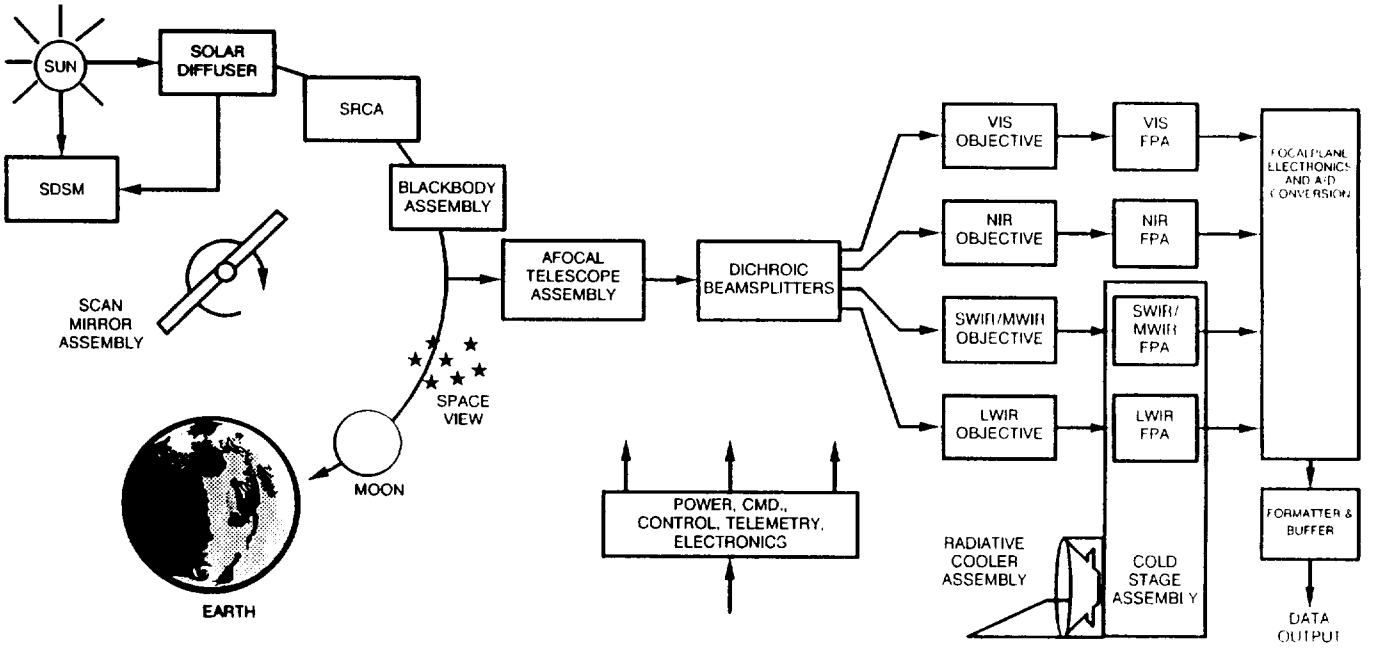

Figure C-1. Conceptual Representation of the MODIS Instrument

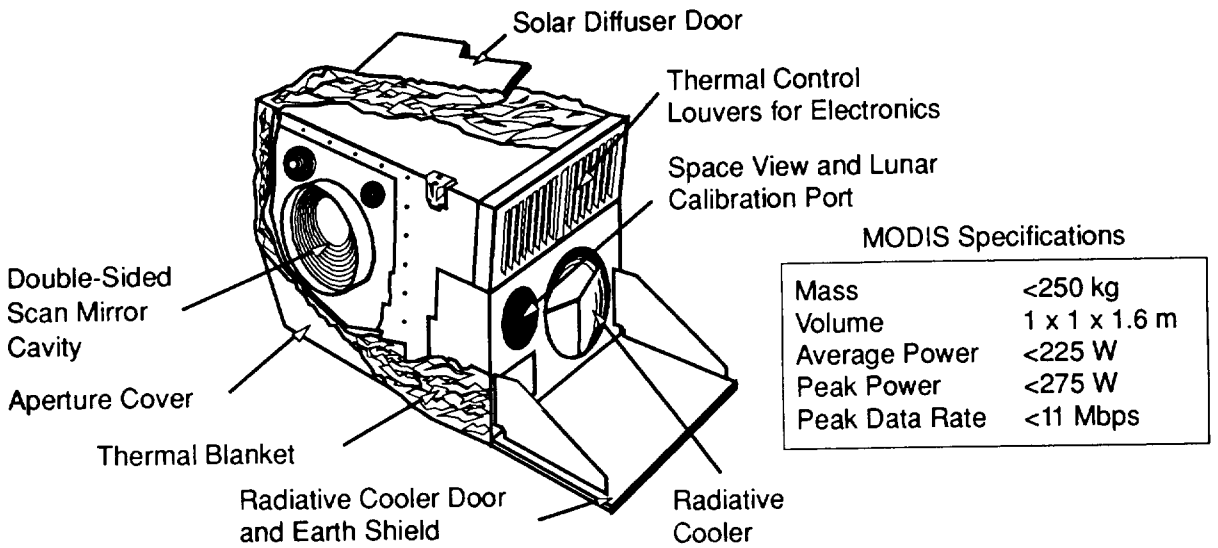

MODIS Specifications

Mass	<250 kg
Volume	1 x 1 x 1.6 m
Average Power	<225 W
Peak Power	<275 W
Peak Data Rate	<11 Mbps

Figure C-2. External View of the MODIS Instrument

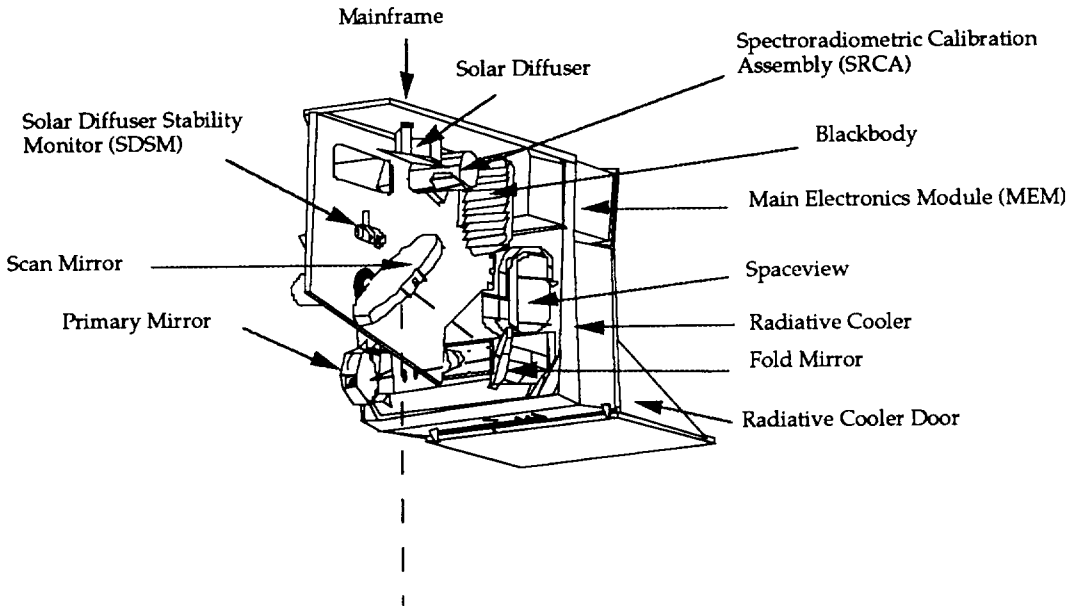

Figure C-3 Physical Arrangement of MODIS Components in the Scan Cavity

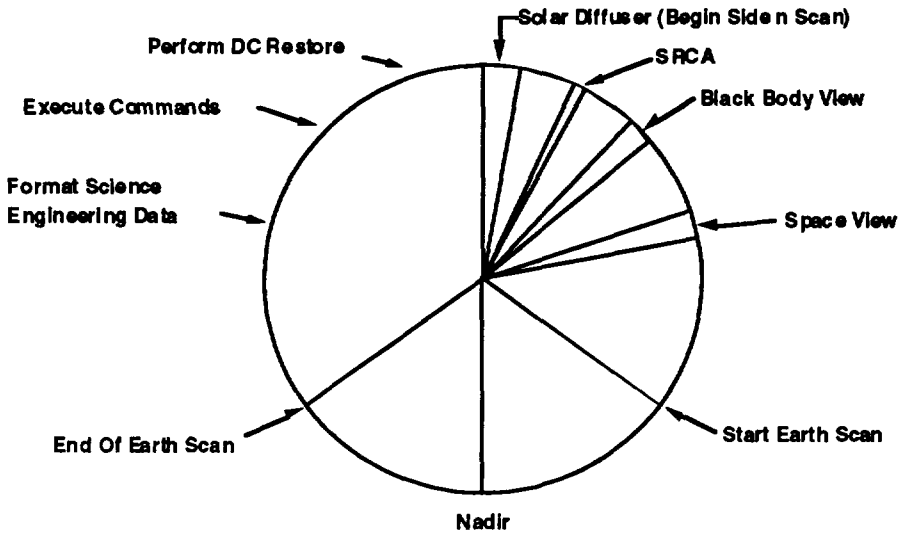

Figure C-4. Data Collection and Processing Sequence for One Scan

Table C-3
Frames of Transmitted MODIS Data Per Scan (as of August,1993)

View	Center Frames	Total Frames	Comments
SD	30/50	50	30 when SD open, 50 for electronic cal.
SRCA	6	10	4 for tolerance
BB	30	50	20 for ghosting analysis
SV	16	50	30 for ghosting, 4 tolerance
Earth	1354		
Engineering	1	1	housekeeping info
Memory Dump	1	1	data package info

As depicted in Figure C-1, the afocal telescope assembly transmits a beam to a series of dichroic beam splitters that split the beam into four separate beams, each in a distinct wavelength domain: visible (VIS), near infrared (NIR), short wave infrared/middle wave infrared (SWIR/MWIR), and long wave infrared (LWIR). The afocal telescope assembly uses only reflective components with optical properties that do not strongly depend on wavelength. The imaging process is completed using four separate refractive objectives with optical properties tailored to the individual wavelength domain. The images are focused onto four distinct focal plane assemblies (FPAs), each with detective elements tailored to the needed observations in the designated wavelength domain. The interference filters that provide the spectral bandpass characteristics for the observations are located just above the detector elements on the focal plane assemblies. The physical layout of the filters and the detector elements is shown in Figure C-5. To simplify the timing of detector readouts, detector elements are separated by a whole number of 1-km element spaces. A total of 490 detector elements is available; two sets of detectors are provided for bands 13 and 14. These dual detector elements are operated in time delay and integration (TDI) mode to enhance radiometric performance. Only 470 detector readout data elements are transmitted to the ground. As shown in Figure C-1, the SWIR/MWIR and LWIR focal plane assemblies are cooled to at least 85 degrees Kelvin using the radiative cooler assembly.

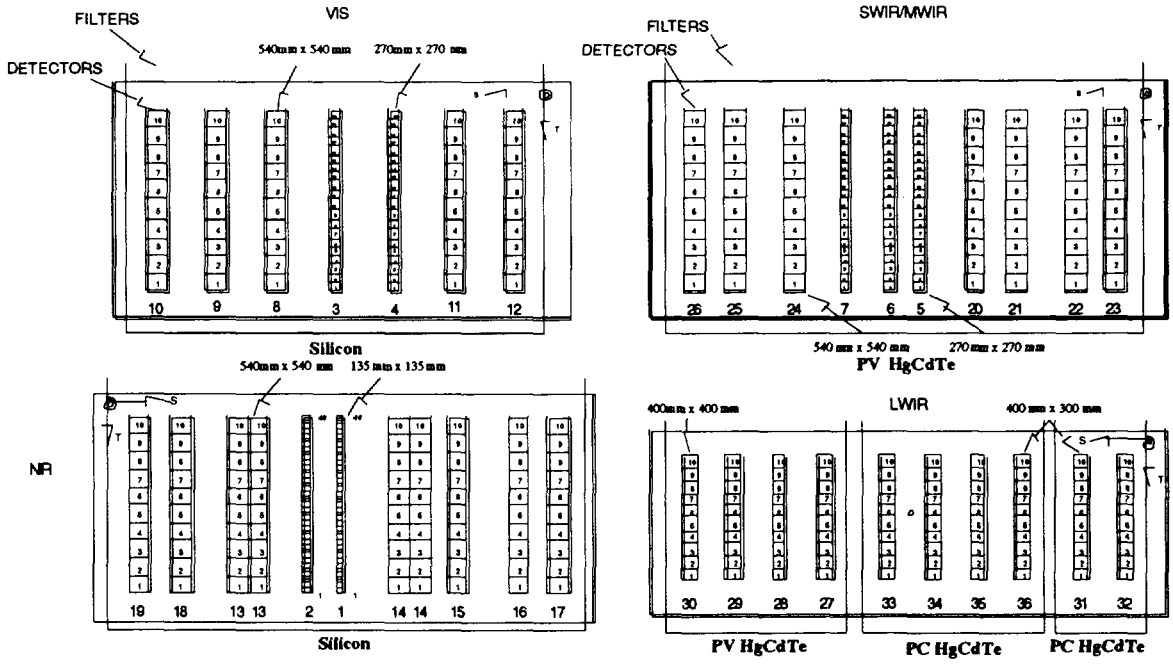

Figure C-5. MODIS Focal Plane Assemblies

To minimize detector lead lengths and maintain signal-to-noise ratio, detector outputs are amplified very close to the detector sites (long detector leads could pick up cross-talk or electromagnetic interference). Outputs from all the detectors are then multiplexed through a programmable analog amplifier that applies an adjustable gain and offset to each sample (operates at better than 12-bit accuracy). Detector output signals are then ready for analog-to-digital (A/D) conversion.

Since 1/f noise in the photoconductive (PC) detectors can cause detector output to drift beyond the dynamic range of the preamplifiers, the dynamic range of the detectors is maintained using a DC-restore process that applies a voltage offset based on detector output while viewing the blackbody. DC-restore voltages are applied to all detectors in all bands and force the detector output to a specified or proper level while viewing the blackbody. As a consequence, all visible bands will give the same relatively low output while viewing the blackbody, and all thermal bands will give the same (or nearly the same) constant output level corresponding to the blackbody temperature (approximately 293 degrees Kelvin). Figure C-6(a) shows the apparent or corrected detector output for two different amplifier gains in the visible bands; note that these two curves intersect on the left at a value corresponding to the slight radiance of the blackbody in the visible region. Corresponding curves for thermal detectors are shown in Figure C-6(b). In this case, the curves are forced to agree at the nominal temperature of the blackbody and the curves for different amplifier gains intersect at the output corresponding to that nominal temperature.

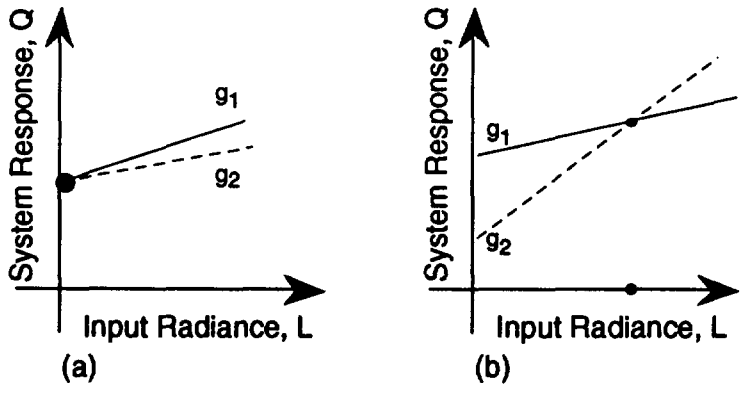

Figure C-6. System Response to Alternative Gains g1 and g2 in the Visible Bands (a) and in the Thermal Bands (b)

Digital output from the A/D converters is buffered and prepared for transmission to Earth in CCSDS-formatted data packets. Because of the spatial offsets between the detectors for the various spectral bands on the focal plane assemblies, data for all the spectral bands corresponding to a given physical pixel on the Earth are not acquired sequentially. To facilitate ground-based processing and minimize the potential effects of lost data packets, data in a CCSDS packet will be arranged in band sequential order, and thus data rearrangement is required from the on-board data

system. The MODIS instrument is equipped with a small computer that performs this function.

The on-board calibration sources shown on the left side of Figure C-1 provide a set of known or calculable radiance sources that can be used to determine instrument responsivity. We shall discuss each of these on-board calibration sources in turn.

The solar diffuser is a flat Spectralon plate that can be illuminated by the Sun to provide a calculable radiance source in the visible, near infrared, and shortwave infrared bands. To eliminate stray radiation from the Earth (Earthshine) on the solar diffuser during calibration periods, calibration using the solar diffuser is done only when the platform is near the solar terminator and the instrument itself is illuminated by the Sun but the Earth below the platform is dark. The solar diffuser will provide two calibration levels, a high level obtained using full solar illumination on the diffuser, and a low level, obtained using an 8.5 percent solar transmission screen over the solar entrance aperture. The solar diffuser entrance aperture is also equipped with an opaque door that eliminates all direct solar radiation on the diffuser plate during most of the orbit period. This door reduces the exposure of the solar diffuser to potentially degrading solar ultraviolet radiation. The MODIS instrument will be mounted at the forward edge of the EOS spacecraft to provide a good view of the sun during solar terminator crossings.

The solar diffuser stability monitor (SDSM) provides information on potential changes in the solar diffuser reflectance by comparing the apparent radiance of the solar diffuser with that of an attenuated solar disk. The SDSM uses a rotatable mirror to alternately view the Sun (through a 2 percent transmission filter) or the solar diffuser. The beam from the mirror is directed into an integrating sphere that contains an array of twelve spectrally filtered detectors. Potential changes in solar diffuser reflectivity can be monitored in each of the twelve spectral regions corresponding to the twelve detectors.

The spectroradiometric calibration assembly (SRCA) uses internal incandescent lamps and a built-in blackbody as radiation sources. Four operating modes are provided:

(1) a radiometric mode that uses calibration lamps, and infrared source and collimating optics to provide a known radiance source in the visible and near infrared.

(2) a spectral calibration mode that uses a grating monochromator (rotating spectral gratings and collimating optics) to provide a temporally varying monochromatic calibration source in the visible and near infrared. Instrument response to one new wavelength can be tested during each rotation of the scan mirror.

(3) a spatial registration mode in which the combined output of a visible/near infrared source lamp and the internal blackbody is transmitted through a reticle

pattern positioned at the focus of the collimating optics to produce an image of the reticle on the MODIS focal plane assemblies. The reticle image provides a known spatial target from which the relative registration of MODIS pixels within a spectral band and between different spectral bands can be obtained. The spatial registration mode of the SRCA will monitor compliance with the 0.2 IFOV band-to-band registration requirement.

(4) an SRCA self-calibration mode that uses a didymium filter, diffraction gratings, and a photodiode to measure the internal stability of the SRCA in the visible and near infrared bands. This is the SRCA self-test mode.

Figure C-7 shows a schematic representation of SRCA calibration functions. The actual hardware implementation of these functions is depicted in Figure C-8. The SRCA provides only a partial aperture source for the MODIS instrument.

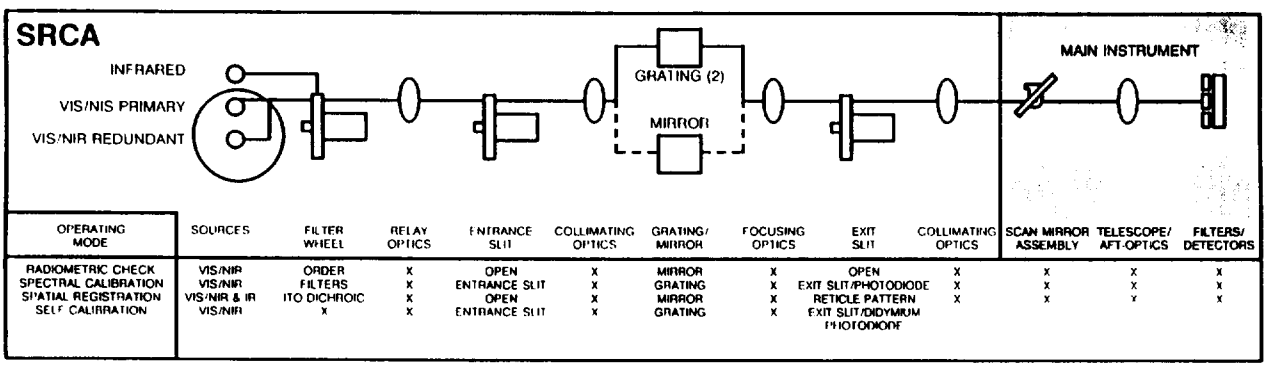

OPERATING MODE	SOURCES	FILTER WHEEL	RELAY OPTICS	ENTRANCE SLIT	COLLIMATING OPTICS	GRATING/ MIRROR	FOCUSING OPTICS	EXIT SLIT	COLLIMATING OPTICS	SCAN MIRROR ASSEMBLY	TELESCOPE/ AFT-OPTICS	FILTERS/ DETECTORS
RADIOMETRIC CHECK	VIS/NIR	ORDER	X	OPEN	X	MIRROR	X	OPEN	X	X	X	X
SPECTRAL CALIBRATION	VIS/NIR	FILTERS	X	ENTRANCE SLIT	X	GRATING	X	EXIT SLIT/PHOTODIODE	X	X	X	X
SPATIAL REGISTRATION	VIS/NIR & IR	ITO DICHROIC	X	OPEN	X	MIRROR	X	RETICLE PATTERN	X	X	X	X
SELF CALIBRATION	VIS/NIR	X	X	ENTRANCE SLIT	X	GRATING	X	EXIT SLIT/DIDYMIUM PHOTODIODE				

Figure C-7. Schematic Representation of SRCA Calibration Functions

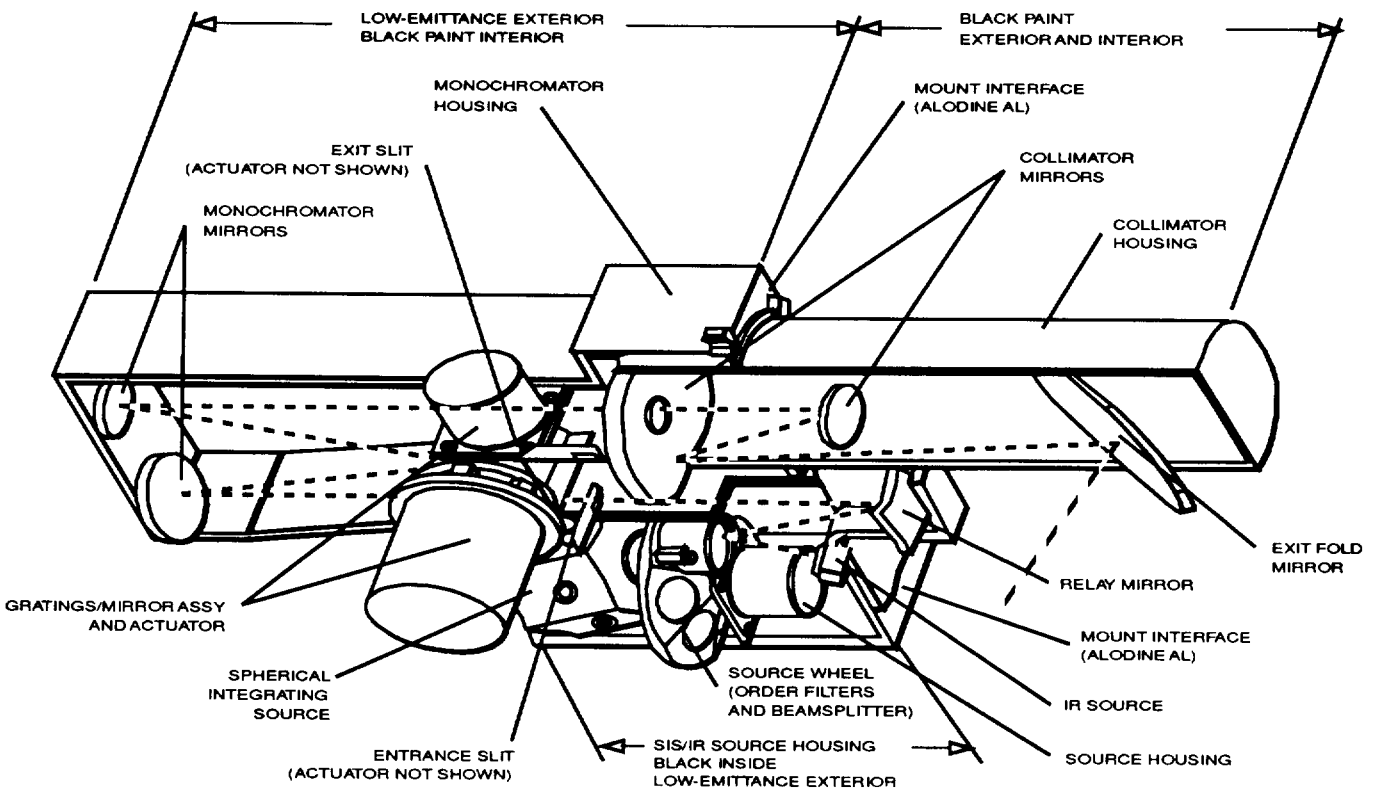

Figure C-8. MODIS Spectral Radiometric Calibration Assembly

Since the solar diffuser can be used only once per orbit (at the terminator crossing), the internal calibration lamps in the SRCA provide an essential measurement of diurnal effects on radiometric stability. SRCA calibration functions can be activated at any point in the orbit. Also, since the absolute radiation output of the SRCA, measured in SI radiometric units, can be established directly in the laboratory before the instrument is launched, the SRCA provides an essential link to absolute or SI-referenced radiometric units during on-orbit operation. The MODIS instrument itself can serve as a transfer radiometer for the transfer of an SI-referenced measurement scale from the SRCA to the solar diffuser plate. Without this reference, solar diffuser radiance in the space environment would be known only relative to solar output.

Experience with spectral filters developed for the Enhanced Thematic Mapper has shown dramatic and largely unexplained shifts in filter transmission when the filters are moved from normal ambient test conditions to the thermal vacuum environment. The spectral calibration mode of the SRCA will provide a means to monitor long-term spectral filter behavior in the space environment.

The on-board blackbody calibrator provides full-aperture thermal calibration in the middle and longwave infrared bands. Two blackbody modes are provided: a normal

calibration mode in which the blackbody temperature floats to equilibrium in the instrument cavity (280-290K) and an elevated temperature mode (315K) in which blackbody temperature is maintained by a Kapton film heater bonded to the blackbody back surface. Volume and weight constraints for the instrument preclude the use of a traditional cavity-type blackbody. As a result, the calibration blackbody is an open, flat plate inscribed with horizontal v-grooves to improve the effective emissivity in the look direction of the MODIS scan mirror. The thermal bands (wavelength greater than 3 μm) must be calibrated to 1 percent absolute uncertainty or better (see Appendix C) and temperature monitoring and control to within 0.1 degree is required to achieve the required accuracy. Twelve electronic temperature sensing devices, each monitoring a "zone" of the blackbody, are embedded beneath the blackbody surface. In the elevated temperature mode, an on/off heater controller is used to maintain the desired temperature to within a 0.02 degrees. Blackbody calibration of the middle and longwave MODIS bands can be achieved once in each instrument scan period. As discussed above, detector output while viewing the blackbody source will be used as a DC-restore reference for all MODIS bands, including those in the visible region.

MODIS calibration also includes a Space View through a port on the starboard side of the instrument. During most MODIS observation periods, the port will view cold space. Detector outputs for these views can be used to establish instrument response levels to unavoidable internal stray radiation when no significant external radiation is present. A measurement of the instrument response corresponding to no external input is essential for determining the slope and intercept of the radiometric response curve. Occasionally, the moon will be visible through this port, and observations obtained during these periods can be used to obtain a lunar calibration of the instrument as well. Space port views are available during each instrument scan period.

Appendix D

MODIS Calibration Strategy

D.1 Overview of Calibration Strategy

The major information sources available for MODIS characterization and calibration are shown in Figure D.1-1. All theses sources are ultimately applied to developing and implementing a calibration algorithm, which converts digital numbers from the instrument into geolocated radiances at the instrument aperture. The instrument calibration algorithm will be comprised of a set of mathematical equations and a set of parameters to be used in the equations. Changes in the basic mathematical structure of the equations will occur infrequently; changes in the specific parameter values to be used in the equations may occur with more regularity and will be checked for on each orbit. If orbital repetition patterns or other repeatable or predictable phenomena become apparent in required parameter adjustments, a mathematical extension of the model to include the observed phenomena may be possible. Initially, the model will likely include few such extensions; the instrument mathematical model may grow in complexity as experience with the instrument increases.

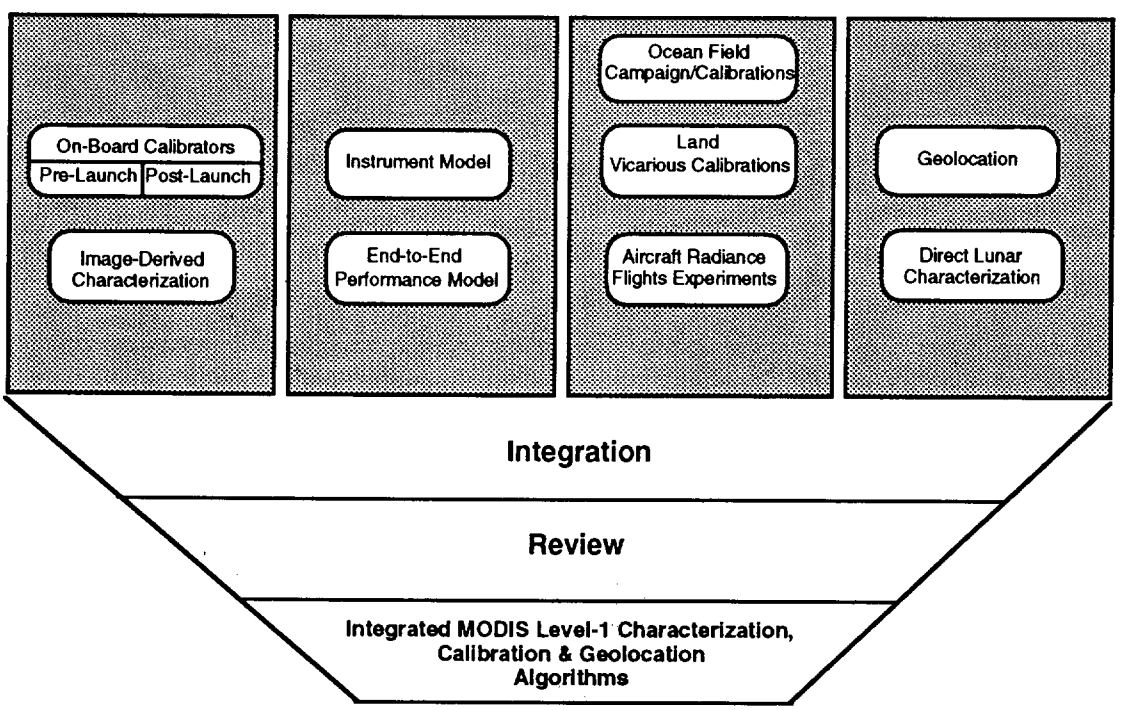

Figure D.1-1. MODIS Characterization and Calibration Data Sources

The End-to-End Performance Model referred to in Figure D.1-1 will relate MODIS calibration accuracy to MODIS science product accuracy. Such a model will initially be helpful in establishing error bar limits for science products. It will also determine what products need to be re-processed if the calibration changes in retrospect. Once the relationship of science product errors to instrument calibration errors become clear, the model may also help to generate potential calibration anomaly alerts based on observed science product anomalies.

The initial calibration baseline will be established using On-Board Calibrator (OBC) systems built into the instrument. A schematic diagram showing components of the OBC is given in Figure D.1-2. Calibration may be referenced to the Sun, using the Solar Diffuser, to the lamps in the Spectroradiometric Calibration Assembly (SRCA) that can operate in either a radiometric, spectral, or spatial calibration mode, to an on-board thermal blackbody and to a Space View that is normally directed at cold space and will occasionally include a view of the Moon. To monitor potential changes in Solar Diffuser characteristics, the on-board calibration systems include a Solar Diffuser Stability Monitor (SDSM) that is equipped with a rotating mirror and can alternately view the Solar Diffuser or the Sun (through an intensity-reducing screen).

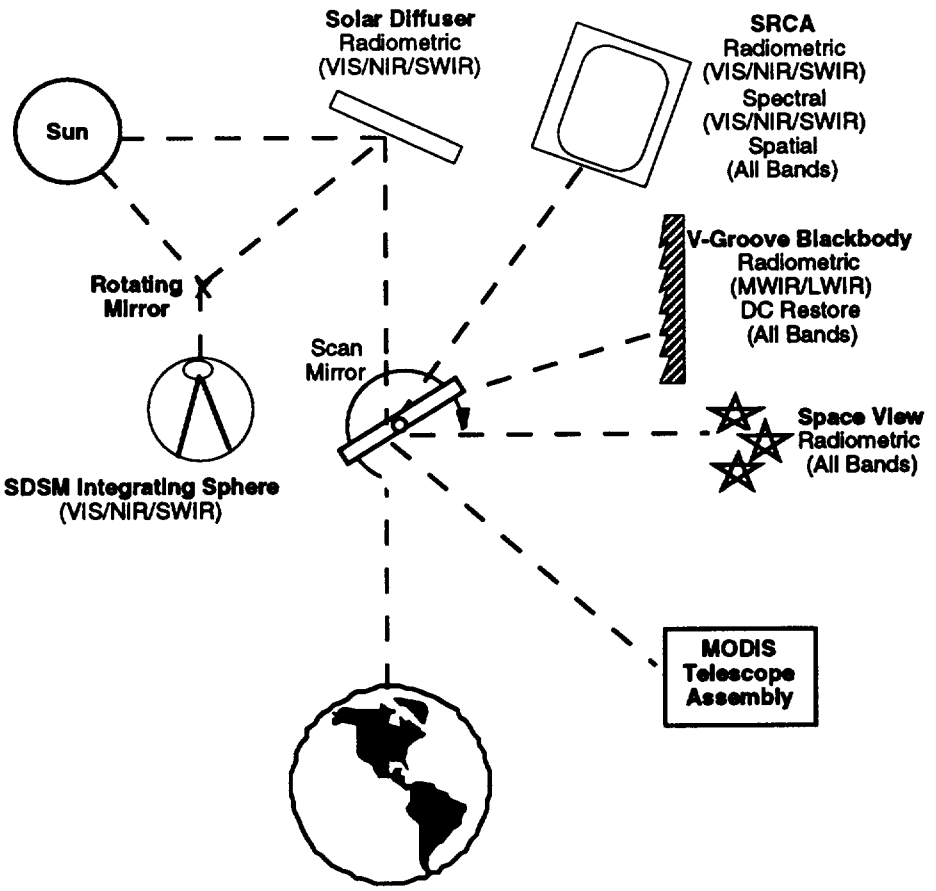

Figure D.1-2 MODIS On-Board Calibration System Components

The Integration function shown at the bottom of Figure D.1-1 attempts to interpret and reconcile characterization and calibration data from disparate sources and, if needed, specify appropriate changes or adjustments in the Calibration Algorithm. The initial Calibration Algorithm will be supplied by the instrument manufacturer and will be based on mathematical models used to design the instrument and on laboratory measurements performed on the instrument during the pre-launch era. To serve as an interpretable reference after instrument launch, on-board calibration systems must also be carefully studied and characterized in the laboratory during the pre-launch era.

The Calibration Algorithm and Instrument Model will serve as the instrument behavior baseline against which all subsequent calibration changes will be evaluated. In the initial on-orbit era, it will be assumed that the on-board calibration systems behave as characterized by the manufacturer, and any calibration adjustments or changes based on observed instrument output from on-board calibration systems will be implemented by the MCST. The statistical procedure known as the null hypothesis test will serve as the primary indicator that changes from the baseline calibration are necessary. During the Activation and Evaluation (A&E) period (the first 3-6 months on-orbit), observable instrument characteristics will be compared with pre-launch values and instrument stability in the space environment will be evaluated.

During the A&E period the entire suite of calibration information sources shown in Figure D.1-1 become available to supplement pre-launch laboratory measurements and on-board calibration systems. Image-Derived Characterization and calibration methodologies determine instrument characteristics from intrinsic image properties and do not require specific Earth or celestial observation targets. Verification of these techniques can begin as soon as the instrument begins Earth observations. Image-derived techniques will be included in the automated Calibration Algorithm only after they have been shown to improve calibration accuracy. Outputs from image-derived techniques will include random, systematic, and coherent noise characteristics, improved images with predictable noise components removed, within-band and cross-band destriping, and simulated dead detector outputs (if any detector elements are inoperative). Table D.1-1 lists eight possible noise effects or exceptional conditions that can be characterized by image-based methods. Possible compensation approaches for these effects are listed.

External-Target-Based Absolute Calibration does require instrument observations of specific targets with known radiances or known locations. Radiance properties of specific ocean sites will be known as a result of ocean field campaigns. Similarly, the reflectances or radiances of specific land sites will be known from a ground-based observation campaign, or radiances will be known from concurrent measurements done by aircraft or obtained from other satellite-based instruments. MODIS calibration plans also include the use of a large number of unsupervised calibration

Table D.1-1
Potential Instrument-Related Corrections

Potential Rectification Issue	Problem Heritage	Mitigation Approaches
Stray Light	Light entering sensor cavity from outside the scan beam can reflect from baffles supports, etc. and influence detectors on all focal planes.	Provide pre-launch and on-orbit tests to allow potential scene dependent de convolution.
Spectral Striping (Shifts in spectral sensitivity)	Undocumented with heritage instruments such as MSS, TM, AVHRR, etc. because they lacked spectral calibrators.	Provide SRCA on-board calibrator to measure spectral shifts by channel within a band with 1 nm resolution and 0.5 nm precision..
Memory Effect	Observed in Landsat Thematic Mapper as scan direction dependent "banding" at edge of bright objects (clouds) with increasing severity for darker backgrounds.	Presumably corrected electronically in the MODIS design Pre-launch tests will permit characterization for potential on-orbit reduction.
Ghost Images	Observed in SeaWiFS instrument due to reflection off focal plane at one location (channel) onto another channel when bright object is in a subset of the channels.	Potentially reducible by design. Will require pre-launch knowledge of the effect if on-orbit processing is required.
Within-Scan Striping	Differences in channel response within a band cause striping even after absolute calibration. Seen in Thematic Mapper.	Histogram equalization methods are applied and each detector channel is normalized to mean or "golden channel."
Between-Scan Striping	Scan correlated shifts were observed in TM. Mean level of output different for different scans independent of scene.	Continuously rotating scan mirrors in MODIS design presumably preclude this specific anomaly; however, there may be effects from differences in the two sides of the scan mirror.
Dark Scene Correlation (Systematic and Coherent Noise)	Many effects (jitter, power supply, thermal snap, scan effects) can cause noise patterns in imagery.	Filtering methods (1-D, 2-D, linear, non-linear) designed for each effect partially remove the noise.
MTF Blur (optical, detector and electronic spread functions)	System MTF results in blurring of image (inherent in imaging systems). Radiometric error increases with scene spatial frequency and contrast.	Deconvolution algorithms can reduce effect of MTF and partially restore image radiometry lost by the MTF, to extent permitted by pre-launch characterization of the system MTF and system design characteristics.

sites distributed along the ground track corresponding to the orbit. Radiance characteristics of these sites will not be independently determined using ground or airborne measurements but will be monitored using the MODIS instrument itself (and perhaps other satellite-borne instruments). The goal of this effort is to choose a number of sites with slowly varying and predictable radiometric characteristics that can be used statistically to determine relative long-term instrument responses and provide normalization references for all 6 MODIS instruments plus the other EOS instruments requiring cross-calibration. Perhaps 10-100 calibration sites will be chosen for each orbit. Potential calibration sites will be monitored and studied for several years after launch before such instrument characterization is applied.

Lunar-based radiometric calibration depends on the successful development of a model of lunar reflectance characteristics as a function of lunar phase. Such a model is under development by Kieffer at USGS. Lunar radiances are being determined for many solar illumination and view geometries in an extensive ground-based measurement program and results are being incorporated into a lunar model with high resolution (equivalent to 15m MODIS instrument resolution at nadir or 4 arc seconds.).

When this model is available, MODIS lunar calibration can be done in either of two modes. A Space View of the Moon can be obtained at those 2-6 times per year when, in the normal observation geometry, the Moon will traverse the space-look port. The moon will be in its waning gibbous phase when visible in this geometry and the statistical base of observations is not sufficiently large to permit direct verification of the lunar reflectance model. Periodically, platform attitude corrections normally required as the platform advances in its orbit will be suppressed to alter the normal observation geometry and provide a direct lunar view as shown in Figure D.1-3. This is known as the active Lunar view mode. The EOS platform would be placed on inertial hold (all three axes fixed with respect to an inertial reference frame) when the nadir view from the platform is toward the Moon. Platform attitude would be maintained while the platform advances and MODIS and other instruments view the Moon to obtain direct lunar calibration.

As displayed in Figure D.1-3, when the EOS spacecraft reaches point *I* in its orbit, it will transition from its nominal nadir pointing mode to an inertial pointing one by ceasing to correct its pointing to track its rotation around the earth. The EOS spacecraft will then be pointing at a place on the celestial sphere which is close to the position of the moon. This procedure doesn't require additional fuel resources for spacecraft maneuvers.

For the EOS AM series with a descending orbit, at point *E*, the moon will rise above the Earth's limb, and calibration will commence. It ends at moonset, indicated by point *B*. Additional pitch and yaw maneuvers to position the moon to various

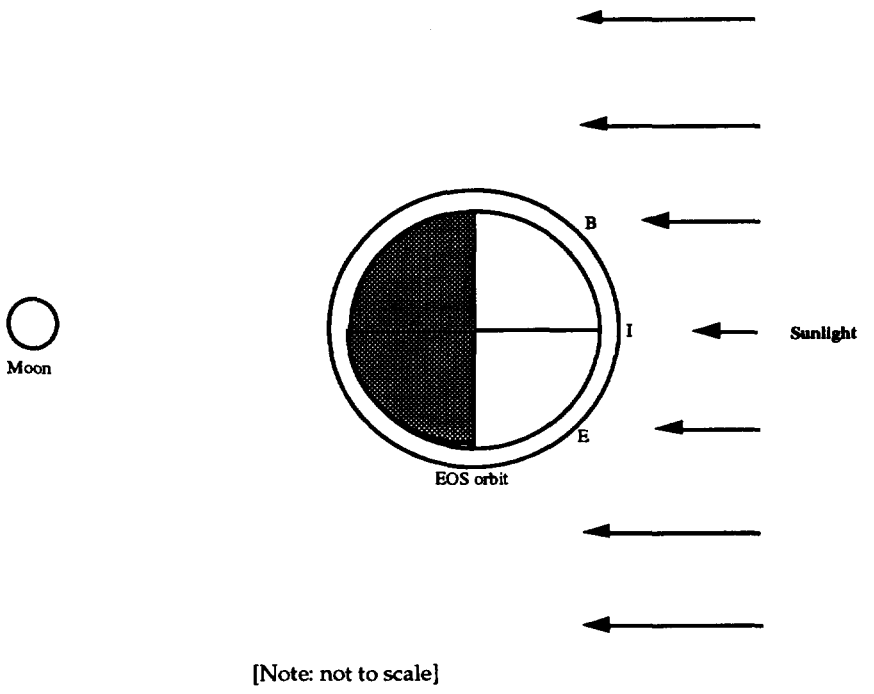

Figure D.1-3 Potential Direct Lunar View Geometry:
Out of Nadir Pointing Maneuver for Scan Angle Calibration on the Lunar Disk

points in the image plane of the MODIS and other EOS instruments may take place during this period. Note: Drawing is not to scale.

Using observations of the moon in both active and passive viewing modes, the MODIS detectors can be characterized both radiometrically and spectrally. With suitably chosen geometries, information on the stray light and unintended internal reflection characteristics of the instrument may also be obtainable using the Earth's limb or Moon as the stray radiation source. Stray radiation will be readily observable against the dark background of cold space, and if image "ghosting" is a problem, information on ghosting effects may be obtainable using this method. Because of the starkly defined limb of the lunar disk, space port and direct lunar views of the lunar surface will also serve as a good Modulation Transfer Function (MTF) estimation source.

In active mode, the roll angle of the EOS platform can be varied to allow the moon to be viewed at all angles of the scan mirror, thereby allowing the mirror to be characterized both radiometrically and spectrally as a function of its scan angle. This mode also allows other EOS instruments to use the moon for calibration, thereby allowing cross-calibration between the MODIS and other EOS AM and PM instruments. The benefits of direct lunar viewing are summarized in Table D.1-2 to

further emphasize the importance of including this mode in the EOS platform operations.

Table D.1-2
Benefits of Direct MODIS Lunar and Space View

Enabled by Direct View	Benefit
Full Lunar Observations	More samples spatially and temporally
Full space look for all detectors	More zero-level samples for all detectors at all mirror angles
Full lunar edge viewed	Good MTF (Modular Transfer Function) test source
Full Lunar illumination of part of focal plane	Ghosting effect data source

D.2 Phasing of Calibration Scene Utilization

Instrument characteristics, including characteristics of on-board calibration systems, may change significantly at launch when the instrument is introduced into the space environment. Vicarious calibration based on external targets may be especially valuable since it accounts for instrument changes occurring at launch and does not depend on the stability of on-board calibration systems. To quickly characterize instrument behavior in the space environment and establish the correspondence between pre-launch instrument characterization and vicarious characterization, target-based, vicarious calibration should be initiated as soon as possible after launch. Vicarious results obtained immediately after launch can serve as a baseline for characterization of further changes in instrument behavior that may occur as the instrument ages in the space environment.

A given calibration procedure cannot provide information on instrument response variations that occur on a time scale shorter than the application interval for the procedure. For example, a calibration procedure that can only be applied once per orbit at a fixed location in the orbit cannot be used to determine any within-orbit variability in response. The expected approximate time validity domains for MODIS on-board and image-derived calibration procedures are shown in Figures D.2-1 and D.2-2 respectively. The validity domains of some procedures overlap, and if all calibration systems function as expected, some redundancy in calibration procedures will exist. Where it exists, such calibration redundancy can be exploited to improve calibration accuracy and confidence. Figure D.2-3 shows an example of how such redundant calibration checks might operate. In the Visible and NIR bands, the SRCA provides primary information on within-orbit instrument response variations. (For the MODIS AM series, solar calibration using the solar diffuser plate can only be done near the Northern terminator crossing.) However, within-band histogram equalization or normalization procedures can also be applied over

several segments of the orbit to obtain detector-to-detector response variations within the orbit. The detector-to-detector response variations obtained using histogram equalization can be compared with those obtained looking directly at the SRCA.

The first step in achieving accurate absolute calibration is the characterization of the instability of the instrument being calibrated. With sufficient measurements, the stability can be characterized at about the level of the NEdL of the instrument. Such a characterization makes use of sources or scenes that have high stability over the measurement period but whose radiances may not be known with any absolute accuracy. The result then is a precise curve of relative calibration with respect to time. A value for the absolute calibration of the instrument at a given time can be found by exposing the entrance pupil to a source or scene of known radiance. This value can be used to anchor the relative calibration curve, thereby converting it to an absolute calibration curve as a function of time. A simple example of the procedure is described in section D.4. The remainder of this section discusses the need for redundancy in calibration.

The factors related to the source that limit the accuracy of absolute calibration are:

1. The accuracy of knowledge of the source's radiance.
2. The suitability of its spectral distribution.
3. Its aperture size with respect to the entrance pupil of the instrument.
4. The radiance uniformity across its aperture.
5. Polarization of its output radiance.

Systematic errors are often related to one or more of these source characteristics, and/or the geometry of the calibration. Thus, precise (repeatable) and sensitive absolute calibration measurements can be made that include an unknown bias. The only way to identify, diagnose and then correct for such systematic error(s) is to compare the results from several independent calibration methods of high precision and apparent absolute accuracy. Only when the results from these calibrations can be made to agree to within their estimated uncertainties can the absolute calibration and its estimated uncertainty be believed.

D.3 Calibration Algorithm Data Transformation Strategy

The final calibrated radiances generated as a result of Level-1 processing are not expressed and stored in floating point format. Instead, for storage and processing efficiency, radiances are written in a 16-bit integer format that must be transformed to the proper physical expression required by the data end user. The 16-bit format assigns the integer zero to an L_{lower} value corresponding to the expected minimum value of observed radiance in the spectral band in question, and it assigns the integer value $2^{16} - 1$ to a maximum expected radiance L_{upper} based on the maximum radiance that the detectors for the spectral band in question were designed to observe and process. The values of L_{lower} and L_{upper} are fixed for each

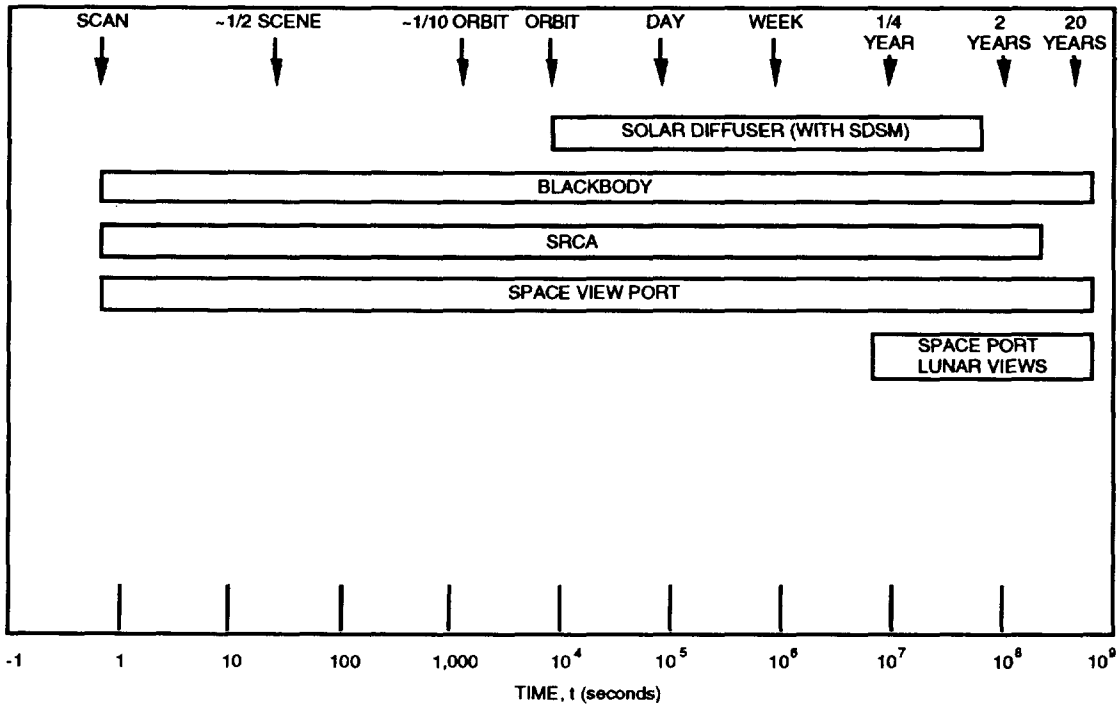

Figure D.2-1 Approximate validity domains (time) for MODIS On-Board Calibration (OBC)

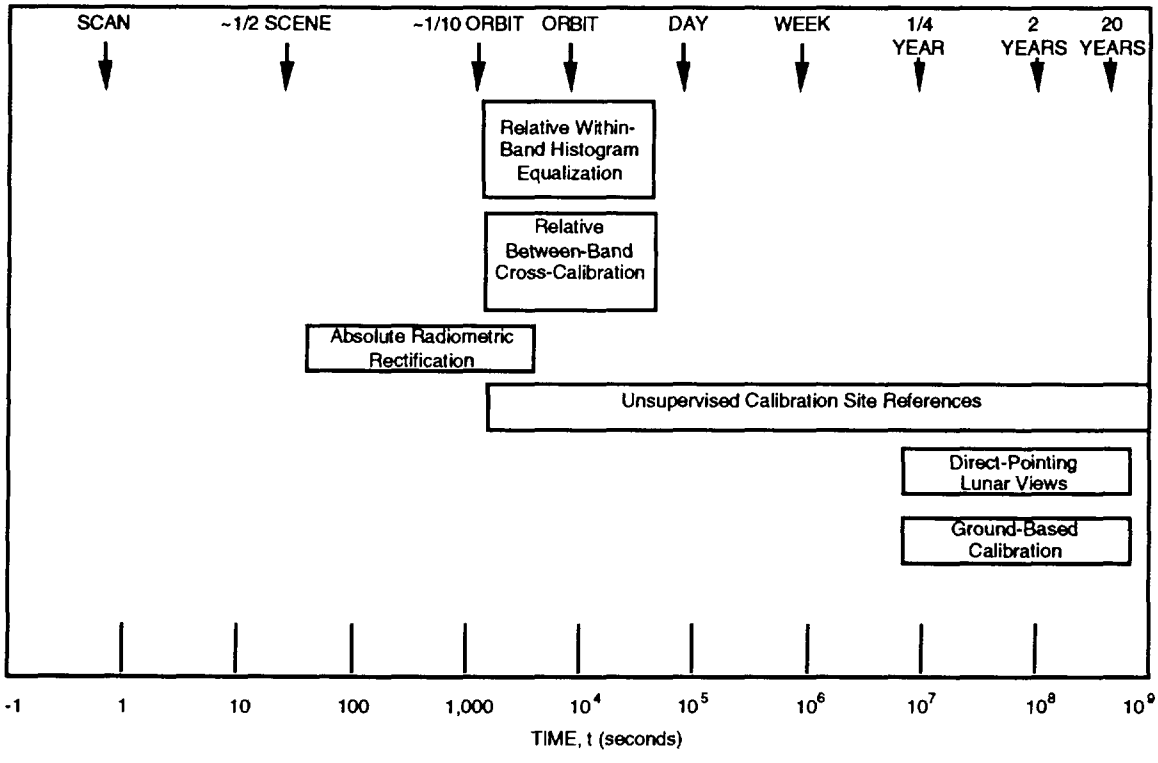

Figure D.2-2 Approximate Validity Domains (time) for MODIS Image-Derived Calibration Technologies

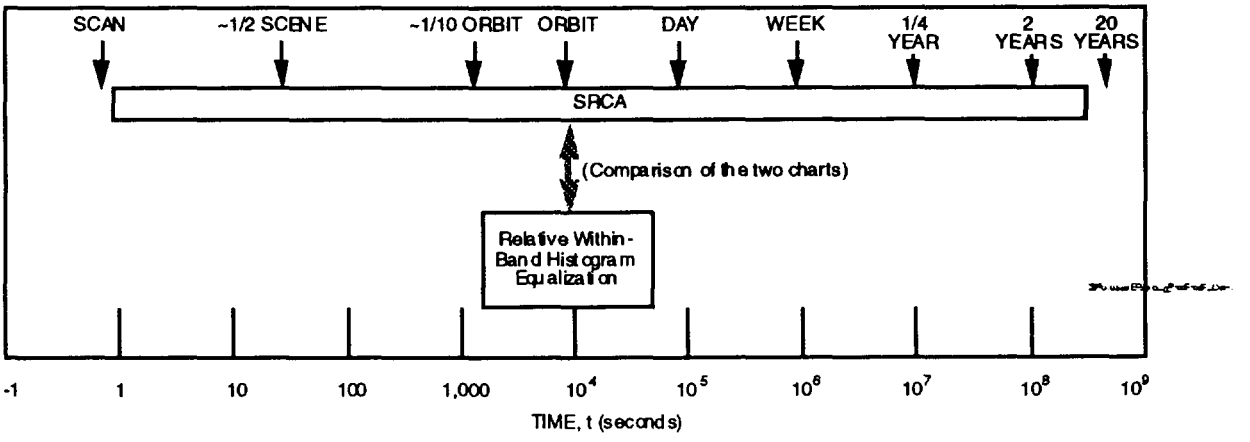

Figure D.2-3 Example of redundant calibration techniques used to verify within-orbit radiometric behavior of instrument as measured by SRCA

spectral band and do not depend on the characteristics of the individual detector that obtained the observation. Details will be provided below; first we shall consider pre-launch calibration measurements and the interpretation of calibration results after instrument launch.

During instrument manufacturing and testing, the manufacturer will conduct measurements relating quantized digital output values of the detector channels (Q) to spectral radiance at the MODIS input aperture (L_λ) as supplied by a reference integrating sphere (IS). Although detector materials can exhibit nonlinear behavior under certain conditions, the manufacturer seeks to establish detector operating conditions that provide linear operation to within a negligible fraction of the radiometric specification. Thus, we shall assume a linear relationship between L and Q; the underlying algorithm structure will provide for higher order terms and a non-linear detector model that can be implemented should the need arise. A response curve for the Landsat MSS (Manual of Remote Sensing, 1985) is shown in Figure D.3-1. The detector was linear in this case.

We shall initially assume a linear relationship between radiance input from the integrating sphere $L_{\lambda,\,IS}$ and digital count output Q from the detector channel as depicted in Figure D.3-2.

The offset in Q for zero radiance input is expected due to stray light and noise which will produce a finite count out of the channel for an apparent zero input at the MODIS aperture. There are 470 detector channels; therefore, there will be at least that number of curves defining pre-launch calibration. If there are variations in

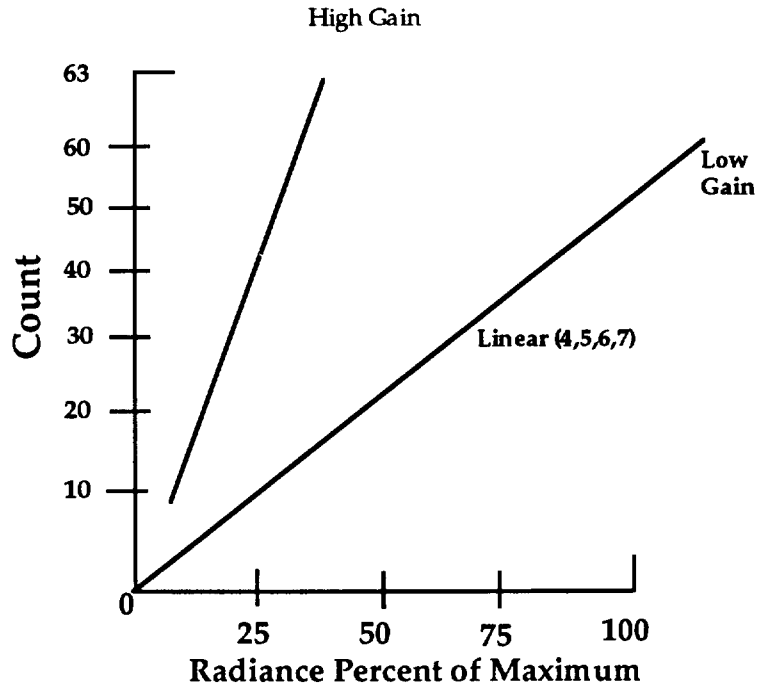

Figure D.3-1 Example of linear detector response (Landsat MSS)

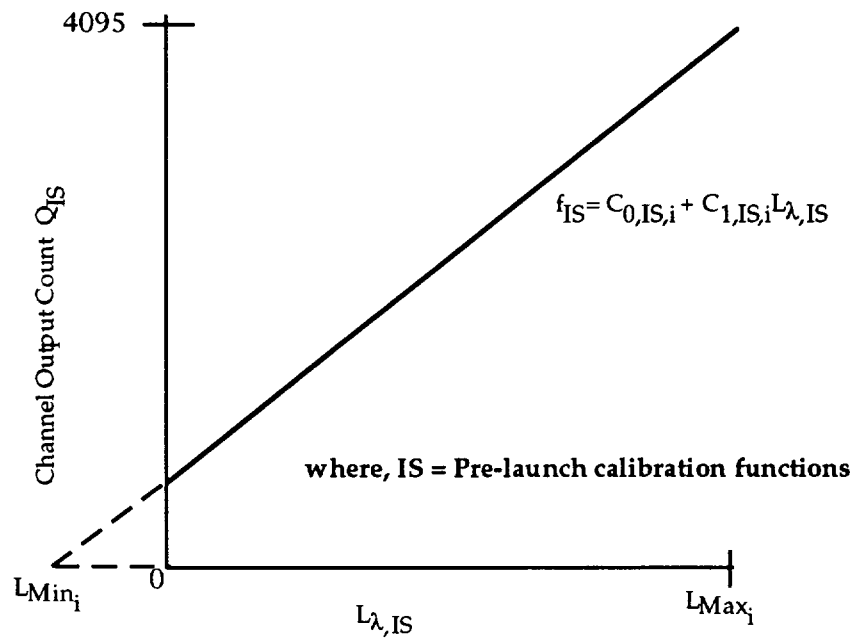

Figure D.3-2 Pre-launch Relationship between Spectral Radiance and Count for Channel i of a band.

mirror Bidirectional Reflectance Distribution Function with mirror side and angle then there could be many more curves per detector channel.

Pre-launch measurements will also establish the relationship between on-board calibration sources and the corresponding instrument digital response. This portion of the measurement program uses the instrument response curves obtained using the integrating sphere (as described above) along with the MODIS instrument itself to obtain effective radiance values for the available on-board calibration sources. In this case, the MODIS instrument itself serves as a transfer radiometer to transfer calibration information from the integrating sphere to the on-board sources. For the SRCA, there are eight possible lamp levels and each is observed through the sensor optics to produce a digital output for each channel. Transfer of calibration from the integrating sphere to the on-board sources involves the determination of radiances from instrument response; this is the inverse of the relationship depicted in Figure D.3-2. The inverse relationship is depicted graphically in Figure D.3-3.

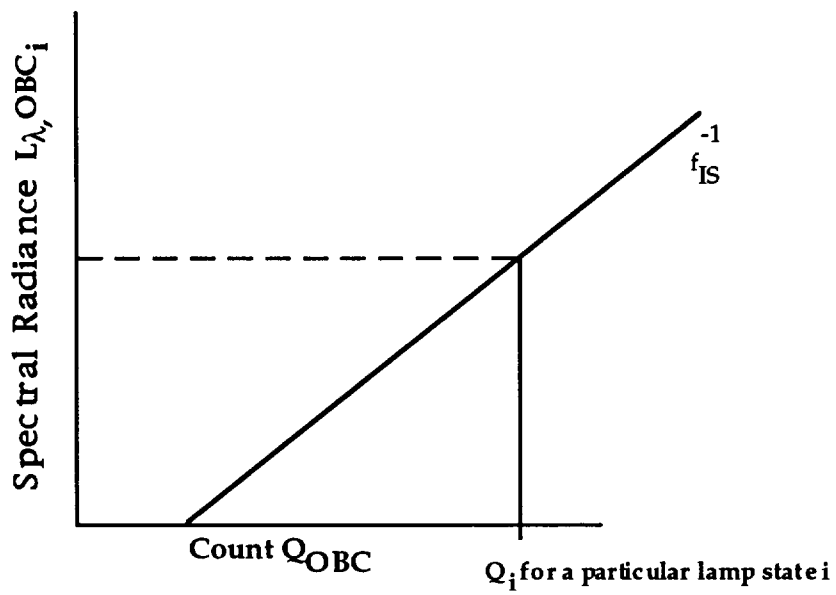

Figure3. Count radiance relationship for an On-Board Calibrator

Figure D.3-3. Count Radiance relationship for an On-Board Calibrator

The SRCA serves as the standard for the transfers of calibration from pre-launch measurements to on-orbit operation. SRCA lamp radiances are assumed to be constant to within the MODIS specification so that if the Q values observed for the various lamp illumination states are significantly different after launch, an instrument calibration adjustment is made. The counts for the lamp states for the 310 reflectance band channels are stored as part of the pre-launch dataset.

Pre-launch calibration measurements also serve to standardize the dynamic range for all detectors in each band. In operation, each of the up to 40 channels in a band can have a different calibration function (i.e., different functional form, or different parameters) and dynamic range. Although the channel gains and biases will be carefully adjusted by the manufacturer, once the instrument is delivered, no further changes are made and slight variations begin to occur. The approach that will be used is to define the standard digital range as zero to the maximum given by the number of bits in the output plus several bits of expansion overhead. For MODIS we will use 0 to 2^{16}-1. The radiance dynamic count range for each band is defined by L_{lower} and L_{upper}. L_{lower} will generally be negative; this is an artifice to allow zero count to be the minimum Q value. The maximum radiance, L_{upper} will be the highest radiance which will not saturate a band, i.e., at least 1.2* L_{max} in the MODIS Specification. Thus, the standard dynamic range for each band will be zero to 2^{16}-1 for count representing a radiance range of L_{lower} to L_{upper} for each band. The MODIS A/D converters digitize to 12 bits, thus the data range is expanded from 0 to 4095 to 0 to 65268. The standard relationship for each band is illustrated in Figure D.3-4.

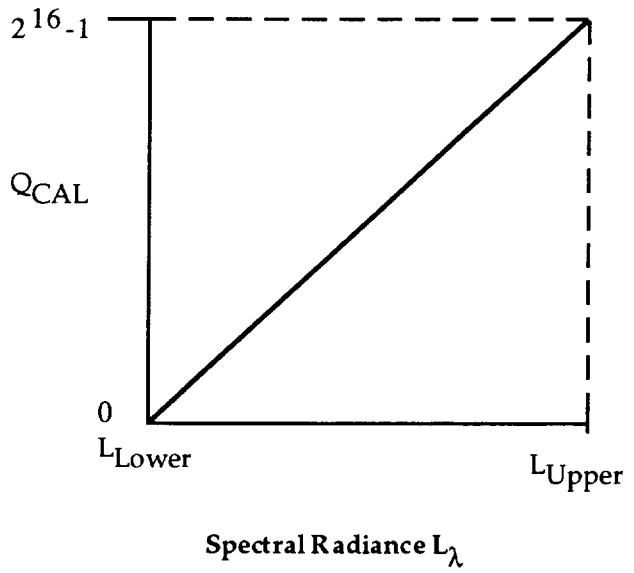

Figure D.3-4. Standard Relationship Between Spectral Radiance At Band Center and Calibrated Digital Values.

Standardization of the response of each channel to the standard for that channel is accomplished by computing a set of C_0 and C_1 coefficients which transform data from each channel to the standard case.

The task for the calibration algorithm is to transform the data from each channel to the standard curve for each band. In the pre-launch phase, the calibration coefficients are obtained from the pre-launch test data as in Figure D.3-2. For each channel, the count is extended for L_{upper} and L_{lower} which in general are all

different than the standard for the channel. A linear transformation is computed for each channel to bring its range to the standard range of 0 to 2^{16}-1.

The steps for the inflight calibration coefficient calculations are:

1. The $Qmax_i$ is computed for each channel:

$$Qmax_i = C_{0,IS,i} + C_{1,IS,i}\, L_{upper}$$

where the L_{upper} is the standard band value. No L_{min} is given in the specification so the mean of L_{min_i} for the set of channels in a band is used:

$$L_{Min} = \frac{1}{N}\sum_{i=1}^{N} -\frac{C_{0,IS,i}}{C_{1,IS,i}} \qquad \text{N=10, 20, or 40}$$

2. The $Qmin_i$ values for the standard minimum radiances are computed:

$$Qmin_i = C_{0,IS,i} + C_{1,IS,i} * L_{lower,i}$$

3. The coefficients from a linear transformation from the original Q range to the standard Q range are computed:

$$Q_{Cal} = C_{0,CAL,i} + C_{1,CAL,i} * Q_i$$

for a system of 2 equations in two unknowns:

$$QCAL = C_{0,Cal,i} + C_{1,Cal,i} * Qmin_i = 0$$

$$QCAL_{max} = C_{0,Cal,i} + C_{1,Cal,i} * Qmax_i = 65268$$

The solution is:

$$C_{1,Cal,i} = \frac{Q_{CalMax} - Q_{CalMin}}{Q_{Maxi} - Q_{Mini}}$$

$$C_{1,Cal,i} = Q_{CALMin} - C_{1,CAL,i} \bullet Q_{Mini}$$

or:

$$C_{1,Cal,i} = \frac{65268 - 0}{Q_{Maxi} - Q_{Mini}}$$

$$C_{0,Cal,i} = 0 - C_{1,CAL,i} \bullet Q_{Min_i}$$

These coefficients are computed for each channel in each band and 470(or more) sets of curves are generated as illustrated in Figure D.3-5.

In the post-launch phase, the counts for given radiances are obtained from the on-board calibration sources and the QCAL calibration coefficients are adjusted in a similar manner to maintain the standard range for each band. In the early on-orbit phase, the SRCA will be the primary source of reflective band calibration data. Pre-launch data provides the expected count values for the lamp states from the SRCA (radiometric mode). These lamp states will be observed by MODIS on-orbit and regression will be performed to obtain the calibration coefficients predicted by the SRCA. This relationship is represented by the plot in Figure D.3-5.

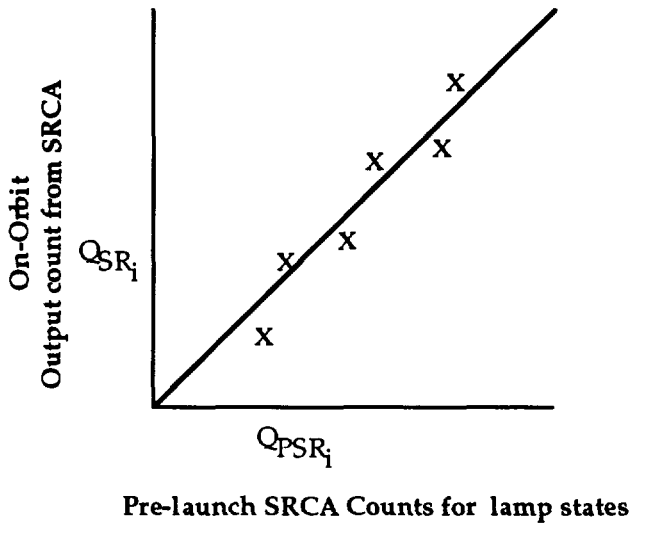

Figure D.3-5. Relationships between Pre-launch and Post-launch counts observed by MODIS for lamp states for channel i.

One such regression curve will be obtained for each reflective band channel (total of 310 for 20 bands) the $C_{0,SR,i}$ will be near zero and the $C_{1,SR,i}$ will be nominally 1 based on the null hypothesis of no change. Significant change in the channel characteristics would be indicated by a change in C_0 and C_1. The same general concept is applied to all other calibration sources in the MODIS suite.

D.4 Integration of Multiple Calibration Source Data

Including results from pre-launch, on-board and vicarious techniques, there will be about ten different calibration data sets available for MODIS. This highly redundant information, properly combined and coordinated, will provide a reliable and accurate set of calibration coefficients as a function of time. However, the issue of

determining the best strategy to combine multiple calibration data sets to achieve the most accurate final result must be addressed. The following procedure has been used successfully by Gellman, 1993, et al., for on-orbit SPOT calibrations. It is based on two considerations. First, that the on-board calibration provides precise relative calibration, at about the ±1% level at monthly intervals (However, for SPOT the uncertainty in the absolute calibration is unknown but estimated at about ±15%). Second, that vicarious absolute calibrations with a ±5% uncertainty are obtained about two or three times a year. By positioning the precise, relative calibration curve to best fit the more accurate absolute calibration points, knowledge of the absolute calibration at any particular time is improved. This occurs since the best-fit relative calibration curve provides a reliable smoothing of the variations in the infrequent absolute calibration results.

The procedure for combining precise relative with less-precise absolute calibration data can be accomplished by an additive method, equivalent to an offset change, or by multiplicative method, equivalent to a gain change. In the SPOT case, the relative calibration data are provided by an on-board lamp and the absolute calibration data are provided by vicarious calibrations at White Sands, NM. In the additive procedure, the sequence of lamp measurements is normalized to the first on-orbit lamp measurement, L_O. The curve is then scaled by multiplying by C_O, the first calibration. Then the scaled lamp measurement L(tj)', at a time tj in days since launch is given by

$$L(t_j)' = \left(\frac{C_o}{L_o}\right) L(t_j), \tag{5}$$

where L(tj) is the unprocessed lamp datum. Next, the relative calibration is fitted to the absolute values by the addition of an offset α. Thus the estimated calibration coefficient E(tj) is given by

$$E(t_j) = \alpha + L(t_j)' \tag{6}$$

In the multiplicative procedure, equation (5) is unnecessary and equation (6) becomes:

$$E(t_j) = \beta\ L(t_j), \tag{7}$$

where β is the multiplicative constant. Note that the multiplicative method does not involve prescaled lamp data. The error x^2 in E(tj), which is a measure of the suitability of the position of the line with respect to the points, is expressed as

$$x^2 = \sum_{j=1}^{N} \left[\frac{V_1 - E(t_j)}{\sigma_j} \right]^2, \tag{8}$$

where V_j is the result from the jth of N vicarious calibrations and σ_j is the uncertainty associated with it. Algorithms published by Press et, al., (Press, 1988) can be used to minimize x^2 for both weighted and unweighted least-squares fits. The latter will be discussed below.

The results for 6.5 years of SPOT-1 calibrations are shown in Figure D.4-1 . They show the lamp curve, which comprises over 300 points with standard deviations of about 1%, as the solid line. This line has been positioned using both the additive and multiplicative procedures to provide a best fit to the vicarious results. The numbers next to the vicarious points represent estimates in the range one to ten of the quality of the calibration. Arbitrarily, uncertainties of between 3.5% and 13.5% were rated as weightings of between ten and one respectively.

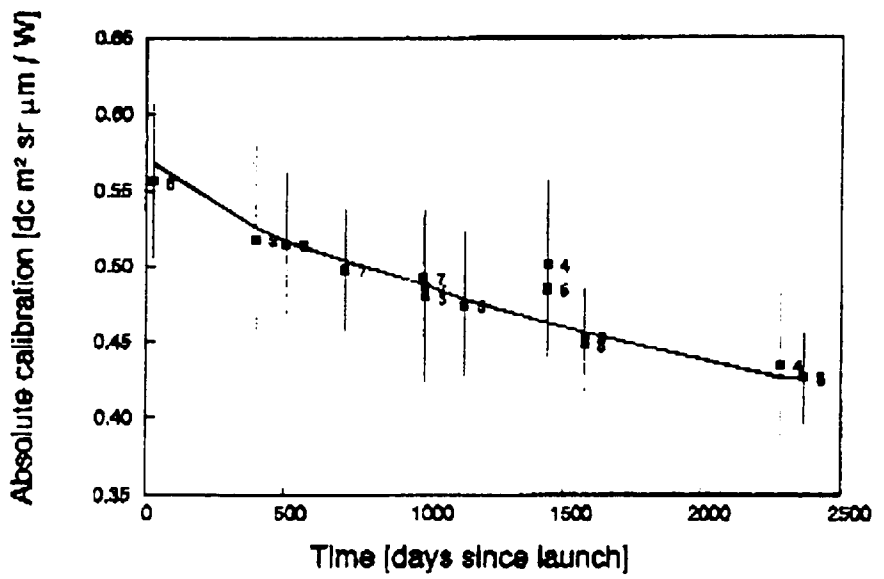

Figure D.4-1. Results of two methods for SPOT-1 HRV1 XS1. Vicarious calibration points are shown with error bars and quality indices.

Two points are worth noting about these results. First, at the scale used for the graph in Figure D.4-1, the lines for the additive and multiplicative methods are barely distinguishable from each other. Second, the unweighted fits produced absolute calibration curves within 1.5% of the weighted fits. This shows that, in this case, the weighting had little influence on the fit. Nevertheless, when dealing with vicarious or other variable accuracy calibrations and particularly as they improve in

sensitivity and accuracy, it is useful to include weighting coefficients to account for variations in calibration conditions, due for example to the presence of clouds.

Thus the calibration results for a high-visibility cloudless day would rate higher weighting than if there were cirrus clouds present. If relative calibrations were being fitted to absolute calibrations provided by a more precise procedure, e.g., perhaps solar-diffuser measurements, variable weightings would not be needed. Preliminary weighting categorizations are listed in Table D.4-1.

Table D.4-1
Fixed and Variable Weightings

Fixed	Variable
Preflight (laboratory)	Reflectance based
Preflight (cross calibration)	Radiance based (ER-2)
SRCA	Radiance based (Moon)
SD/SDSM	Ocean measurements
Deep space	Radiometric rectification
	On-orbit cross calibration

The quantification of weighting factors and the detailed procedures for combining the results of the calibration methods listed in Table D.4-1 will depend largely on the reliability of the on-board calibration systems. This will be impossible to ascertain until on-orbit experience has been developed. Provided one of the fixed weighting methods yields a reliable, temporal, relative calibration, then the variable weighting methods can be used to determine the absolute calibration in the manner described here for SPOT. Of course, the anticipation is that at least one of the fixed weight methods will provide a reliable, accurate, temporal, absolute calibration. This will improve the confidence in, and probably the accuracy of, the overall calibration.

Appendix E

Algorithm Theoretical Basis Document for the Vicarious, In-flight, Radiometric Calibration of MODIS

Principal Investigator: Philip N. Slater
Contract Number: NAS5-31717

Report compiled by Kurtis J. Thome
Contributions by Stuart F. Biggar

Remote Sensing Group of the Optical Sciences Center
University of Arizona
Tucson, Arizona 85721
August 2, 1993

1.0 Introduction

1.1 Algorithm Identification and Data Product

The Algorithm Theoretical Basis Document (ATBD) describes the algorithm to be used for the in-flight, vicarious, radiometric calibration of the MODerate resolution Imaging Spectroradiometer (MODIS) which is part of the National Aeronautics and Space Administration's Earth Observing System (EOS). There is no standard data product produced by this algorithm. It is used to provide calibration coefficients used in converting raw digital number (DN) to radiance. These calibration coefficients are to be supplied to the MODIS Calibration Science Team (MCST) for use in determining the absolute radiometric calibration of MODIS.

1.2 Algorithm Overview

The vicarious calibration discussed has separate approaches for the different parts of the electromagnetic spectrum. One approach is applied to the solar-reflective portion of the spectrum which covers the visible and near infrared (VNIR) and the short-wave infrared (SWIR). The second approach is used for the thermal infrared (TIR). Both approaches are similar in philosophy but different in implementation.

The reflectance-based method, developed by the Remote Sensing Group (RSG) at the University of Arizona for use in the solar reflective portion of the spectrum, relies on ground-based measurements of the surface and atmosphere at a selected site to predict top-of-the-atmosphere radiances. (Slater et al., 1987). This technique has been modified for large footprint sensors for cases when it is not feasible to characterize the surface for several sensor pixels (Teillet et al., 1990, and Teillet et al. 1991). Measurements of the surface are performed for a number of pixels by transporting radiometers/spectrometers across a selected test site and measuring upwelling radiance. Upwelling radiance is converted to reflectance by comparing it with measurements from a panel of known reflectance. Atmospheric characterization is performed using measurements from solar radiometers located at the test site. These measurements are converted to atmospheric transmittances (Gellman et al., 1991) and used to determine the aerosol properties and columnar absorber amounts over the site (Biggar et al., 1990, Thome et al., 1992). The results of these measurements are used as input to a Gauss-Seidel iteration radiative transfer code (RTC) to predict the top-of-the-atmosphere (TOA) radiance. The digital numbers reported by the sensor are compared to these predicted radiances to give a radiometric calibration.

An improvement on the atmospheric characterization is made by using measurements of the diffuse skylight irradiance and comparing it to the total downwelling irradiance (Biggar et al., 1991). Further improvements in the atmospheric characterization are expected through the use of an aureole camera (Grotbeck et al., 1993). Better surface characterization is expected by using a recently developed SWIR spectroradiometer (Smith, 1992).

If it is not feasible to measure the surface reflectance for several MODIS pixels, the above technique is used to calibrate a high-spatial-resolution (HSR) sensor. This calibration is then transferred to a low-spatial-resolution (LSR) sensor using radiances reported by the HSR sensor and comparing them to the DNs reported by the LSR sensor for the appropriate pixels. The difficulties of this technique are ensuring the two images are properly registered and accounting for spectral differences between the two sensors. Both the direct calibration and transfer calibration methods are being investigated for application to MODIS. If it is necessary to transfer the calibration from a HSR sensor, data from the Advanced Spaceborne Thermal Emission and Reflectance radiometer (ASTER) will be used.

A variation of the reflectance-based method is the radiance-based method using airborne radiometer measurements (Slater et al. 1987). The instrument flown in the aircraft is a well-calibrated radiometer and the measured radiances are corrected for the intervening atmosphere between the aircraft and the satellite to predict the at-satellite radiance. This method is more accurate because the atmospheric correction is not as important.

The method for the vicarious calibration in the TIR is similar in philosophy but different in measurement and atmospheric correction. The differences are the surface measurements are of temperature and emissivity not reflectance, the atmospheric measurements are profiles of temperature and water vapor, and the RTC calculations are concerned with emission and absorption rather than scattering. The philosophy remains the same in that the surface and atmosphere are characterized and this characterization is used in a radiative transfer code to predict the radiance seen by the satellite.

1.3 Document Scope

This document addresses the algorithms used by the RSG as part of this project. The document limits itself to describing the algorithm used. The plan for implementing the algorithm is not discussed here. Instead, the ATBD gives background information about the algorithm. It is related to and part of a package of documents used to describe the conversion of the algorithm to production code. The purpose of this document is to allow the team leader to make informed decisions regarding the use and implementation of the algorithm and indicate areas which may be problematic in implementation.

Other documents as part of this package include the Algorithm Development and Test Plan, Software and Data Management Plan, and the Science Computing Facilities document. The Algorithm Development and Test Plan discusses plans for implementing these algorithms. The Software and Data Management Plan describes how the code developed from the algorithms is to be maintained and integrated within the EOS project. The Software and Computing Facilities document describes the hardware and operating software needed for producing the code.

1.4 Document Organization

The ATBD first describes the overall algorithm in detail. Background information and overview are given first including the experimental objective of the algorithm, an historical perspective, and instrument characteristics of interest.
The detailed algorithm description is from a theoretical standpoint with discussions of the physical basis of the problem, the mathematical solution, and an estimate of the variance or uncertainty. Also as part of the algorithm description is a discussion of practical considerations for implementation of the algorithm. The next section covers limitations, constraints, and assumptions.

Appendixes are included in which component algorithms are discussed in detail. It should be noted that the component algorithms are not discussed in

great detail in the main portion of the document for clarity. Each section devoted to a component algorithm will follow the format described above.

2.0 Overview and background information

This section has three parts. The first gives the experimental objective. The second section gives an historical perspective of the algorithm. The last part describes the instrument characteristics important to this algorithm.

2.1 Experimental Objective

The purpose of vicarious calibration is to provide an absolute-radiometric calibration for the sensor of interest such that DNs reported by the sensor are converted to absolute units such as radiance. This opposed to a relative calibration typically produced by on-board systems where system degradation may be tracked but no conversion from measured DNs to a physical quantity may be made. The results from the vicarious calibration will be used by the MCST as part of a larger algorithm to determine the calibration for the sensor used to report satellite-measured radiances.

2.2 Historical Perspective

The reflectance-based method has a proven history of use since the mid-1980s. It has been used to radiometrically calibrate Systeme Probatoire d'Observation de la Terre (SPOT) -1 and -2 (Begni et al., 1986, Gellman et al. 1993) and Landsat-4 and -5 Thematic Mapper (TM) (Slater et al. 1987, and Thome et al. 1993). The radiance-based method has also been used with great success and better accuracy (Biggar et al., 1991 and Slater et al. 1987). The method for transferring calibration from a high spatial resolution sensor to a low resolution sensor has been applied to the National Oceanic and Atmospheric Administration's (NOAA) -9 and -11 Advanced Very High Resolution Radiometers (AVHRR) (Che et al., 1991, Teillet et al., 1990, and Teillet et al., 1991). A similar method has also been proposed for the calibration of Sea viewing Wide Field-of-view Sensor (SeaWiFS). The method for vicariously calibrating bands in the thermal portion of the spectrum has only a recent history of use by the RSG (Palmer, 1993).

2.3 Instrument Characteristics

The intent of this process is to produce calibration coefficients for all bands of MODIS. The method relies on near-nadir views of the test sites and data will be coincident with that of ASTER. We require raw DNs, but geometrically corrected data are preferred. The data cannot be radiometrically corrected.

3.0 Algorithm Description

This section has two parts. The first part is a theoretical discussion of the algorithm including a description of the physics of the problem, a mathematical discussion of the algorithm, and an error analysis. The second part of this section covers practical considerations of implementing the algorithm, including a discussion of validation plans. Also included in this part are planned methods of quality control, a discussion of data dependencies, and a description of the output product.

3.1 Theoretical Description

3.1.1 Physics of Problem: This section gives a description of the algorithm and how each of the data sets used is related. To emphasize the overall calibration process, detailed descriptions of the component algorithms used in the process are not given here. These algorithms are discussed in detail in the Appendix of this document. The component algorithms are denoted in this section by bold-faced type.

The physical basis for the reflectance-based method is that TOA radiance may be predicted by adequately characterizing the atmosphere over the surface of a selected test site during the overpass of the sensor to be calibrated. The predicted radiance is from RTC results based on models of scattering, absorption, and emission of radiation in the earth-atmosphere system. The radiometric calibration for the sensor is found by comparing the predicted radiances to the DNs reported by the sensor.

The process relies heavily on selecting the proper site. The desired characteristics of the surface are it should be flat, have high reflectance/emissivity, and be uniform/homogeneous. The atmosphere over the site should be clear with low aerosol loading and the climate should be dry to reduce the chances of cloudiness during satellite overpass. A dry climate also reduces the effects of surface moisture. All of these factors serve to reduce the uncertainties involved in characterizing the radiative transfer in the earth-atmosphere system. One last desirable characteristic is that the site should be readily accessible. The RSG currently uses two sites: White Sands Missile Range and Rogers Dry Lake for our calibration. We also have an alternative site at the Maricopa Agricultural Center that is used for verification studies.

Atmospheric characterization is performed using data collected from solar radiometers, a line-of-sight radiometer, meteorological instrumentation, and a pyranometer. An improved atmospheric characterization can be made by measuring diffuse and global downwelling irradiances. Radiosonde data are collected to determine the height distribution of temperature and pressure. Surface characterization is performed using data collected by radiometers

attached to our reflectomobile. At times a well-calibrated radiometer is flown in an aircraft to measure the upwelling radiance.

The solar radiometer data is used as input to the **Langley method algorithm** (Gellman et al., 1991) to determine the exo-atmospheric signals, or zero-airmass intercepts, for the solar radiometer. These intercepts are necessary for the computation of the atmospheric transmittance at the time of satellite overpass. The intercepts are typically computed prior to calibration campaigns and stored for use in the calibration.

The exo-atmospheric intercepts for the solar radiometers are used to compute the total optical depths for all measurements and all channels for which there is no strong gaseous absorption. This is performed in the **component optical depth algorithm** (Biggar et al., 1990a). This algorithm also determines the columnar ozone amount and Junge aerosol size distribution. Once the aerosol size distribution and ozone are known, the component optical depths for the sensor wavelengths are computed by this algorithm as well.

In wavelength regions of strong gaseous absorption, the Langley method algorithm is not valid. In these cases a **modified-Langley algorithm** (Thome et al., 1992) is used. This algorithm uses the results from the component optical depth algorithm to remove scattering effects in the solar radiometer bands where strong absorption occurs. This algorithm is currently only used for the 0.94 μm water vapor band. The exo-atmospheric intercept computed from this method is used in the **columnar water vapor algorithm** (Thome et al., 1992) to compute the columnar water vapor.

To characterize the surface, the reflectomobile is used to transport radiometers/spectrometers across the site around satellite overpass time. These radiometers measure the upwelling surface radiance which is compared to the upwelling radiance from a panel of known reflectance to give the surface reflectance. The surface reflectance for several pixels is computed and averaged by the **surface reflectance algorithm** to give the average site reflectance. This algorithm also finds the surface reflectance for each band of the satellite sensor, based on the reflectance measured in the spectral bands of the ground-based instrument. A separate algorithm, the **surface emission algorithm** (Palmer, 1993), computes the average surface temperature and emissivity of the site. This algorithm also finds the surface emissivity for the spectral bands of the sensor to be calibrated using the emissivities determined for the bands of the ground-based instrument.

An improvement on the atmospheric correction is made using the **diffuse-to-global algorithm** (Biggar, 1990). This method uses measurements of the downwelling diffuse irradiance and of the total downwelling irradiance. By comparing the two measurements, information regarding the aerosol content and their scattering properties is obtained.

At this point the atmosphere and surface have been characterized. The results for the VNIR and SWIR are used in the **Gauss-Seidel radiative transfer algorithm** (Herman et al., 1965) to predict TOA radiances over the site at the time of sensor overpass. In order to compute these radiances the radiative transfer algorithm requires the aerosol scattering phase function as found by the **Mie phase function algorithm**. The radiative transfer algorithm also requires a model atmosphere which is used to divide the atmosphere into plane-parallel layers. Ancillary data such as satellite view angle, solar zenith angle, ground elevation and slope are also required. In the TIR, the surface and atmospheric measurements are used in the **TIR radiative transfer algorithm** to compute the TOA radiances. The reason for separate radiative transfer algorithms is the TIR is dominated by emission while the VNIR and SWIR are dominated by scattering. Predicted at-satellite radiances from the radiative transfer algorithms are combined with the measured satellite digital counts in the **gain and offset algorithm** to compute the calibration coefficients for the sensor.

As previously mentioned, a secondary approach is the radiance-based method, which is similar to the reflectance-based method except the reflectomobile data are replaced with radiances measured by a well-calibrated radiometer in an aircraft. The radiative transfer code need only correct these radiances for the atmosphere between the aircraft and the satellite. This reduces the uncertainties by lessening the effect of the atmospheric correction and errors in the measured surface reflectance. This method does not require any new algorithms to implement, but does require extensive work to characterize the radiometer used in the aircraft.

All of the above algorithms are typically used to calibrate a HSR sensor such as ASTER. Because the reflectomobile now allows us to collect surface reflectance over a larger area and in less time than the previous method of walking, it may be possible to apply the above-described methods directly to MODIS. This will be done if a large enough area of the selected site can be measured for surface reflectance/emissivity, and this area can be located on the satellite image. If it is not feasible to use the reflectance- or radiance-based approaches directly on MODIS, a transfer of calibration from an HSR sensor (such as ASTER) to MODIS is performed using the **HSR-LSR calibration transfer algorithm** (Che et al., 1991).

Past calibrations using this method have transferred calibration from SPOT to AVHRR. The difficulties with this approach are overpass times vary and the view and solar geometries change. These problems are avoided with an ASTER to MODIS calibration transfer since they are on the same platform and will view the site with the same geometry at the same time. The basic approach is to resample the HSR data to the resolution of the LSR sensor. The images are registered to one another and uniform 3x3 pixel areas are

located. The radiances for these areas are determined from the HSR sensor data and compared to the average digital counts for the same areas of the uncalibrated LSR sensor. By comparing the radiances and digital counts a calibration coefficient is determined for the LSR sensor.

This algorithm will also account for the spectral differences between the HSR and LSR sensors. This will involve extensive field work to accurately characterize the spectral reflectance of the ground surfaces used in the calibration. In an ASTER-to-MODIS calibration transfer the differences in spectral bandpass will be one of the larger sources of uncertainty in the calibration. As such, the actual method for accounting for spectral differences is still under investigation to ensure that uncertainties are minimized as much as possible.

3.1.2 Mathematical Description of Algorithm: The mathematics of the overall problem are contained within each of the component algorithms. The reader is directed to the discussion of each separate algorithm for a mathematical treatment of the problem.

3.1.3 Variance/Uncertainty Estimates: Recall the scattering and absorption of light in the atmosphere is computed using radiative transfer models and codes. The RTC output is TOA radiance for a measured ground reflectance. This radiance is compared to the average digital count from the image, for the ground area measured, to give a calibration coefficient in units of counts per unit radiance.

Table 1 lists the error sources we have identified for a wavelength region in the green portion of the visible spectrum corresponding to the second band of TM ($_c \approx 0.58$ μm) or the first spectral band of the HRV (XS1, $_c \approx 0.55$ μm). This also relates to MODIS bands 4 and 12, and ASTER band 1. The error column is the percent error in the quantity listed in the source column. The total error column is the error in radiance in percent at the sensor caused by the item in the source column. The total is the root sum of squares of all the error sources. The choice of the root sum of squares is not necessarily valid as the sources are not known to be independent.

These uncertainties will depend on the wavelength. For example, the uncertainty in the atmospheric correction increases with shorter wavelengths and the ozone correction is very small or insignificant at longer wavelengths. The results in the table are for a typical calibration day at White Sands: cloud free with good visibility of 100 km or more. The total error reported in Table 1 (and subsequent tables) is representative of the reflective portion of the spectrum.

TABLE 1
Reflectance-based method error sources, with reference to solar exoatmospheric irradiance. The values are quoted as one-sigma percentages.

Source	Error	Total Error
Choice of aerosal complex index (1.44-0.005i)		2.0
Choice of aerosal size distribution		3.0
Type (see text)		
Size limits		0.2
Junge parameter		0.5
Optical depth measurement	5.4	1.1
Extinction optical depth	5.0	
Partition into Mie and Rayleigh	2.0	
Absorption computations		1.3
O_3 amount error	20.0	
Vertical distribution	1.0	1.0
Inherent code accuracy	1.0	1.0
Non-polarized vs polarization code	0.1	0.1
Non-lambertian ground characteristic	1.2	1.2
Ground reflectance measurement		2.1
Reference panel calibration (BRF)	2.0	
Diffuse field correction	0.5	
Measurement	0.5	
Uncertainity in the value of $\mu_s = \cos(-s)$	0.2	0.2

* Included in the total error for choice of aerosol size distribution

Change in radiance with change in imaginary part of the index, real part = 1.44 for 3 ground reflectance values.

As seen from the table, the largest sources of error are in the atmospheric characterization, specifically the choice of the complex index of refraction of the aerosols and the determination of the size distribution of the aerosol particles. In our modeling of the atmosphere at White Sands, we have chosen an index of refraction for the aerosols of 1.44-0.005i. This choice was based on recommendations by Herman (1989) and Santer (1987). RTC results, with the index varied as a parameter and other inputs appropriate for a typical White Sands day show differences in TOA radiance of +1.7% to -1.4% for a change in imaginary part of the index of -0.004 and +0.005 with a ground reflectance of 0.5. See Figure 1 for details and other reflectance values. The change in the radiance due to a change in the real part of the index is much smaller (Kastner, 1985).

The choice of the aerosol particle size distribution entails a larger uncertainty. In most of our calibration work at White Sands, we use a Jungian distribution to describe the size distribution. We fit the aerosol extinction optical depth to a power law giving a Junge parameter (Biggar et al., 1990). The standard deviation of the Junge parameter from this fit is typically between 0.1 and 0.7. If the wrong Junge parameter is derived from the extinction data, a small error in the radiance occurs. In RTC simulations with nominal White Sands conditions, an error of +0.5 in the Junge parameter (3.0 instead of 2.5) gives an increase in TOA radiance of 0.45% at a solar zenith angle of 45 degrees. This error decreases at smaller zenith angles. The percentage change in radiance as a function of Junge parameter for three ground reflectances is presented in Figure 2.

Percentage change in TOA radiance with Junge parameter, refractive index = 1.44-0.005i for three ground reflectances.

Two other parameters which affect the scattering when using a known Junge parameter are the small and large particle radius limits. With normal aerosol loading, the choice of the large radius limit causes negligible error in TOA radiance because there are so few very large particles. An error in the choice of the small radius limit can, however, lead to a change in the radiance. A change in the small radius limit from 0.1 μm to 0.01 μm gives less than a 0.1% change in TOA radiance. A change from 0.1 to 0.2 μm gives a similar change in the radiance. Larger changes in the small radius limit give rise to larger changes in radiance although a choice of 0.1 μm is reasonable.

A much larger possible error can be the assumption of a Junge size distribution on a day where this size distribution is not appropriate. King et al. (1978) and Hart (1990) investigated the inversion of spectral optical depths to obtain the aerosol size distribution. Hart finds as high as a 3.6% change in the calibration using an inverted size distribution rather than a Junge size distribution and as low as 0.2%. This shows we must carefully choose the

appropriate size distribution for our calibration efforts in order to minimize errors.

The RTCs used in our calibrations require the optical depth components due to Rayleigh scattering and aerosol scattering and absorption. The starting point for determining these optical depths is the measured extinction optical depth. The accuracy of this measurement depends on the calibration of the solar radiometer and the stability of the atmospheric conditions during the period of measurements. If the radiometer is accurately calibrated, we can use "instantaneous" measurements of the optical depth. The error in the measurement then depends on the accuracy of the calibration of the zero-airmass intercept (Gellman et al., 1991). At the airmasses used during calibrations, the error in percent is nearly equal to the error in percent in the intercept. For a carefully calibrated instrument, this error should be no more than 5 percent. If the radiometer is not calibrated, we can use a Langley plot technique to determine the optical depth if the atmosphere is stable during the period of measurement. The uncertainty is then unknown as certain temporal variations in the optical depth can give a straight line Langley plot and an erroneous value for the optical depth, (Shaw, 1976).

Once the extinction optical depth is measured, we determine the components of the optical depth. The contribution to the optical depth due to Rayleigh scattering is computed from the barometric pressure at the surface. This measurement has an uncertainty of 0.1% resulting in an optical depth component known to better than 2% when the atmospheric profiles are nominal. If the extinction optical depth is measured to within 4% and the size distribution is Jungian, we can determine the ozone contribution to the optical depth to within about 20%, (Biggar et al., 1990). If the radiometer wavelengths are chosen to be free from known absorption bands of other atmospheric constituents, the optical depth components are partitioned into the necessary components at about the 5% level. With these errors, RTC results show a 1% difference in TOA radiance. The 20% uncertainty in ozone amount translates to an error of only about 1.3% in TOA radiance as the ozone absorption is a small effect. This error is strongly wavelength dependent due to the spectral variation in the ozone absorption coefficient. The ozone absorption contribution is modeled with a custom version of the 5S code, (Tanré et al., 1990).

There are several other uncertainties related to the RTC. The code's authors claim an inherent code accuracy of no worse than 1%. Comparisons between independent codes making similar assumptions (Mie scattering by the aerosols, Junge size distributions, etc) but different numerical techniques, give results which compare at the 1% level. In our work, we use a scalar code that does not account for polarization of the scattered radiation. We also use a code which does include polarization but have found the TOA radiance changes by less than 0.1%. This is an insignificant error as long as the sensor

being calibrated is not sensitive to the polarization of the light incident at the sensor. If this is not the case, the polarization code must be used and the polarization characteristics of the sensor must be well understood to eliminate calibration errors. This effect is most prominent in clear atmospheres when the scattering is nearly Rayleigh and the view angle of the sensor is 90 degrees to the solar zenith angle.

Another consideration is the accuracy of the measured surface nadir reflectance factor. The reflectance factor is measured by reference to a field reflectance standard, usually painted barium sulphate ($BaSO_4$) or Spectralon (a diffuse panel material made by Labsphere). The directional reflectance of the standard is measured in the laboratory (Biggar et al., 1988) or field (Jackson et al., 1987) with respect to pressed polytetrafluoroethylene made according to a National Institute of Standards and Technology prescription. We estimate the directional reflectance error of the field standard is no more than 2% and the precision of the radiometer measurements of the sand and the standard are about 0.5% due to sampling errors and limitations of the instruments and data loggers. We correct the nadir reflectance factor for the component of diffuse light in the field which is not present during the laboratory calibration of the standards. This correction has an uncertainty of about 0.5%. Simulations with the code show an error in nadir reflectance factor gives the same error in TOA radiance for conditions similar to those normally found at White Sands. Simulation results are presented in Figure 3. Errors also exist in the leveling of equipment and measurement of time and position which translates to an error in our knowledge of the cosine of the solar zenith angle $__S$. We estimate this error to be about 0.1 degree which gives a 0.2% error in the $\cos(__S)$ for $__S = 45°$.

Percentage change in radiance with ground reflectance, refractive index of 1.44-0.005i, Junge parameter of 2.5.

We must recognize that the total of these errors could add to much more than the root sum of squares. Also, these are in reference to the exoatmospheric solar irradiance. We have used the solar irradiance data from Neckel and Labs (1984) in which the authors claim an uncertainty of ±1.0% or less in the region between 0.33 and 1.25 μm.

We note that a sensor calibration made under a given set of conditions may not apply accurately under different conditions. Sensor-related errors, which may vary with the scene under observation can change the calibration by a few percent. Examples, whose magnitudes can vary substantially from sensor to sensor, are: stray light, non-linear response, spectral-bandpass changes and the memory effect, listed elsewhere for TM (Slater, 1988). Furthermore, all sensors exhibit a modulation transfer function that modifies the radiometry of the image depending on the spatial frequency content of the scene.

The improved reflectance-based method uses many of the measurements made for the basic reflectance-based method along with the measurement of the diffuse-to-global irradiance ratio at the ground (Biggar et al., 1990b). This measurement is made at the time of satellite sensor overpass and at the solar zenith angle corresponding to the sensor view zenith angle (_v). The errors and the estimated values are given in Table 2. The extinction optical depths and ground reflectance measurement entries are identical with those of the reflectance-based method.

TABLE 2.
Improved reflectance-based method error sources, with reference to solar exoatmospheric irradiance. The values are quoted as one-sigma percentages.

Source	Error	Total Error
Extinction optical depth	5.0	1.0
Ground reflectance measurement	2.1	2.1
Spherical albedo and atmospheric reflectance		1.0
Atmospheric model error	1.0	
Diffuse-to-global ratio measurement		2.3
Field measurement	2.0	0.5*
Blocked diffuse component	2.0	0.5*
Extrapolation to new angles	1.0	0.25*
Panel BRF correction (-s~ 50°)	2.2	2.2*
Uncertainty in μ_s and μ_v	0.4	0.1
Total Error (root sum of squares)		3.5

* Included in the Total Error for Diffuse-to-global ratio measurement

In the improved method, two quantities are calculated by the radiative transfer code that were not explicitly used in the previous method. The computation of the spherical albedo and the atmospheric reflectance depend on the atmospheric model chosen (Biggar, 1990). The choice of the wrong model for equivalent conditions at White Sands can give an error of up to 1%. These two terms are normally of opposite sign however and an error in one is usually counterbalanced to a degree by an opposite error in the other. As the terms enter directly into the computation of the apparent reflectance

(which is directly proportional to the TOA radiance), the error in either term contributes to an error of the same sign and amount in the calibration.

The largest error source in the improved method relates to the measurement of the ratio of diffuse to global (total) irradiance. Currently we measure the total irradiance using a 1-degree field-of-view radiometer viewing a reflectance panel at nadir. The panel is leveled on a stand about 0.5 to 0.75 m above the ground. The diffuse irradiance is measured by shadowing the panel with an aluminum panel on the end of a 3.5-m long pole. We make a correction for the part of the diffuse field that is blocked by the shadower. This correction depends on the optical depth and the aerosol size distribution.

Simulations show the error in the computation of the blocked diffuse component can be as large as 2% but due to the way the ratio enters the computation, the error in the apparent reflectance will be about 0.5%. A similar error in the measurement of the ratio (due to the radiometer, data logger, and other equipment) is possible. If we extrapolate the ratio measurements to a view angle that is not measured, an error of about a percent in the ratio is the maximum expected. This gives rise to an error of about 0.25% in the final result. Finally, we correct for the non-lambertian reflectance of the panel. We computed a maximum error of 2.2% for a $BaSO_4$ panel with a solar zenith angle of about 50 degrees. This is about worst case for calibrations at White Sands. We can reduce this error by accurately computing the distribution of diffuse light on the panel from the RTC and by using a more lambertian panel (such as Spectralon). The root sum of squares of these uncertainties is about 3.5%.

The radiance-based method relies on a different realization of a radiometric scale than the reflectance-based methods. The scale of spectral irradiance is the base rather than diffuse spectral reflectance. In this method, we use a carefully calibrated portable radiometer to measure the radiance at some altitude above the site. The radiance is measured at the time of sensor overpass in a similar view geometry. The sources of uncertainty for this method are listed in Table 3.

The largest error is the calibration of the radiometer. We normally use a calibrated FEL (ANSI designation) type quartz-halogen lamp to illuminate a reflectance panel. The lamp illuminates the panel with a given irradiance at a given distance when the lamp is aligned correctly with the optical axis of the calibration setup. The lamp calibration itself suffers from both scale and transfer uncertainty as given by the calibration laboratory. The lamp positioning causes an uncertainty as the lamp-to-panel distance may not be the exact distance specified and any deviation causes a change in irradiance proportional to $1/r^2$. The lamp output depends in a complicated way on the lamp current. In most cases, the precision constant-current-power supplies maintain the lamp output to a precision of better than 0.5%. The lamp

current is set and monitored by measuring the voltage across a precision shunt. There is a small measurement error which is almost always less than 0.5% (the worst case three-sigma limits for the precision voltmeter and shunt calibration).

Currently we use a standard reflectance panel in our calibration of the radiometer. This panel directional reflectance is probably known to no worse than 2% as stated above. Penny (1991) has recently developed a detector-based absolute radiometer that should improve our uncertainty in determining the panel radiance as it provides a direct measure of the lamp irradiance or panel radiance. The three-sigma uncertainty in the irradiance measurement should be less than 0.6% and the radiance less than 1.0%.

TABLE 3.
Radiance-based method error sources. The values are quoted as one-sigma percentages.

Source	Error	Total Error
Radiometer Calibration		2.5
Panel calibration	2.0	
Lamp calibration	1.3	
Scale uncertainty	1.2	
Transfer uncertainty	0.5	
Lamp positioning	0.3	
Lamp current stability	0.5	
Voltage measurement error	0.5	
Measurement Accuracy		1.3
Data logger accuracy	0.5	
Radiometer stability	0.5	
Pointing angle errors (± 10°)	1.1	
Correction For Altitude Difference		< 0.1
Uncertainty in the reflectance-based method	5.0	
Total Error (root sum of squares)		2.8

The calibrated radiometer is then carried to altitude in an aircraft or helicopter. Data from the scene are recorded by a data logger that digitizes the

radiometer output. The radiometer stability (temperature drifts, etc) and data logger errors are less than 0.5% each. A video camera is bore-sighted with the radiometer in order to locate measurements on the ground after data collection. In this way, we ensure that only radiances from the test site are used. A calibration uncertainty can be introduced by pointing errors as the helicopter may not maintain the same geometry as the sensor. Simulation with a radiative transfer code has shown that a pointing error of up to 10 degrees can give a maximum error of 1.1% in radiance.

The final source of uncertainty in the radiance-based method is the transfer of the measured radiance at some intermediate altitude in the atmosphere to the top of the atmosphere. The RTC is run with measured values of optical depths and ground reflectance to compute the normalized radiance at the aircraft or helicopter altitude and at the top of the atmosphere. The atmospheric correction is normally on the order of 2%. The error in the atmospheric correction is the same as that in the reflectance-based method and should be less than 5%. A 5% error in a 2% correction adds a negligible uncertainty compared to the radiometer calibration and measurement accuracy. If the radiometer is accurately calibrated and the data collection system is stable and accurate, the radiance-based method gives the lowest uncertainty.

We intend to refine these three methods to apply them to the calibration of MODIS and ASTER. We plan to improve the accuracy of the BRF and reflectance measurements with new equipment. This includes measuring the solar aureole to allow us to improve the characterization of the aerosol scattering phase function which depends on refractive index and size distribution. We plan to design and build an instrument to measure the spectral diffuse-to-global ratio and a camera system to determine the surface bi-directional reflectance distribution function (BRDF). With these improvements, we anticipate the uncertainty in the three methods can be reduced to between 2 and 3% by the time Eos instruments are being calibrated in flight.

These error budgets were presented for TM band 2 (or SPOT band XS1, MODIS bands 4 and 12, or ASTER band 1) but are representative of the range from 0.4 to 1.1 μm. We have calibrated TM bands 1-5 and 7, however bands 5 and 7 involve extrapolation of measured data and hence the uncertainty in the calibration is higher. We intend to extend the wavelength range over which measurements are made for the three methods using a spectrometer with a nominal 15-nm operating resolution covering the range from 1.1 to 2.4 μm (Smith, 1992). We plan to improve the automatic tracking solar radiometer we use to collect spectral extinction optical depths to extend the wavelength coverage from 0.37 to about 2.5 μm. The diffuse-to-global instrument will use a silicon-array-detector spectrometer covering the range 0.4 to 1.1 μm. We

also plan to use the SWIR spectrometer with this instrument to investigate the spectral variation of the irradiance ratios.

If MODIS is calibrated by reference to another satellite sensor, most likely ASTER, then additional uncertainties will be induced. An error analysis has been previously performed with relation to the in-flight calibration of NOAA-11 AVHRR with reference to SPOT-2 HRV (Che et al., 1991). In that study it is noted that the uncertainty in gain introduced by inaccurate registration of the images is 2% in the worst case. Much of this error is due to the difference in scale between the two sensors. Selecting 3x3 areas minimizes this uncertainty but does not reduce it to zero. Grant (1989) showed that a 0.5 AVHRR pixel error in any direction gives rise, on average, to a change in gain of 1% for the gypsum areas and generally larger errors for darker areas.
The error in the double application of the Herman-Browning code is estimated to be 1%. Although the code itself is more exact than this, its use in a single path calculation can typically give results with uncertainties as large as 4.4% due to errors in the inputs for optical depth, complex index of refraction of aerosols, etc (Biggar, 1990). However these errors are to a large extent self-compensating when the code is used in both the up and down directions as is the case here (Teillet et al., 1990).

Non-coincidence and spectral reflectance uncertainties are estimated to be 2% for reflectance larger than 0.5 and 4% for lower reflectance. The non-coincident uncertainties relate to the time difference of about four hours between the HRV and AVHRR acquisitions of the same scene. The largest effect here is due to the change in the BRDF of the surface as observed from sensors in orbits of different inclination, the non-lambertian characteristics of flat areas, or surface relief variations. This is particularly noticeable for the lava bed area sometimes used in our work which is to the north of our White Sands site. These lava beds exhibit changes from 0.03 to 0.15 in BRF depending on illumination and viewing conditions.

Many of these problems indicated above are less critical for the calibration of MODIS with reference to ASTER. Because both sensors are on the same platform and acquire the image under the same illumination and viewing conditions, the registration uncertainty is reduced and the BRDF problem is eliminated. There remains a spectral-band mismatch but a band-averaged value that includes two to four MODIS bands will still be of great value for MODIS calibration and cross-calibration purposes in general. We estimate the error due to the mis-registration between the images should be reduced to 0.5%. Errors due to spectral band mismatch should decrease to 1.0%, and the errors in the atmospheric correction should be 0.5%. Assuming the case for which ASTER is radiometrically corrected to 2%, it should be possible to radiometrically calibrate MODIS to better than 3%.

The above discussion has focussed on the vicarious calibration in the VNIR, and SWIR. Because work for the thermal portion does not have as long a history of use by the RSG, we do not have a detailed error analysis at this time. However, results from a recent thermal calibration of Landsat-5 TM indicate the method is most sensitive to measurements of the surface temperature and emissivity and inclusion of atmospheric profiles. Secondary effects include more accurately assessing the upwelling and downwelling atmospheric radiances.

3.2 Practical Considerations

This section describes anticipated techniques for algorithm implementation. A detailed plan for implementation is not given here. This section focuses on the practical issues involved in algorithm implementation. This includes programming and procedural issues as well as validation, quality control, data dependencies, exception handling, and a detailed description of the output product.

3.2.1 Implementation Plans: The software will be developed to allow for future upgrades. We do not anticipate major algorithmic changes in the final version since many of the algorithms have a long history of use. This, however, will not preclude improvements as knowledge of the problem becomes greater. To avoid problems caused by software upgrades, we will develop all software with backward compatibility. This will allow older data sets to be re-processed to determine the effect of any upgrades. This will also allow for traceability of the results.

3.2.2 Programming/Procedural Considerations: The primary programming effort in this project focuses on the integration of the separate component algorithms into a coherent package. The software will also be designed so as to limit user intervention and increase user friendliness. To enhance user friendliness, the software will be based on an X-windows graphical user interface. The use of point and click techniques will be implemented for user-defined parameters in the calibration process.

There are also several other programming and procedural considerations. Look-up tables could be used to store radiative transfer and phase function computations to greatly save computation time. This, however, will not be done since the loss of accuracy incurred is not worth the time savings. Since the software is not intended to run at the Distributed Active Archive Center (DAAC) for real-time processing, this should not be a problem.

As mentioned, the software will be made as automated as possible to allow for repeatability of results and to speed processing. This will also allow the software to be used at alternate sites, yet achieve the same results. Currently, a great deal of subjectivity comes into play in the calibration. Much of this

subjectivity is from expert users adjusting the calibration technique to obtain optimal results. By implementing an expert system approach, this subjectivity will be avoided. This could, however, slightly increase the uncertainty of the results if the rules developed for the expert system are not stringent enough. On the otherhand, if the rules become too stringent we may inadvertently limit the use of marginal data sets which could still give adequate results.

The only data required from outside of the RSG are the image and associated ancillary data from ASTER and MODIS. The satellite data should be in raw form, with no radiometric correction. Preferably it should be geometrically corrected. It is also desirable that the data from the two sensors be registered to one another.

Since this algorithm will not be implemented at the DAAC, the size of the package and processing time are not critical. The output will be calibration coefficients and will be stored to disk. All ground-based input data will be archived to allow reprocessing if necessary.

3.2.3 Calibration and Validation: Validation of this algorithm is difficult because of the lack of knowledge of the true calibration state of the sensor. We will perform validation studies of the reflectance-based and improved reflectance-based methods using the measurements from the well-calibrated radiometer flown in an aircraft for the radiance-based method. Validation will be obtained by comparing the predicted radiances at the aircraft altitude to the measured radiances by the radiometer. We currently, have no planned method for validation of the radiance-based method.
3.2.4 Quality Control and Diagnostics: Quality control will be performed on all of the ground-based collected data. This will be built into the expert system algorithms. These assessments will be used to indicate the reliability of the calibration coefficients. Quality assessment of the satellite data will not be performed by the RSG. We will rely on cloud-screening algorithms developed by ASTER and MODIS Science Teams to assess the quality of the scene. We will also rely on software resident at the DAAC for quality assessment of the image data.

3.2.5 Exception Handling: Exception handling will be treated in a similar manner as quality assessment. We will examine all data collected by our group for problems. We will rely on those algorithms developed by the science team for exception handling of the image data. We will attempt to anticipate all problems which could affect the results. These problems include detecting and correcting for equipment failure. Lack of a certain type of data will be handled and their effect on the final output product assessed and reported.

3.2.6 Data Dependencies: Data dependencies are minimal. We require MODIS raw DNs. We require ASTER raw DNs. All other data will be collected by the RSG. We will handle all problematic data dependencies other than the image data.

3.2.7 Output Product: The output product of this algorithm is the calibration coefficient for the sensor. This will be reported for all MODIS bands. All intermediate results of the algorithm will be available on request. This includes atmospheric optical depths, columnar ozone and water vapor, surface reflectance measurements, and predicted-top-of-the-atmosphere radiances. In addition, all ancillary data such as meteorological information will be available. An estimate of accuracy of each parameter and a breakdown of each component's contribution to the overall error will be included. These data may be useful to other investigators for validation studies. The measured optical depths, and retrieved aerosol parameters may especially be of interest to the MODIS Science Team, as well as to the Multi-angle Imaging SpectroRadiometer (MISR) Science Team.

4.0 Constraints, Limitations, and Assumptions

The assumptions made are given in greater detail for each of the component algorithms. Constraints are primarily the ability to characterize the atmosphere and the surface. Limitations are determined by examining the assumptions. As more of the assumptions break down, the algorithm becomes less valid. Eventually, the results become invalid.

The constraints to the method can be ascertained from the previous section. These include using appropriate test sites of uniform high reflectance located in regions of low aerosol loading. The method is limited to days when the satellite can observe the test site, and preferably to days when no clouds are present. If no atmospheric transmittance data are collected, the results of the method are greatly compromised. If no ground-based reflectance data or aircraft-based radiance data are available, the method cannot be used.

5.0 Component Algorithm Descriptions

As described earlier, the vicarious calibration algorithm is actually several independent algorithms. Since detailed descriptions of these algorithms would make the ATBD prohibitively long, descriptions of each component algorithm are contained in the appendix of this document. The descriptions are given in the same form as used above for the overall method. The first part in each appendix contains the objective of the algorithm, an overview of the algorithm, and an historical perspective. The second part describes the algorithm in a mathematical and physical basis. This section also discusses errors and uncertainties in the algorithm. The last two sections describe

computational considerations and constraints and limitations on the algorithm. It should be noted that many of these algorithms have a long history, and as such we will not give lengthy mathematical derivations for several of the algorithms. In these cases a brief description of the algorithms history will suffice and references for derivations will be given.

Overall there are 12 algorithms which are described. These are as follows:

A. Langley method
B. Modified-Langley method
C. Component optical depth
D. Columnar water vapor
E. Diffuse-to-global
F. Surface reflectance
G. Surface emissivity
H. Mie phase function retrieval
I. Gauss-Seidel radiative transfer
J. TIR radiative transfer
K. Gain and offset
L. HSR-to-LSR calibration transfer

Each of these algorithms has been previously implemented in some fashion by the RSG. The difficulty of the current project is to implement these diverse algorithms as part of a larger more efficient package. Because of this diversity, it is important that the history, derivation, and limitations of each algorithm be known so their effects on the overall calibration process is understood. It is for this reason that each algorithm is discussed in detail in the appendix.

6.0 References for Appendix E

Begni, G, M. C. Dinguirard, R. D. Jackson, and P.N, Slater, "Absolute calibration of the SPOT-1 HRV cameras," *Proc. SPIE*, **660**:66-76, 1986.

Biggar, S. F., *In-flight methods for satellite sensor absolute radiometric calibration*, Ph.D. dissertation, University of Arizona, 153 pp., 1990.

Biggar, S. F., D. I. Gellman, and P. N. Slater, "Improved evaluation of optical depth components from Langley plot data," *Remote Sens. Environ.* **32**:91-101, 1990a.

Biggar, S. F., J. Labed, R. P. Santer, P. N. Slater, R. D. Jackson, and M. S. Moran, "Laboratory calibration of field reflectance panels," *Proc. SPIE* **924**:232-240, 1988.

Biggar, S. F., M. C. Dinguirard, D. I. Gellman, P. Henry, R, D, Jackson, M. S. Moran, and P. N. Slater, "Radiometric calibration fo SPOT-2 HRV - a comparison of three methods," *Proc. Spie*, **1493**:155-162, 1991.

Biggar, S. F., R. P. Santer, P. N. Slater, "Irradiance-based calibration of imaging sensors," *Proceedings IGARSS 90*, **1**:507-510, 1990b.

Che, N., B. G. Grant, D. E. Flittner, P. N. Slater, S. F. Biggar, R. D. Jackson, and M. S. Moran, "Results of calibrations of the NOAA-11 AVHRR made by reference to calibrated SPOT imagerey at White Sands, N. M.," *Proc. SPIE*, **1493**:182-194.

Gellman, D. I., Biggar, S. F., Slater, P. N. and Bruegge, C. J., "Calibrated intercepts for solar radiometers used in remote sensor calibration," *Proc. SPIE* **1493**:175-180, 1991.

Gellman, D. I., S. F. Biggar, M. C. Dinguirard, P. J. Henry, M. S. Moran, K. J. Thome, and P. N. Slater, "Review of SPOT-1 and -2 calibrations at White Sands from launch to the present," *Proc. SPIE*, **1938**, 1993.

Grant, B. G., *Calibration of the Advanced Very High Resolution Radiometer*, M. S. Thesis, Univeristy of Arizona, Tucson, Arizona, 71 pp, 1989.

Grotbeck, C. and R. Santer, "Solar aureole instrumentation and inversion techniques for aerosol studies: Part 2, data acquisition and inversion," *Proc. SPIE*, **1968**, 1993.

Hart, Q. J., *Surface and aerosol models for use in radiative transfer codes*, M.S. Thesis, University of Arizona, 66 pp., 1990.

Herman, B. M. and S. R. Browning, "A numerical solution to the equation of radiative transfer," *J. Atmos. Sci.*, **22**:559-566, 1965.

Herman, B. M., Personal communication, Department of Atmospheric Sciences, University of Arizona, 1989.

Jackson, R. D., M. S. Moran, P. N. Slater, and S. F. Biggar, "Field calibration of reference reflectance panels," *Remote Sens. Environ.* **22**:145-158, 1987.

Kastner, C. J. (now Bruegge), *In-flight absolute radiometric calibration of the Landsat thematic mapper*, Ph.D. dissertation, University of Arizona, 195 pp., 1985.

King, M. D., D. M. Byrne, B. M. Herman, and J. A. Reagan, "Aerosol size distributions obtained by inversion of spectral optical depth measurements," *J. Atmos. Sci.* **35**:2153-2167, 1978.

Neckel, H. and D. Labs, "The solar radiation between 3300 and 12500 Å," *Solar Physics* **90**:205-258, 1984.

Palmer, J. M., "Calibration of Thematic Mapper band 6 in the thermal infrared," *Proc. SPIE*, **1938**, 1993.

Penny, I. R., *Detector-based absolute radiometric calibration of lamps and reflectance panels*, M. S. Thesis, University of Arizona, 69 pp., 1991.

Santer, R. P., Personal communication, Laboratoire d'Optique Atmosphérique, l'Université des Sciences et Techniques de Lille, 1987.

Shaw, G. E., "Error analysis of multi-wavelength sun photometry," *Pure and Applied Geophysics*, **114**:1-14, 1976.

Slater, P. N., "Review of the calibration of radiometric measurements from satellite to ground level," *Int. Archives of Photogrammetry and Remote Sensing*, **27**:B11:726-734, 1988.

Slater, P. N, S. F. Biggar, R. G. Holm, R. D. Jackson, Y. Mao, M. S. Moran, J. M. Palmer, and B. Yuan, "Reflectance- and radiance-based methods for the in-flight absolute calibration of multispectral sensors," *Rem. Sens. Env.*, **22**:11-37, 1987.

Smith, M. W., "Design and initial performance evaluations of a portable short wave infrared spectrometer," *Proc. SPIE* **1762**, 1992.

Tanré, D., C. Deroo, P. Duhaut, M. Herman, J. J. Morcrette, J. Perbos, and P. Y. Deschamps, "Description of a computer code to simulate the satellite signal in the solar spectrum: the 5S code," *Int. J. Remote Sensing* **11**:659-668, 1990.

Teillet, P. M., P. N. Slater, Y. Ding, R. P. Santer, R. D. Jackson, and M. S. Moran, "Three methods for the absolute calibration of the NOAA AVHRR sensors in-flight," *Rem. Sens. Env.*, **31**:105-120, 1990.

Teillet, P. M., P. N. Slater, Y. Mao, Y. Ding, B. Yuan, R. J. Bartell, R. P. Santer, R. D. Jackson, and M. S. Moran, "Absolute radiometric calibration of the NOAA AVHRR sensors," *Proc. SPIE*, **924**:196-207, 1991.

Thome, K. J., D. I. Gellman, R. J. Parada, S. F. Biggar, P. N. Slater, and M. S. Moran, "In-flight radiometric calibration of Landsat-5 Thematic Mapper from 1984 to present," *Proc. of SPIE*, **1938**, 1993.

Thome, K. J., B.M. Herman, and J.A. Reagan, "Determination of precipitable water from solar transmission," *J. of Appl. Met.*, **31**:157-165, 1992.

Acronyms for Appendix E

ASTER	Advanced Spaceborne Thermal Emission and Reflectance radiometer
ATBD	Algorithm Theoretical Basis Document
AVHRR	Advanced Very High Resolution Radiometer
BRDF	Bi-directional Reflectance Distribution Function
BRF	Bi-directional Reflectance Factor
DAAC	Distributive Active Archive Center
DN	Digital Number
EOS	Earth Observing System
HRV	Haute Resolution Visible
HSR	High Spatial Resolution
LSR	Low Spatial Resolution
MCST	MODIS Characterization Support Team
MISR	Multi-angle Imaging SpectroRadiometer
MODIS	MODerate resolution Imaging Spectroradiometer
NOAA	National Oceanic and Atmospheric Administration
RTC	Radiative Transfer Code
RSG	Remote Sensing Group (of the Optical Sciences Center at the University of Arizona)
SeaWiFS	Sea-viewing Wide Field-of-view Sensor
SPOT	Systeme Probatoire d'Observation de la Terre
SWIR	Short-Wave Infrared
TOA	Top-Of-Atmosphere
TIR	Thermal Infra-Red

Appendix F

Glossary

Absolute Calibration. The determination of calibration factors by comparison with a standard with output known in SI units.

Accuracy Precision. *Accuracy* is an estimate characterizing the closeness of a measurement to the true measurand. It can given as one minus the absolute value of relative uncertainty (negative values are set to 0), or as a percentage after multiplication by 100. Note that while accuracy assumes reference to a standard or knowledge or error sources, *Precision* is a relative measure of the agreement amongst a set of measurements. Also, with accuracy higher numbers are better, and with uncertainty lower numbers are better.

Ancillary Data. Data other than instrument data required to perform an instrument's data processing. They include orbit data, attitude data, time information, spacecraft or platform engineering data, calibration data, data quality information, and data from other instruments.

Attitude Data. Data that represent spacecraft orientation and onboard pointing information. Attitude data includes:

- Attitude sensor data used to determine the pointing of the spacecraft axes, calibration and alignment data, Euler angles or quaternions, rates and biases, and associated parameters.
- Attitude generated on-board in quaternion or Euler angle form.
- Refined and routine production data related to the accuracy or knowledge of the attitude.

Browse Data Product. Subsets of a larger data set, other than the directory and guide, generated for the purpose of allowing rapid interrogation (i.e., browse) of the larger data set by a potential user. For example, the browse product for an image data set with multiple spectral bands and moderate spatial resolution might be an image in two spectral channels, at a degraded spatial resolution. The form of browse data is generally unique for each type of data set and depends on the nature of the data and the criteria used for data selection within the relevant scientific disciplines.

Calibration. The set of operations which establish, under specified conditions, the relationship between values indicated by a measuring instrument and the corresponding known values of a standard.

Calibration Data. The collection of data required to perform calibration of the instrument science data, instrument engineering data, and the spacecraft or platform engineering data. It includes pre-flight calibration measurements, in-flight calibrator measurements, calibration equation coefficients derived from calibration software routines, and ground truth data that are to be used in the data calibration processing routine.

Channel. (See Detector Channel).

Characterization. The measurement of the typical behavior of instrument properties which may affect the accuracy or quality of its response or derived data products. The results of a characterization may or may not be directly used in the calibration of the instrument response, but may be used to determine its performance.

Correlative Data. Scientific data from other sources used in the interpretation or validation of instrument data products, e.g., ground truth data and/or data products of other instruments. These data are not utilized for processing instrument data.

Correlative Measurements. Spatially and temporally coincident measurement of the parameters deduced from a given sensor, made with independent surface, aircraft, or separate in-orbit instrumentation. These activities require coordination with other ground stations, EOS validation teams, concurrent intensive field campaigns, or long-term monitoring stations.

Data Product. The final processed data sets associated with the various measured and derived geophysical parameters.

Data Product Levels. Data levels 1 through 4 as defined in the EOS Data Processing Levels (table F.1).

Data Product Validation. The process of assessing, by independent means, the uncertainty of observable or geophysical parameters derived from sensor output. Accurate calibration, data transmission, and processing algorithms are prerequisite to data validation. Data product validation can further be divided into correlative measurements or data product verifications.

Data Product Verification. Perform product validation analyses by simulation, checks with physical bounds, or self-consistency analyses. Comparisons with routine data products from other in-orbit sensors, or utilization of existing databases for trend analyses are included.

Detector Channel. A detector and all of its associated optics and electronics.

EDOS Production Data Sets. Data sets generated by EDOS using raw instrument or spacecraft packets with space-to-ground transmission artifacts removed, in time

order, with duplicate data removed, and with quality/accounting (Q/A) metadata appended. Time span, number of packets, or number of orbits encompassed in a single data set are specified by the recipient of the data. These data sets are equivalent to level zero data formatted with Q/A metadata. For EOS, the data sets are composed of:

- instrument science packets,
- instrument engineering packets,
- observatory housekeeping packets, or
- onboard ancillary packets

with quality and accounting information from each individual packet and the data set itself and with essential formatting information for unambiguous identification and subsequent processing.

EDOS Quick Look Production Data Sets. Data sets generated by EDOS using raw instrument or spacecraft packets from a single TDRSS acquisition session and delivered to a user within minutes of receipt of the last packet in the session. Transmission artifacts are removed, but time ordering and duplicate packet removal is limited to packets received during the TDRSS contact period.

Emissive Bands. MODIS bands 20-25 and 27-36.

Engineering Data. All data available on-board about health, safety, environment, or status of the platform and instruments.

- Platform Engineering Data – The subset of engineering data from platform sensor measurements and on-board computations.

- Instrument Engineering Data – All non-science data provided by the instrument.

- Housekeeping Data – The subset of engineering data required for mission and science operations. These include health and safety, ephemeris, and other required environmental parameters.

Ephemeris Data. (See Orbit Data)

Ground Calibration. See Vicarious Calibration.

In-Flight Calibration. See On-Orbit Calibration.

Ground Truth. Geophysical parameter data, measured or collected by other means than by the instrument itself, used as correlative or calibration data for that instrument data. It includes data taken on the ground or in the atmosphere. Ground truth data are another measurement of the phenomenon of interest; they are not necessarily more "true" or more accurate than the instrument data.

Housekeeping Data. (See Engineering Data)

In Situ Data. (See Ground Truth)

Instrument Data. Data specifically associated with the instrument, either because they were generated by the instrument or included in data packets identified with that instrument. These data consist of instrument science and engineering data, and possible ancillary data.

Instrument Engineering Data. (See Engineering Data)

Instrument Housekeeping Data. (See Engineering Data)

Instrument Science Data. Data produced by the science sensor(s) of an instrument, usually constituting the mission of that instrument.

Metadata. Information about data sets which is provided to the ECS by the data supplier or the generating algorithm and which provides a description of the content, format, and utility of the data set. Metadata may be used to select data for a particular scientific investigation.

On-Orbit Calibration. The calibration of an aircraft or satellite based sensor while in flight. This may be through ground calibration exercises, or through use of an on board calibration system.

Operational Data. Data created by an operational instrument (i.e., NOAA).

Orbit Data. Data that represent spacecraft locations. Orbit (or ephemeris) data include: Geodetic latitude, longitude and height above an adopted reference ellipsoid (or distance from the center of mass of the Earth); a corresponding statement about the accuracy of the position and the corresponding time of the position (including the time system); some accuracy requirements may be hundreds of meters while other may be a few meters.

Playback Data. Data that have been stored on-board the spacecraft for delayed transmission to the ground.

Pre-Flight Calibration. See Pre-Launch Calibration.

Pre-Launch Calibration. The calibration of a sensor prior to launch.

Prototype Product. Data product generated as part of a research investigation, of wide research utility, requiring too much data or computer power for generation at the investigator SCF, and accepted as a candidate Standard Product by the IWG. Prototype Products will be generated at DAACs, but their routine generation is not guaranteed and will not interfere with other Standard Product generation.

Quick-Look Data. Data received during one TDRSS contact period which have been processed to Level 0 (to the extent possible for data from a single contact). These are data that have been identified to EDOS as requiring priority processing.

Quick-Look Product. Product produced at a PGS by applying science algorithms to Quick-Look Data.

Real-Time Data. Data that are acquired and transmitted immediately to the ground (as opposed to playback data). Delay is limited to the actual time required to transmit the data.

Reflective Bands. MODIS bands 1-19, and 26.

Relative Calibration. The determination of the correction by comparison with a standard with output not necessarily known in physical units, but which is established in ratio or as a fraction of the value of the standard.

Science Computing Facilities (SCFs). Project-funded facilities at instrument team member locations used to develop and test algorithms and assess data quality.

Special Data Products. Data products which are considered part of a research investigation and are produced for a limited region or time period, or data products which are not accepted as standard products.

Spectral Regions.

VIS	400-700nm
NIR	700-1060nm
SWIR	1060-3000nm
MWIR	3000-6000nm
LWIR	6000-14400nm

Standard Products. (1)Data products generated as part of a research investigation, of wide research utility, accepted by the IWG and the EOS Program Office, routinely produced, and in general spatially and/or temporally extensive. Standard Level 1 products will be generated for all EOS instruments; standard Level 2 products will be generated for most EOS instruments. (2)All data products which have been accepted for production at a PGS, including (1) above as well as prototype products.

Vicarious Calibration. The radiometric calibration of an in-orbit sensor through an intensive field-campaign. This calibration is established via a

•1. reflectance-based ground calibration in which atmospheric and surface reflectance characteristics are measured and used to compute exo-atmospheric radiances, or

•2. radiance-based ground calibration in which helicopter or aircraft sensors are used to map radiances and extrapolate to the required exo-atmospheric radiances.

Table F.1
EOS Data Processing Levels

Raw Data	Data in their original packets, as received from the observatory, unprocessed by EDOS.
Level-0	Raw instrument data at original resolution, time ordered, with duplicate packets removed.
Level-1A	Level 0 data, which may have been reformatted or transformed reversibly, located to a coordinate system, and packaged with needed ancillary and engineering data.
Level-1B	Radiometrically corrected and calibrated data in physical units at full instrument resolution as acquired.
Level-2	Retrieved environmental variables (e.g., ocean wave height, soil moisture, ice concentration) at the same location and similar resolution as the Level 1 source data.
Level-3	Data or retrieved environmental variables that have been spatially and/ or temporally resampling may include averaging and compositing.
Level-4	Model output and/or variables derived from lower level data which are not directly measured by the instruments. For example, new variables based upon a time series of Level 2 or Level 3 data.

Appendix G

Acronyms & Symbols

G.1 Acronyms

A/D	Analog to Digital Converter
A&E	Activation and Evaluation
AEM	Analog Electronics Module
AIRS	Atmospheric Infrared Sounder
AM1	First EOS AM platform to be launched
AM2	Second EOS AM platform to be launched
AM3	Third EOS AM platform to be launched
ASTER	Advanced Spaceborne Thermal Emission and Reflection Radiometer
ATBD	Algorithm Theoretical Basis Document
AVHRR	Advanced Very High-Resolution Radiometer
AVIRIS	Airborne Visible Infrared Imaging Spectrometer
BBR	Band-to-Band Registration
BRDF	Bidirectional Reflectance Distribution Function
BW	Bandwidth
BWT	Bandwidth Tolerance
Cal ATBD	Calibration Algorithm Theoretical Basis Document
CCSDS	
CDR	Critical Design Review
CERES	Clouds and Earth's Radiant Energy System
COB	Close of Business
COLOR	Follow-on to SeaWiFS satellite
CTIA	Capacitance transimpedance Amplifier
CW	Center Wavelength
CWT	Center Wavelength Tolerance
CZCS	Coastal Zone Color Scanner
DAAC	Distributed Active Archive Center
DADS	Data Archive and Distribution System

DC	Direct Current
DN	Digital Number
DR	Data Rates
EDOS	EOS Data and Operations System
EM	Engineering Model of MODIS
EOC/ICC	EOS Operation Center / Instrument Control Center
EOS	Earth Observing System
EOS AM	Descending sun-synchronous satellite with a 10:30 AM equatorial crossing
EOS PM	Ascending sun-synchronous satellite with a 1:30 PM equatorial crossing
ER-2	Second Earth Resources U-2 Aircraft
ESDIS	Earth Science Data and Information System
FFT	Fast Fourier Transform
FOV	Field-of-View
FPA	Focal Plane Assemblies
FS	Full Scale
GFOV	Ground Field-of-View
GIFOV	Ground Instantaneous Field-of-View
GOES	Geostationary Operational Environmental Satellite
GSFC	Goddard Space Flight Center
GSD	Ground Sample Distance
GSE	Ground support Equipment
HIRIS	High-Resolution Imaging Spectrometer
HIRS	High-Resolution Infrared Sounder
HRV1	First High-Resolution Visible scanner on SPOT
HS	Half Scale
IFOV	Instantaneous Field of View
IMC	Information Management Center
IR	Infrared
Landsat	Land Remote-Sensing Satellite, formerly ERTS
LWIR	Long Wavelength Infrared
MCST	MODIS Characterization Support Team
MeV	Million Electron Volts
MISR	Multi-Angle Imaging Spectroradiometer
MODIS	Moderate-Resolution Imaging Spectroradiometer
MSS	Multispectral Scanner
MTF	Modulation Transfer Function

NASA	National Aeronautics and Space Administration
MWIR	Medium Wavelength Infrared
NDVI	Normalized Difference Vegetative Index
Nimbus-7	Satellite
NIR	Near-infrared bands
NIST	National Institute of Standards and Technology
OBC	On-Board Calibrators
OC	Operating/Duty Cycle
PA	Pointability Angle of Optical Axis
PC	Photo conductive
PF	Polarization Factor
PI	Principal Investigator
PV	Photo Voltaic
PM1	First EOS PM platform to be launched
PM2	Second EOS PM platform to be launched
PM3	Third EOS PM platform to be launched
PRF	Point Response Function
PSF	Point Spread Function
RDC	Research and Data Systems Corporation
RMM	Radiometric Math Model
SBRC	Santa Barbara Research Center, a subsidiary of Hughes
S/MWIR	Short and Medium Wavelength Infrared
SD	Solar Diffuser
SDSM	Solar Diffuser Stability Monitor
SDST	Science Data Support Team
SeaWiFS	Sea-Viewing Wide Field Sensor
SI	Systeme Internationale
SIS(100)	Spherical Integrating Source
SNR	Signal-to-Noise Ratio
SPOT	Systeme pour l'Obsservation de la Terre
SPOT-1	First SPOT instrument
SRCA	Spectroradiometric Calibration Assembly
STE	System Test Equipment
SV	Space Viewpoint
SWIR	Short Wavelength Infrared
TBD	To be determined

TBW	Band Width Tolerance
TCW	Center Wavelength Tolerance
TDI	Time Delay and Integration
TIR	Thermal Infrared bands
TM	Thematic Mapper
TOY	Time of Year
USGS	United States Geological Survey
VIS	Visible bands
VQW	Vector Quantization using n-by-n texture window

G.2 Symbols

$L\lambda$	Spectral radiance - $^{w}/m^2$-sr-um
L	Radiance - $^{w}/m^2$-sr
Q	Quantized data value - Integer
f	General symbol for a function
σ	Standard deviation (unit say the variable derived from)
P	Reflectance (unitless)
T	Temperature (K, KeLvin)
Ln	Natural logorithm
Q_{cal}	Calibrated quantized data (integer)
$C_o, C_{1,...}$	Calibration coefficients
μ	General symbol for the mean (unit of the variable derived from)
M,N	Number of samples processed by the expression
W	Watts (unit of power)
MeV	Million electron volts (unit of electrical potential)
NEΔL	Noise equivalent spectral radiance
sr	Sterradian (solid angle of 1 radian)
μm	Micrometer (10-6 meter)
NEΔT	Noise equivalent temperature
P	General symbol for reflectance (sometimes used for correlation coefficient)
R	Also used for reflectance
L_{typ}	Typical spectral radiance- $^{w}/m^2$-sr-μm
L_{max}	Maximum spectral radiance
π	Constant 3.14159...

d	General distance symbol
$E_{sun,\lambda}$	Mean solar exoatmospheric spectral radiance $\frac{W}{m^2 - sr - \mu m}$
θ,ϕ	General angle symbol
P_{12}	Covariance between two variables
e	Base of natural logarithms
$i,j,h,$	General variable indices
H_i	Histogram count for bin i
R	General symbol for convolution product
c_i	General calibration coefficients
$s(\lambda)$	Solar spectral radiance- W/m^2-sr-μm
τ	General time variable
C	Degradation ratio
$L(\lambda)$	Spectral radiance as a function of λ
$E(\lambda)$	Emissivity as a function of λ
$T_i(X_i)$	General linear transformation symbol used in radiometric rectification illustration (general slope parameter m_i and offset 6_i unique ti this section- not general terms)
S^2	Variance- units of the variable squared
$F_{\alpha/2}$	Statistical F test parameter for confidence level $\alpha/2$
$Z_{\alpha/2}$	Statistical τ test parameter for confidence level $\alpha/2$
$I_{max,min}$	Radiance maximum or minimum used in polarization calculation
L_{cloud}	Typical radiance from cloud surface
$\Delta\lambda$	Bandwidth (nanometers)
λ	Wavelength (nanometers)
$L_{upper,lower}$	Upper and lower spectral radiance used in calibration transformations
$Q_{max,min}$	Maximum and minimum Q values used in calibration equations
QSR	Observed post-launch count from SRCA
QPSR	Pre-launch count from SRCA
L_o	Initial lamp measurement used in calibration source integration discussion
$L(tj)$	Lamp measurement at time t_j:

Appendix H

Bibliography and References

1988 Abel, P., G. R. Smith, R. H. Levin and H. Jacobowitz. "Results from Aircraft Measurements over White Sands, New Mexico, to Calibrate the Visible Channels of Spacecraft Instruments."

1991 Ardanuy, P., D. Han and V. Solomonson. "The Moderate Resolution Imaging Spectrometer (MODIS) Science and Data System Requirements." IEEE Transactions on Geoscience and Remote Sensing , 29, No. 1, January.

1993 Asrar, G., and D. J. Dokken. "EOS Reference Handbook." NASA Publication.

1991 Balick, L. K., C. J. Golanics, J. E. Shines, S. F. Bigger and P. N. Slater. "The In-Flight Calibration Of A Helicopter-Mounted Daedalus Multispectral Scanner." Proc. SPIE, in press.

1983a Barker, J. L., D. L. Ball, K. C. Leung and J. A. Walker. "Prelaunch Absolute Radiometric Calibration of the Reflective Bands on the Landsat-4 Protoflight Thematic Mapper." Landsat-4 Science Characterization Early Results: Thematic Mapper, 2, part 1, pp. 277-371, NASA/GSFC Publication.

1983b Barker, J. L., R. B. Abrams, D. L. Ball and K. C. Leung. "Radiometric Calibration and Processing Procedure for Reflective Bands on Landsat-4 Protoflight Thematic Mapper." Landsat-4 Science Characterization Early Results: Thematic Mapper, 2, part 1, pp. 47-86, NASA/GSFC Publication.

1983c Barker, J. L., R. B. Abrams, D. L. Ball and K. C. Leung. "Characterization of Radiometric Calibration of Landsat-4 TM Reflective Bands." Landsat-4 Science Characterization Early Results: Thematic Mapper, 2, part 1, pp. 373-474, NASA/GSFC Publication.

1984 Barker, J. L. "Reflective Radiometric Calibration of Landsat TM Reflective Bands." Landsat-4 Science Investigations Summary: Includes Dec. 1983 Workshop Results, 1, pp. 140-180, NASA/GSFC Publication.

1988 Barker, J. L. and L. Wanchoo. "Radiometric Performance of Calibrators On The Landsat Thematic Mappers." Invited Paper No. A. 3. 1. 1 of Topical Meeting No. A. 3, XXVII COSPAR Meeting in Espoo, Finland, July 18-29.

1992 Barker, J. L., B. L. Markham and J. W. Burelbach. "MODIS Image Simulation from Landsat TM Imaging." Proc. of ASPRS Convention, August 3 - 8, 1, pp. 156-165.

1993 Barker, J. L., J. Harnden, P. Anuta, J. Smid and D. Hoyt. "MODIS Radiometric Sensitivity to Spectral Band Characterization." In preparation.

1993b Barker, J. L., J. Harnden, T. Bryant, and G. Kvaran. "MCST Plan for the Level-1 Calibration Algorithm." Goddard Space Flight Center Presentation, February 5.

1993 Barnes, W. L. and V. Salomonson. "MODIS: A Global Imaging Spectroradiometer for the Earth Observing System." Proceeding of 16-17 November 1992, Optical Technologies for Aerospace Sensing CR47 in Critical Reviews of Optical Science and Technology.

1986 Begni, G., M. C. Dinguirarad, R. D. Jackson and P. N. Slater. "Absolute Calibration of the SPOT-1 HRV." Cameras, Proc. SPIE, 660, Earth Remote Sensing Using the Landsat Thematic Mapper and SPOT Sensor Systems, pp. 66-76.

1979 Berthold, K., P. Horn and R. Woodham. "Destriping Landsat MSS Images by Histogram Modification." Computer Graphics and Image Processing, 10, pp. 69-83.

1978 Chu, N. and C. D. McGillem. "Methods and Performance Bounds for Constrained Image Restoration." LARS Tech. Rept. TR 061678. Purdue Univ., West Lafayette, IN.

1979 Chu, N. and C. D. McGillem. "Image Restoration Filters Based On A 0-1 Weighting Over The Domain Of Psp." IEEE Trans. Acoustics Speech and Signal Processing, ASSP-27, no. 5, pp. 457-464.

1984 Crist, E. P., and R. C. Cicone. "A Physically-Based Transformation of Thematic Mapper Data: The TM Tasseled Cap." IEEE Transactions on Geoscience and Remote Sensing, GE22, no. 3, pp. 256-263.

1988 Conel, J. E., R. O. Green, J. S. Margolis, C. Bruegge, G. A. Vane, R. E. Alley, P. N. Slater and R. D. Jackson. "Field, Radiometric, And Spectral Calibration Of The Airborne Visible And Infrared Imaging Spectrometer." Proc. SPIE, 924, pp. 179-195.

1961 Dollfus, A. "Polarization studies of the planets, in Planets and Satellites." G. P. Kuiper and B. M. Middlehurst, eds., pp. 343-399.

1973 Duda, R. and P. Hart. "Pattern Classification and Science Analysis." Wiley.

1987 Ebert, E. "A Pattern Recognition Technique for Distinguishing Surface and Cloud Types in the Polar Regions." Journal of Climate and Applied Meteorology, 26, pp. 1412-1427, October.

1993 Evans, R. Personal Communication.

1991 Flittner, D. E. and P. N. Slater. "Stability of Narrow-Band Filter Radiometers in the Solar-Reflective Range." Photogrammetric Engineering and Remote Sensing, 57, No. 2, pp. 165-171, February.

1974 Frieden, B. R. "Image Restoration By Discrete Convolution Of Minimum Length." Jour, of the Optical Soc. of Amer., 64, no. 5, pg. 682.

1975 Frieden, B. R. "Image Enhancement and Restoration." Topics in Applied Physics, 6. Picture Processing and Digital Filtering, edited by T. S. Huang, Springer Verlag, Berlin-New York.

1976 Frieden, B. R. "A New Restoring Algorithm For The Preferential Enhancement Of Edge Gradients." Jour. of the Optical Soc. of Amer., 66, no. 3, pg. 280.

1980 Frieden, B. R. "Statistical Models For The Image Restoration Problem." Computer Graphics and Image Processing, 12, pg. 40.

1991 Frieden, B. R. "Probability Statistical Optics and Data Testing." Springer-Verlag, New York.

1987 Frouin, R. and C. Gautier. "Calibration of NOAA-7 AVHRR, GOES-5, and GOES-6 VISSR/VAS Solar Channels." Remote Sensing of Environment, 22, pp. 73-101.

1964 Gehrels, T., T. Coffeen and D. Owings. "Wavelength Dependance Of Polarization. III. The Lunar Surface." Astron. Jour., 69, pp. 826-852.

1993 Gellman, D. I., S. F. Biggar, M. C. Dinguirard, P. J. Henry, M. S. Moran, K. J. Thome, and P. N. Slater. "Review of SPOT-1 and -2 Calibrations at White Sands from Launch to the Present." Spie Proceedings, Vol. 1938-13, Orlando, Florida, 12-16 April.

1993 Goddard Space Flight Center. "Specification for the Moderate-Resolution Imaging Spectroradiometer (MODIS), 422-20-02, Revision A." Goddard Space Flight Center, Greenbelt, MD, March 24.

1993 Goff, T. E. "MODIS Data Rates, Volumes and Processing Performance with the Proposed Computerized Data Structures."

1987 Hall, F. G., and G. D. Badhwar. "Signature-Extendable Technology: Global Space-Based Crop Recognition." IEEE Trans. Geosci. Remote Sens. GE-25,1

1991 Hall, F. G., D. E. Strebel, J. E. Nickeson and S. J. Goetz. "Radiometric Rectification: Toward a Common Radiometric Response Among Multidate, Multi-Sensor Images." Remote Sensing of the Environment., 5, 1991, pp. 11-27.

1992 Hall, F. G., K. F. Huemmrich, S. J. Goetz, P. J. Sellers and J. E. Nickeson. "Satellite Remote Sensing of Surface Energy Balance: Success, Failures and Unresolved Issues in FIFE, Journal of Geophysical Research." 97, No. D17, pp. 19.

1979 Haralick,R. M. "Statistical And Structural Approaches To Texture," Proc. of the IEEE, pp. 786-804, May.

1992 Helder, D. L., B. K. Quirk and J. Hood. "A Technique for the Reduction of Banding in Landsat Thematic Mapper Images." Photogrammetric Engineering & Remote Sensing, 58, no. 10, October, pp. 1425-1431.

1987 Helfenstein, P. and J. Veverka. "Photometric Properties Of Lunar Terrain Derived From Hapke's Equation." Icarus, 72, pp.342-357.

1967 Helstrom, C. W. "Image Restoration By The Method Of Least Squares." J. of Optical Soc. of Amer., 57, pg. 297.

1992 Hickey, J. R. and D. J. Brinker. "Studies Of Effects On Optical Components and Sensors: Ldef Experiments Ao-147 (Ereb Components) And S-0014 (Apex)." Second LDEF Post-Retrieval Symposium Abstracts, June 1-5, San Diego, CA, NASA Conference Publication 10097, pg. 106.

1979 Horn, B. and R. Woodham. "Destriping LANDSAT MSS Images by Histogram Modification." Computer Graphics and Image Processing,10, pp. 69-83.

1992 Hughes, Santa Barbara Research Center. "Moderate Resolution Imaging Spectroradiometer (MODIS)." Calibration Management Plan, Hughs Santa Barbara Research Center (SBRC).

1983 Irons, J. "An Overview of Landsat-4 and the Thematic Mapper." Landsat-4 Science Characterization Early Results: Thematic Mapper, 2, part 1, pp. 15-46, NASA/GSFC Publication.

1976 Kauth, R. J. and G. S. Thomas. "The Tasseled-Cap: A Graphic Description of the Spectral-Temporal Development of Agricultural Crops as Seen by Landsat: Symposium on Machine Processing of Remote Sensed Data. June 29 - July 1, 1976, Purdue University, LARS."

1985 Kieffer, H. H. and R. L. Wildey. "Absolute Calibration Of Landsat Instruments Using The Moon." Photogram. Eng. and Remote Sens., 51, pp. 1391-1393.

Krishniah, P. R. and L. S. Kanal, eds. "Classification, Pattern Recognition, And Reduction Of Dimensionality." Handbook of Statistics, 2,Amsterdam, North Holland.

1984 Kurucz, R. L., I. Furenlid, J. Brault, and L. Testerman. "Solar Flux Atlas from 296 to 1300 nm." National Solar Observation Atlas 1.

1973 Lane, A. P. and W. M. Irvine. "Monochromatic Phase Curves And Albedos For The Lunar Disk." Astron. Jour., 78, pp. 267-277.

1983 Lansing, J. C. and J. L. Barker. "Thermal Band Characterization of Landsat-4 Thematic Mapper." Landsat-4 Science Investigations Summary: Includes Dec. 1983 Workshop Results, 1, pp. 186-188, NASA/GSFC Publication.

1983 Lu, S. Y. "Pattern Classification Using Self-organizing Feature Map." Proceedings IJCNN'91., Febuary 22-28, 1983.

Lyot, B. "Annuals Observatoire Meudon." 8, part 1.

1985 Malaret, E., L. Bontolucci, F. Lozano, P. Anuta and C. McGillan. "Landsat-5 Thematic Mapper Data Quality Analysis." Photogrammetric Engineering & Remote Sensing, LI, no. 9, September, pp. 1407-1416

1985 Markham, B. L. and J. L. Barker. "Spectral Characterization of the Landsat Thematic Mapper Sensors." Landsat-4 Science Characterization Early Results: Thematic Mapper, 2, part 1, pp. 235-276, NASA/GSFC Publication.

1985b Markham, B. L., and J. L. Barker. "Special Issue LIDQA Final Symposium: Landsat Image Data Quality Analysis." Photogrammetric Engineering & Remote Sensing, LI, pp. 1245-1493.

1986 Markham, B. L. and J. L. Barker. "Landsat-MSS and TM Post-Calibration Dynamic Ranges, Exoatmospheric Reflectances and At-Satellite Temperatures." EOSAT Landsat Technical Notes, No.1, August, pp. 3-8.

1970 McCord, T. B. and T. V. Johnson. "Lunar Spectral Reflectivity (0. 3 To 2. 50 Microns) And Implications For Remote Mineralogical Analysis." Science, 169, pp. 855-858.

1972 McCord, T. B., M. P. Charette, T. V. Johnson, L. A. Lebofsky, C. Pieters and J. B. Adams. "Lunar Spectral Types." J. Geophys. Res., 77, pp. 1349-1359.

1981 McCord, T. B., R. N. Clark, B. R. Hawke, L. A. McFadden, P. D. Owensby and C. M. Pieters. "Moon: Near-Infrared Spectral Reflectance, A First Good Look." J. Geophys. Res., 86(B11), 10, pp. 833-10892.

1975 McGillem, C. D., T. E. Riemer and M. Mobassire. "Resolution Enhancement Of Erts Imagery." Proc. Conf. on Machine Processing of Remotely Sensed Data, Purdue Univ., West Lafayette, IN, June 3-5.

1980 Moik, J. G. "Digital Processing of Remotely Sensed Images." NASA SP-431, NASA, Washington, D. C.,.

1984 Neckel, H., and D. Labs. "The Solar Radiation Between 3300 and 12500 A." Solar Physics, 90, 205.

1992 Pagano, T. S. "Design of the Moderate Resolution Imaging Spectrometer-Nadir." Proceedings ASPRSIACSMIRT, Remote Sensing Data Acquisition, 4, pp. 374-385, August.

1993 Pagano. T. S., Hughes SBRC. "Moderate Resolution Imagine Spectroradiometer (MODIS)." Presentation at MODIS Science Team Meeting, March 23.

1993 Pagano. T. S., and R. Durham. "Moderate Resolution Imaging Spectroradiometer". SPIE Aerospace Sensing Symposium, April 12-16, 1993, Orlando, FL. Conference 1939 - Sensor Systems for the Early Earth Observing System Platforms. TAP93-0164.

1986 Pairman, D. and J. Kittler. "Clustering Algorithm for use with Images of Clouds." Int. J. Remote Sensing, 7, no. 7, pp. 855-866.

1989 Pan, J. J. "Spectral Analysis and Filtering Techniques in Digital Spatial Data Processing." Photogrammetric Engineering and Remote Sensing, 55, no. 8, August, pp. 1203-1207.

1988 Pieters, C. M. and J. F. Mustard. "Exploration Of The Crustal/Mantle Material For The Earth And Moon Using Reflectance Spectroscopy." Remote Sens. of Environ., pg. 24.

1977 Riemer, T. E. and C. D. McGillem. "Optimum Constrained Image Restoration Filters." IEEE Trans-on Aerospace Eng., 13, no. 2.

1993 Running, S. W. and C. Justice. "Terrestrial Remote Sensing and Algorithms Planned for EOS/MODIS."

1987 Salomonson, V. V. and J. L. Barker. "Recent Data Quality and Earth Science Results from the Landsat Thematic Mapper." Adm. Space. Res. 7, pp. (11) 217-(11)226.

1989 Salomonson, V. V., W. L. Barnes, P. W. Maymon, H. E. Montgomery, O. Harvey, "MODIS: Advance Facility Instrument for Studies of the Earth as a System," IEEE Transactions on Geoscience and Remote Sensing, 27, No. 2, March, pp. 145-153.

1990 Salomonson, V. V. and D. L. Toll. "Execution Phase (C/D) Spectral Band Characteristics Of The EOS Moderate Resolution Imaging Spectrometer (Modis-N) Facility Instrument." Advances in Space Research, 2(3), pp. 231-236.

1992 Salomonson, V. V. and J. L. Barker. "EOS Moderate Resolution Imaging Spectrometer: Phase C/D Status and Comments on Calibration and Georeferencing Approaches." 15th Annual AAS Guidence and Control Conference, Paper AAS 92-004, Keystone, CO, Febuary 8-12.

1967 Sarri, J. M. and R. W. Shorthill. "Isothermal And Isophtic Atlas Of The Moon: Contours Through A Lunation." NASA Contractors Report CR-855, pp. 186.

1986 Saunders, R. W. "An Automated Scheme for the Removal of Cloud Contamination from AVHRR Radiances over Western Europe." Int. J. Remote Sensing, 7, no. 7, pp. 867-886.

1985 Schowengerdt, R. A., C. Archwanety and R. C. Wrigley. "Landsat Thematic Mapper Image-Derived MTF, Photogrammetric Engineering and Remote Sensing," 51, No. 9, September, pp. 1395-1406.

1972 Shorthill, R. W. "The Infrared Moon: A Review." In Thermal Characteristics of the Moon, J. W. Lucas, ed., Progress in Astronautics and Aeronautics, 28, the MIT Press, pp. 3-49.

1987 Slater, P. N., S. F. Biggar, R. G. Holm, R. D. Jackson, Y. Mao, M. S. Moran, J. M. Palmer and B. Yuan. "Reflectance-Based And Radiance-Based Methods For The In-Flight Absolute Calibration Of Multi-Spectral Sensors." Rem. Sens. of Environ., 22, pp. 11-37.

1986 Strang, G. "Introduction To Applied Mathematics," Wellesley-Cambridge Press.

1990 Teillet, P. M., P. N. Slater, Y. Ding, R. P. Santer, R. D. Jackson and M. S. Moran. "Three Methods for the Absolute Calibration of the NOAA AVHRR Sensors In-Flight." Remote Sensing Environment, 31, pp. 105-120.

1988 Teillet, P. M., P. N. Slater, Y. Mao, B. Yuan, R. J. Bartell, S. F. Biggar, R. P. Santer, R. D. Jackson and M. S. Moran. "Absolute Radiometric Calibration Of The Noaa AVHRR Sensors." Proc. SPIE, 924, Recent Advances in Sensors, Radiometry and Data Pro.

1985 Tilton, J., B. Markham and W. Alford. "Landsat-4 and Landsat-5 Coherent Noise: Characterization and Removal." Photogrammetric Engineering and Remote Sensing, Vol LI, No. 9, September, pp. 1263-1279.

1992 Townshend, J. R. G., C. O. Justice, C. Gumey and J. McManue. "The Impact of Misregistration on Change Detection." IEEE Transactions on Geoscience and Remote Sensing, 30, No. 5, September.

1968 Van Trees, H. L. "Detection, Estimation and Modulation Theory." Wiley.

1989a Weinreb, M. P., R. Xie, J. H. Lienesch and D. S. Crosby. "Destriping GOES Images by Matching Empirical Distribution Functions." Remote Sensing of the Environment, 29, pp. 185-195.

1989b Weinreb, M. P., R. Xie, J. H. Lienesch and D. S. Crosby. "Removing Stripes in GOES Images by Matching Empirical Distribution Functions." NOAA Technical Memorandum NESDIS 26, National Oceanic and Atmospheric Administration, Washington, D. C., May.

1985 Wertz, J., ed. "Spacecraft Attitude Determination And Control." D. Reidel Publishing Company.

1976 Wildey, R. L. "A Digital File Of Lunar Normal Albedo: The Moon." 16, pp. 231-277.

Index

A&E period 3, 107
A/D converters 15, 17, 18, 99
Afocal telescope assembly 98
Algorithm
  A&E phase 11
  classification masking 24
  control flow diagram 12
  operational phase 11
Analog Electronics Module 17
Band properties 94
Bidirectional Reflectance Distribution Function 16, 17, 116
Bidirectional Reflectance Distribution Function (16
Blackbody 19-20, 82, 99, 100, 103
Calibration
  absolute 112
  accuracy 8
  algorithm 105
  algorithm changes 4
  algorithm data transformation 112
  algorithm status 1
  coefficients 15-22, 23, 117
  consistency 7
  defined 1
  electronic 17-18, 20
  error 2
  extreme-target-based absolute 107
  geometric error 44
  image-derived 107, 111
  in-flight 90
  lunar 103, 109
  lunar-based radiometric 109
  lunar-view
  on-board 111, 119
  pre-launch 3, 116, 119
  pre-launch cross-sensor 7
  processing 4
  radiometric coefficients 5
  radiometric equation 4
  reference standards 7
  requirements 7-9, 91, 109
  sites 107
  specification 8-9

strategy 9
uncertainty 2, 103
units 7
vicarious 3, 111, 119, 120, 123
weighting factors 122
Calibration Management Plan 91
Capacitance transimpedance amplifier 17
Center wavelength 83
Characterization
defined 1
Earth scan 20
LIDQA 4
lunar view 20, 21
noise 21-22
on-board calibrator 15-22
requirements 83
Coefficients
calibration 23
emissive 22
OBC/Lunar 22
potential calibration 30
projected 22
projected calibration for next orbit 31
reflective 22
Coordinate systems 4, 11-13
Data
dark image 21
frames of 15
Level-1 calibration and utility mask product 3
Level-1A product 4
MOD01, geolocation raw data 1
Level-1B product 4
MOD02, geolocated radiance 1
Level-2 products 7
MOD18, MODIS utility mask 1, 23
product sensitivity 7
product uncertainty 7
Degradation 88
ratio 16
Detector lead lengths 99
Detector readout data elements 98
Detectors
dead 23, 24, 107
photoconductive 18, 99
photovoltaic 17
Earth view 86

Earthshine 100
Edge range 83
End-to-End Performance Model 106
Error budgets 41-45
Fields of view 79
Filters, interference 83
Geolocation 4, 11-13, 105
    accuracy 87
    algorithm development 1
    attitude data 51
    attitude information 55
    data fields 53
    data products
        Level-0 53
        Level-1A 51, 52
        Level-1B 52
        Level-2 53
        Level-3 53
    Earth location algorithm 51-75
        ancillary input data sets 55-56
        computational load 69
        control point data 71
        coordinate conversion 69, 70
        coordinate systems 57-58
        coordinate transformations 58, 60
        digital elevation data 70
        digital elevation model 55
        Ellipsoidal Look Vector intersection 63
        exception handling 74
        fields of view 60
        fields of view,ground 51, 53
        geometric parameter estimation 72-73
        ground locations 56
        mathematical development 56-69
        MISR, coordination with 70
        MODIS line of sight intersection 69
        product validation 71-72
        quality control 73
        SOM projection 70
        terrain intersection search geometry 66
        uncertainty estimates 67-69
        viewing geometry 60-61
    Earth location data fields 51
    Earth location height 53
    geodetic position 51
    multiple detector geometry 54

- off-nadir satellite imagery 54
- other satellites
  - AVHRR 54
  - Landsat 54
  - SPOT 54
- sample timing adjustments 54
- satellite viewing angles 53
- scan to scan overlap in cross-track scanning mirror 55
- solar angles 54
- spacecraft ephemeris 55
- sub-pixel misalignments 54
- sub-pixel offsets 54

Ground sample distance 86
Ground Support Equipment 92
Histogram equalization 26-28
Instantaneous fields of view 9, 19, 86-87, 88, 94, 98
Instrument
- characteristics 9
- dynamic range requirements 80, 81
- failure 77
- integration and test 79
- lifetime 77
- mount 100
- mounting surfaces 87
- optical axis 87
- stability 3
- storage 79
- table of physical requirements 78

Interference fringes 87
Kieffer, Hugh 20, 109
Launch schedule
- COLOR 2
- EOS AM 2-3
- EOS PM 2-3
- SeaWiFS 2

Linear detector response 115
Lunar ephemeris prediction module 20
Lunar view 109
Lunar View geometry 110
Math models
- extension of 105
- instrument 8
- radiometric 42, 87, 90
- structural 90, 91
- thermal 90

Metadata 30-31

Modis Characterization Support Team
  relevent activities 90
  responsibilities 1, 7, 11, 92, 107
MODIS Science Data Support Team
  responsibilities 1, 11
Modulation Transfer Function 4, 9, 29, 45, 87, 88, 92, 108, 110
NIST standards 83
Nyquist frequency 88
On-board calibrator 11, 15, 21, 22, 23, 30, 90, 106
Orbit patterns 21-22
Out-of-band response 83
Planetary reflectance
  effective at-satellite equation 5
Platform attitude 109
Pointing accuracy 9
Polarization 87
Radiance
  detector specific 21
  lamp 116
  lunar 109
  properties 107
  spectral 79, 80, 81
  uncertainty 8
Radiation
  diffracted 88
  scattered 88
  stray 100
  transient 88
Radiometric accuracy 82, 87
Response points 83
RMS deviation 82
Signal-to-noise ratio 83, 86
Solar diffuser 8, 15, 18, 90, 95, 100, 106
Solar input 79
South Atlantic radiation anomaly 79
Space View 17, 18, 20, 21, 22, 103, 106, 109, 111
Space Viewport 20, 95
Specification references
  ¶(2.0) 77
  ¶(3.1.1) 78
  ¶(3.1.4) 90
  ¶(3.1.4.1) 91
  ¶(3.1.4.2) 91
  ¶(3.1.4.3) 91
  ¶(3.1.4.4) 91
  ¶(3.1.4.5) 91

¶(3.1.4.6) 91
¶(3.1.4.7) 91
¶(3.2.1) 78
¶(3.2.2) 91, 92
¶(3.2.3) 77, 78
¶(3.2.4.1) 78
¶(3.2.4.2) 78, 79
¶(3.3.1) 86
¶(3.3.2) 87
¶(3.3.3) 83
¶(3.3.3.2) 83
¶(3.3.3.3) 79, 83
¶(3.3.3.4) 83
¶(3.3.4) 79
¶(3.3.4.1) 79
¶(3.3.4.2) 82
¶(3.3.5) 87
¶(3.4.1) 79
¶(3.4.10.1) 92
¶(3.4.10.2) 92
¶(3.4.10.3) 92
¶(3.4.10.4) 78
¶(3.4.2) 87
¶(3.4.3) 82
¶(3.4.4) 89
¶(3.4.5.1) 83
¶(3.4.5.2) 82, 83
¶(3.4.5.3.1) 82
¶(3.4.5.3.2) 77, 83
¶(3.4.5.3.3) 88
¶(3.4.5.4) 86
¶(3.4.5.5) 83
¶(3.4.6) 87
¶(3.4.6.1) 87
¶(3.4.6.2) 87
¶(3.4.6.3) 86
¶(3.4.7.4) 86
¶(3.4.7.5) 83
¶(3.4.8.1) 88
¶(3.4.8.2) 88
¶(3.4.8.3) 88
¶(3.4.8.4) 89
¶(3.4.9) 90
¶(3.4.9.1) 90
¶(3.4.9.2) 90
¶(3.4.9.3) 90

¶(3.4.9.4) 90
¶(3.4.9.5) 90
¶(3.5.1) 91
¶(3.5.2) 91
¶(3.5.2.1) 91
¶(3.5.3) 91
¶(3.6.2.1) 78
¶(3.6.2.2) 78
¶(3.6.2.4.1) 78
¶(3.6.2.4.2) 78
¶(3.6.2.4.3) 78
¶(4.1) 91
¶(4.1.1) 91
¶(4.1.2) 91
¶(4.1.3) 91
¶(4.1.4) 91
¶(4.2) 91
¶(5.0) 91
¶(5.1) 91
¶(5.1.1) 91
¶(5.1.2) 91
¶(5.1.3) 91
¶(5.1.4) 91
¶(5.1.5) 91
¶(5.1.6) 91
¶(5.1.7) 91
¶(5.1.8) 91
¶(5.2) 91
¶(5.3) 91
¶(5.4.1) 91
¶(5.4.2.1) 91
¶(5.4.2.2) 91
¶(5.4.2.3) 91
¶(5.4.2.4) 91
¶(5.4.2.5) 91
¶(5.4.3) 91
¶(5.4.4) 91
¶(5.5) 91
¶(6.1) 92
¶(6.3) 92
¶(6.4) 92
¶(6.5) 92
Specification, references 77-92
Spectral bands
alignment 86
LWIR 77, 88, 98

MWIR 77, 88, 98
NIR 18, 19, 77, 88, 89, 93, 98, 111
properties 93
shape 83
solar reflective, units 5
SWIR 18, 19, 77, 88, 93, 98
thermal 82
thermal emissive, units 5
VIS 18, 19, 77, 88, 89, 93, 98
Spectral radiance 83
Spectral response 83
Spectralon plate 100
Spectroradiometric calibration assembly 18-19, 22, 28, 92, 95, 97, 100, 101, 102, 106, 111, 116, 119, 122
geometric mode 19
radiometric mode 18
spectral mode 19
Systematic errors 112
Systematic noise
analysis 13
characterization 21-22
corrections 107
crosstalk 13, 87
dark scene correlation 109
electronic crosstalk 88
formulas 14
Fourier notch filtering 15
ghost images 13, 20, 109, 110
image blurring 87
instrument-related corrections 108
Kalman filtering 15
memory effect 109
MTF blur 109
occurances 2
pre-processing 13-15
stray light 13, 87, 109, 110, 114
stray light tests 88-90
striping 26
between-scan 109
spectral 109
witin-scan 109
transforms
nonlinear
Hadamard 14
spectral
brightness 14

greenness 14
tasseled cap 14
Temperature
effective at-satellite equation 5
Transient response 87, 89

REPORT DOCUMENTATION PAGE

Form Approved
OMB No. 0704-0188

Public reporting burden for this collection of information is estimated to average 1 hour per response, including the time for reviewing instructions, searching existing data sources, gathering and maintaining the data needed, and completing and reviewing the collection of information. Send comments regarding this burden estimate or any other aspect of this collection of information, including suggestions for reducing this burden, to Washington Headquarters Services, Directorate for Information Operations and Reports, 1215 Jefferson Davis Highway, Suite 1204, Arlington, VA 22202-4302, and to the Office of Management and Budget, Paperwork Reduction Project (0704-0188), Washington, DC 20503.

1. AGENCY USE ONLY *(Leave blank)*

2. REPORT DATE
May 1994

3. REPORT TYPE AND DATES COVERED
Technical Memorandum

4. TITLE AND SUBTITLE
MODIS Technical Report Series
Volume 2, MODIS Level 1Geolocation, Characterization and Calibration Algorithm Theoretical Basis Document, Version 1

5. FUNDING NUMBERS
Code 920
NAS5-31331

6. AUTHOR(S)
John L. Barker, Joann M. K. Harnden, Harry Montgomery,
Paul Anuta, Geir Kvaran, Ed Knight, Tom Bryant,
Al McKay, Jon Smid, and Dan Knowles, Jr.

7. PERFORMING ORGANIZATION NAME(S) AND ADDRESS (ES)
Laboratory for Terrestrial Physics
Goddard Space Flight Center
Greenbelt, Maryland 20771

8. PEFORMING ORGANIZATION REPORT NUMBER
94B00069

9. SPONSORING / MONITORING ADGENCY NAME(S) AND ADDRESS (ES)
National Aeronautics and Space Administration
Washington, DC 20546-0001

10. SPONSORING / MONITORING ADGENCY REPORT NUMBER
NASA TM-104594, Vol. 2

11. SUPPLEMENTARY NOTES
J. Barker, J. Harnden, H. Montgomery: Goddard Space Flight Center, Greenbelt, Maryland; P. Anuta, G. Kvaran, E. Knight, T. Bryant, A. McKay, J. Smid, D. Knowles, Jr.: Research and Data Systems Corporation, Greenbelt, Maryland.

12a. DISTRIBUTION / AVAILABILITY STATMENT
Unclassified - Unlimited
Subject Category 19

12b. DISTRIBUTION CODE

13. ABSTRACT *(Maximum 200 words)*

The EOS Moderate Resolution Imaging Spectrometer (MODIS) is being developed by NASA for flight on the Earth Observing System (EOS) series of satellites, the first of which (EOS-AM-1) is scheduled for launch in 1998. This document describes the algorithms and their theoretical basis for the MODIS Level 1B characterization, calibration, and geolocation algorithms which must produce radiometrically, spectrally, and spatially calibrated data with sufficient accuracy so that Global change research programs can detect minute changes in biogeophysical parameters. The document first describes the geolocation algorithm which determines geodetic latitude, longitude, and elevation of each MODIS pixel and the determination of geometric parameters for each observation (satellite zenith angle, satellite azimuth, range to the satellite, solar zenith angle, and solar azimuth). Next, the utilization of the MODIS onboard calibration sources, which consist of the Spectroradiometric Calibration Assembly (SRCA), Solar Diffuser (SD), Solar Diffuser Stability Monitor (SDSM), and the Blackbody (BB), is treated. Characterization of these sources and integration of measurements into the calibration process is described. Finally, the use of external sources, including the Moon, instrumented sites on the Earth (called vicarious calibration), and unsupervised normalization sites having invariant reflectance and emissive properties is treated. Finally, algorithms for generating utility masks needed for scene-based calibration are discussed. Eight appendices are provided, covering instrument design and additional algorithm details.

14. SUBJECT TERMS
EOS, MODIS, Calibration, Algorithm, Geolocation.

15. NUMBER OF PAGES
196

16. PRICE CODE

17. SECURITY CLASSIFICATION OF REPORT
Unclassified

18. SECURITY CLASSIFICATION OF THIS PAGE
Unclassified

19. SECURITY CLASSIFICATION OF ABSTRACT
Unclassified

20. LIMITATION OF ABSTRACT
UL